UNIVERSITY OF NATAL

AEROSOLS AND ATMOSPHERIC CIRCULATION CHARACTERISTICS OVER DURBAN

M. Z. RAHMAN

AEROSOLS AND ATMOSPHERIC CIRCULATION CHARACTERISTICS OVER DURBAN

by

Muhammad Ziaur Rahman

Submitted in the partial fulfillment of the
requirements for the degree of
Master of Science, in the School of
Life and Environmental Sciences,
University of Natal, Durban.

Durban
October, 2000.

ABSTRACT

The main objective of this study was to investigate the vertical distribution of aerosols over Durban in relation to the vertical stability structure and horizontal transport of air masses. The importance of aerosols in the region is well recognised and recently there have been many international experiments which have focused on aerosol distribution over the subcontinent. Durban is situated at the approximate centre of a giant plume that is known to transport aerosols and trace gases off the east coast of southern Africa and is therefore strategically located for an investigation of the vertical distribution of aerosols.

The vertical distribution of aerosols over Durban was measured using a LIDAR (Light Detection And Ranging) system on selected cloud free days in 1997. Backward trajectory modelling was used at selected pressure (standard) levels to determine the origin and transport pathways of aerosols. Six case studies are presented in an attempt to gain insight into the relationship between the vertical distribution of aerosols and absolutely stable layers.

The results of the study revealed that the occurrence of absolutely stable layers governs the vertical distribution of aerosols in the troposphere. An absolutely stable layer at ~5km (~500hPa) appears to be the most effective in capping and trapping aerosols in the atmosphere. Below 5km, the atmosphere was charcterised by marked stratification and relatively higher concentration of aerosols. Above 5km, the concentrations were much lower, but generally increased slightly with height. Low aerosol concentrations are observed during post-frontal situations and relatively higher concentrations during anticyclonic conditions.

The background to the problem and the objectives of this investigation are elaborated in Chapter 1. A description of the data sets and derived meteorological variables, along with the methodologies applied in this thesis, are given in Chapter 2. A theoretical review of aerosols, including their sources, effects and distribution over the globe and southern Africa, is discussed in Chapter 3. Atmospheric circulation and weather patterns

and their relationship to the transport and dispersion of aerosols are described in Chapter 4. The results of the study and an analysis of the major findings are presented in Chapter 5. Finally, Chapter 6 summarises the major findings of this dissertation.

PREFACE

The work described in this dissertation was carried out in the School of Life and Environmental Sciences, University of Natal, Durban, from September 1998 to June 2000, under the supervision of Professor Roseanne D. Diab.

The study represents original work by the author and has not been submitted in any form for any degree or diploma to another university. Where use was made of the work of others, it has been duly acknowledged in the text.

ACKNOWLEDGEMENTS

This thesis required the help, assistance and guidance of several people without whom successful completion of this study would not have been possible. To give due credit to everyone involved would be impossible. In particular, I would like to thank the following persons for their assistance and support:

A special word of thanks to my supervisor, Professor Roseanne Diab, for all the support, advice and encouragement she provided throughout the duration of this project. It was she who had the initial idea for this project. I really enjoyed working under her. I believe that under her supervision and inspirational guidance, I have been able to acquire some knowledge and techniques in atmospheric science. These should stand me in good stead for future research. I would like to wish her well for the future and thank her for all she has taught me.

I owe a great deal to several people for obtaining data for me. A special thanks must go out to Ashokabose Moorgawa of the Physics Department, University of Natal, Durban, for giving me the opportunity to work on his aerosol data and helping me to understand the functioning of the Durban LIDAR system. I would also like to thank Tali Freiman of the Climatology Research Group, University of the Witwatersand, for teaching me to work on the Trajectory Model and for helping me to acquire necessary data for this study.

I am deeply indebted to Frank Sokolic, School of Life and Environmental Sciences, University of Natal, Durban, for writing necessary computer programmes for data processing and also for coming to my rescue on numerous occasions.

Thanks to Hem Hurrypursad, School of Life and Environmental Sciences, University of Natal, Durban, for assisting with the preparation of many of the diagrams.

Thanks to Isaac Abboy, School of Life and Environmental Sciences, University of Natal, Durban, for allowing me to use books and SAWB reports on many occasions.

To all my friends in the department for helping me to settle into a new culture, in a new place, especially to Kirsten, a true and special friend, who assisted me in proof reading this document and organising my secondary information. Her help during my work is beyond any words.

A very special word of thanks must go out to my parents and sister and her family for their support and patience. Without their love this would not have been possible.

Finally, my sincerest and grateful thanks go to the School of Life and Environmental Sciences, University of Natal, Durban for giving me the opportunity to work on this project.

TABLE OF CONTENTS

LIST OF FIGURES

LIST OF TABLES

LIST OF PLATES

CHAPTER 1

INTRODUCTION

1.1 Background

In recent years, substantial progress has been made in evaluating the impact of aerosols on climate and atmospheric chemistry. It has been recognised that aerosols play an influential role in the earth's climate through their interaction with global radiation and cloud albedo (Andreae and Crutzen, 1997). Aerosols in the lower atmosphere, resulting from combustion of fossil fuels, biomass burning and other sources, can have regional to continental scale effects on climate. Locally, the influence of aerosols on surface temperature can be large enough to more than offset the warming due to greenhouse gases (Intergovernmental Panel on Climate Change (IPCC), 1996). Such observations provide cause for concern and strong support for research into the behaviour of atmospheric aerosols at a regional scale.

Aerosols have indeed become a major issue and are the focus of much research in the southern African context. The first and largest international experiment undertaken was the Southern African Fire-Atmosphere Research Initiative (SAFARI-92) conducted during 1992, where attention was focused on the relationship between fires and savanna ecology and the atmospheric impacts of biomass burning emissions over southern Africa (Lindesay *et al.*, 1996). A recent and ongoing experiment, the Aerosol Recirculation and Rainfall Experiment (ARREX), has been initiated to investigate the physical and chemical properties of aerosols and their transport over South Africa (Swap and Annegarn, 1999). Moreover, owing to the success of SAFARI-92 and building upon its the scientific legacy, SAFARI 2000 is about to follow to explore and study the linkages among land-atmosphere processes, principally the biogenic, pyrogenic and anthropogenic emissions occurring in this region, their transport and transformations in the atmosphere, their influence on regional climate and meteorology

and their eventual deposition and effects on the functioning of the ecosystems of this region (Swap and Annegarn, 1999).

During SAFARI-92 and the Southern African Atmosphere Research Initiative (SA'ARI-94), biomass burning was considered as the major contributor to the total aerosol loading over southern Africa. However, recently some other major sources have been identified in relation to total aerosol loading in the atmosphere over southern Africa (Piketh *et al.*, 1999a; 1999b). Piketh *et al.* (1999a; 1999b) found that soil-derived aerosols are the major contributors to aerosol loading in the dry winter periods over the plateau of South Africa. These studies have shown that regardless of seasonal variations in aerosol composition, soil-derived aerosols dominate the composition of aerosol loading throughout the year. Along with soil-derived aerosols, the contribution of marine aerosols to aerosol loading has been found to be significant along the marine boundary layer in South Africa for both summer and winter.

Recently Tyson *et al.* (1996) identified that surface derived dust, biomass burning products and aerosols are trapped in a dust pall beneath the ~500hPa stable discontinuity to form a haze layer over southern Africa. This prominent stable layer at 500hPa acts as a barrier to the vertical transport and dispersal of trace gases and aerosols (Tyson and Whyte, 2000). Recirculation has a major influence on the transport patterns of trace gases and aerosols over this sub-continent. During the process of recirculation, trace gases and aerosols are trapped beneath absolutely stable layers over South Africa. When westerly or easterly winds occur, these pollutants move as far as Amsterdam Island (5000km to the south-east) and Ascension Island (4000km to the north-west) respectively (Tyson *et al.*, 1996).

The strategic location of Durban on the east coast, at the approximate centre of the giant plume that exits the subcontinent to the Indian Ocean, makes it an ideal location at which to investigate aerosol concentrations. In the past several studies were conducted by Kuppen (1992; 1996) and Moorgawa (1997) using a LIDAR (Light Detection And Ranging) to measure aerosol concentrations. Their studies concentrated on the detection of both low and high altitude aerosols. Kuppen (1992; 1996) identified aerosol layers at

3, 5, 25 and 60km over the KwaZulu-Natal coast during the sugar cane burning season (June to September 1996). Moorgawa (1997) identified aerosol layers at 3, 5, 9 and 27km. However, none of these studies examined the relationship between the identified aerosol layers and vertical temperature stratification in the atmosphere.

A new LIDAR was installed by the French-South Africa collaboration in April 1999. This new LIDAR operates on 2 channels. Channel A receives signals from 10 to 60km and channel B receives signals from 0 to 12km. It uses a 'Nd_Yag' laser beam. Moorgawa (1999) has initiated an experiment with this new LIDAR to investigate the relative aerosol density and temperature profiles within the stratosphere level over Durban. Unfortunately due to problems experienced with the Channel B sensor, it has not yet been possible to use the new LIDAR to investigate tropospheric aerosol profile. However, it has been possible to utilise tropospheric measurements from the earlier instrument in this study.

Since studies of the relationship between vertical aerosol distribution and atmospheric dynamics have never been undertaken, it is appropriate that research be conducted on this topic.

1.2 Aim and Objectives

Tropospheric aerosol concentrations fluctuate over the subcontinent on a day-to-day basis. This study aims to analyse the variability in aerosol profiles over Durban due to the atmospheric circulation, including both horizontal transport and vertical dispersion.

The objectives of this study are:

1. To describe the nature and characteristics of the vertical distribution of aerosols in the troposphere over Durban.

2. To investigate the relationship between the vertical distribution of aerosols and atmospheric stability, vertical wind structure and air mass origin.

3. To investigate the relationship between the vertical distribution of aerosols and local synoptic weather situations (e.g. established high-pressure system, pre-frontal situation and post-frontal situation).

These objectives will be achieved based on an analysis of six aerosol profiles over Durban measured by a LIDAR over the period July to October 1997. Although it is acknowledged that this is a very small sample, it represents all the available data and in view of the fact that tropospheric aerosol profiles have not been previously described, the data were deemed worthy of investigation.

CHAPTER 2

DATA AND METHODOLOGY

2.1 Introduction

In this chapter, data used in this study are outlined, together with a discussion of the methodologies used to describe the characteristics of aerosol and meteorological data.

2.2 Data

2.2.1 Aerosol Data

The aerosol data set was obtained from the Light Detection And Ranging (LIDAR) system operated by the Physics Department, University of Natal, Durban. This instrument is situated on the top of a five-storied building, which is located on the university campus at an altitude of 100m above sea level.

This LIDAR system is a remote-sensing tool that consists of two main components: viz. a transmitter and a receiver. The transmitter is a bright light source (usually a laser beam), while the receiver is a telescopic arrangement with light detection optics at the focus. Short pulses of laser light are emitted into the atmosphere. Depending on the wavelength of operation, it interacts with particular atmospheric constituents. The scattered light is then collected by the telescope. The return signal gives a direct indication of the altitude from which the scattering takes place. The intensity of the return signal is related to the density of the scatterer. In this way, profiles of aerosol density can be plotted (Kuppen, 1996). Full details of the LIDAR system operated in Durban are given by Kuppen (1992; 1996) and Moorgawa (1997).

Aerosol profiles used in this study were taken between approximately 20:00 and 20:15. Data collection was undertaken in 1997 on six selected clear sky days, July 3 and 23, August 8 and 21, September 26 and October 20. Aerosol concentrations were measured from the ground to the lower stratosphere but for the purposes of this study, only the aerosol data from a height of 1km to 10km have been considered and analysed.

The Durban LIDAR is a monostatic, uniaxial system, consisting of a transmitting and a receiving component. The transmitter consists of a 'flashlamp-pumped dye laser'. The dye used is Rhodamine 6G in a concentration of 0.5×10^{-4} moles/ litre of methanol. This produces an output laser beam of 589nm. The receiver consists of a 1.5m back silvered parabolic search light mirror with a focal length of 654mm. Collimating optics are located at the focus of the mirror. The photomultiplier tube is placed immediately after the collimating optics (Kuppen, 1996).

A 'flashlamp-pumped dye laser beam' is fired into a prism, which is steered by a motor controller (Fig. 2.1). The photocathode, which is placed at the back of the laser cavity, detects the emitted laser beam and sends the voltage pulse to the pulse counting system with counts recorded by the computer. The pulse counting system consists of two electronic counters, which integrate the signal from the photomultiplier and give the system a vertical resolution of 150m. Two computers are used in this system.

The prism is set by a computer so that the light sent to the atmosphere falls on the field of view of the receiving search light mirror. The other computer controls the data acquisition and storage. The Pascal programme 'Hlidar.pas' written by Kuppen (1992) has been utilised to calculate the number of counts after every shot and to store data. A more complete description of this programme will be given in the latter part of this chapter.

The laser beam strikes the directing prism from where it is reflected upwards into the sky (Fig. 2.2). As it interacts with the atmospheric molecules and aerosols, the scattered laser comes straight back and is collected by the mirror and focused onto the aperture.

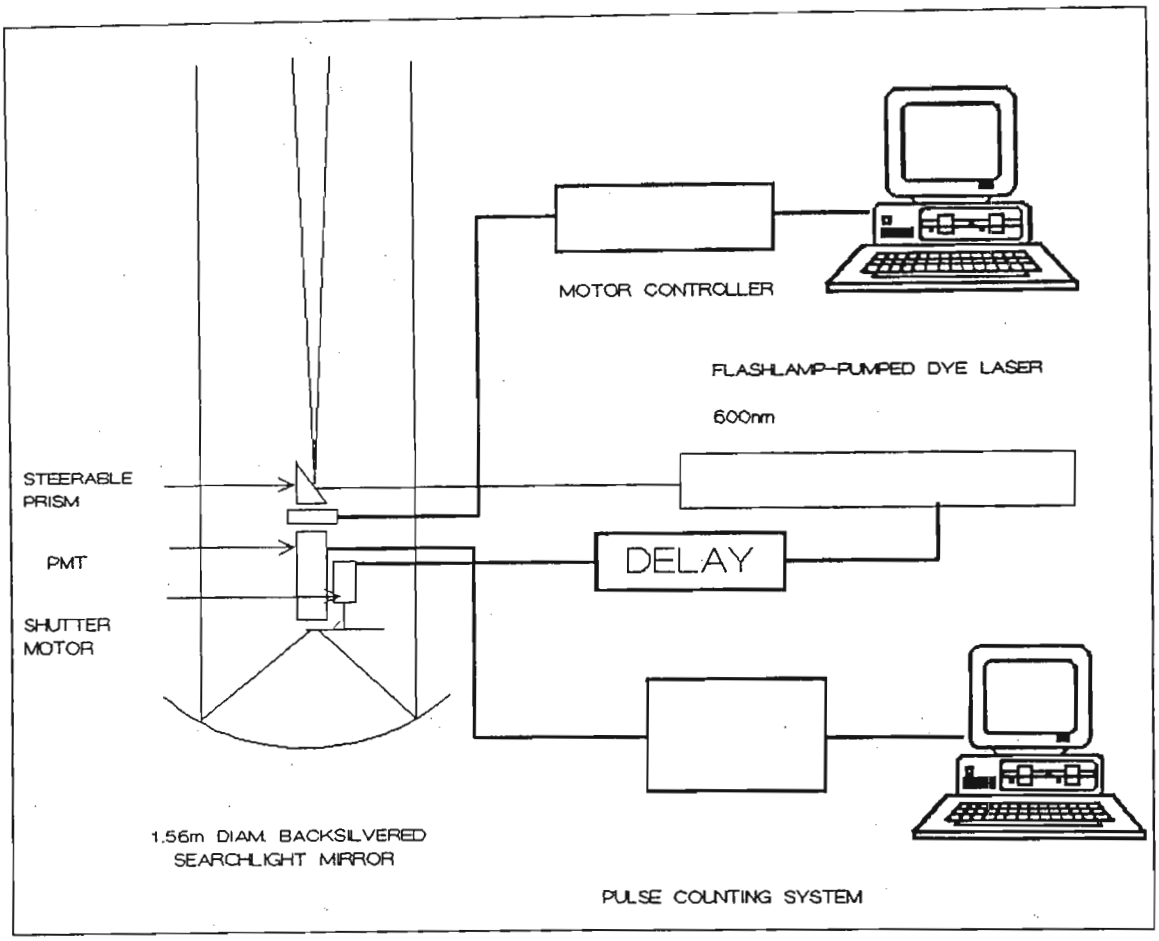

Figure 2.1: Structural diagram of the Durban LIDAR system (after Kuppen, 1996).

The light then passes through the aperture and strikes the photocathode on the photomultiplier. The light incidents on the photocathode consist of a large number of photons. The photomultiplier detects the backscattered photons and sends pulses to the pulse counting system, which are recorded as counts by the computer. The pulse counting system starts counting records the moment the laser is fired and integrates counts for every microsecond. A number of laser shots are taken with a resolution of 150m and the counts are added to produce a single profile.

As mentioned earlier, the return counts, which are raw data, are numerical signals for backscattered photons. The return signals are plotted as counts against altitude to produce all the aerosol profiles, which are used in this study.

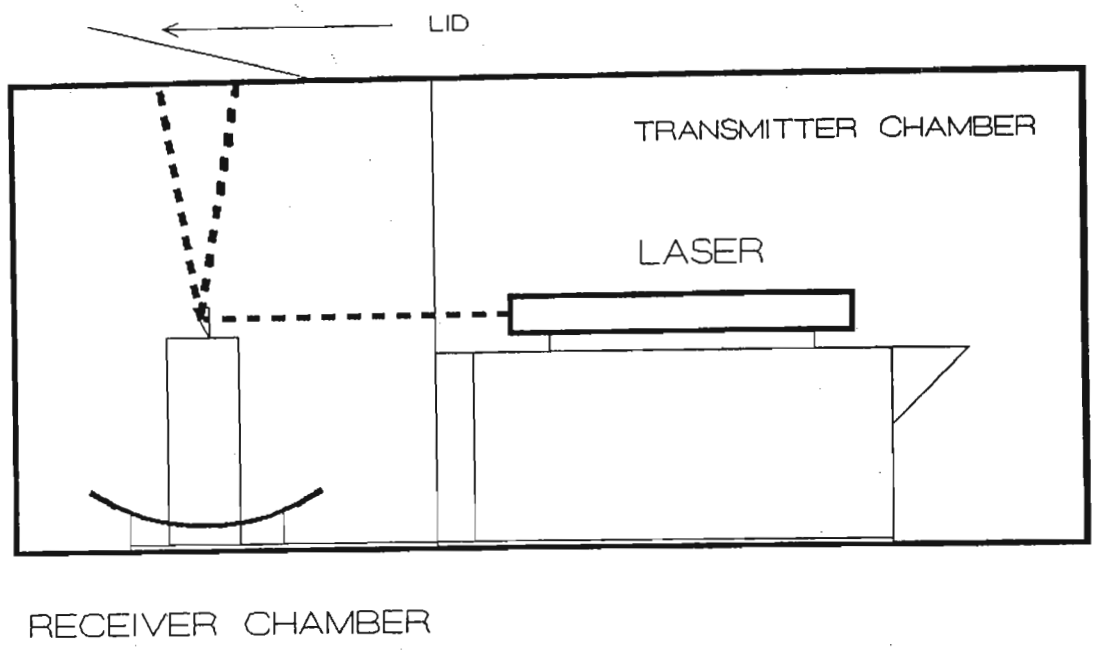

Figure 2.2: Internal layout of the lidar system (after Kuppen, 1996).

A wavelength of 589nm is used in the laser beam to detect all particles, such as sea-salt, pollens, particulates from biomass burning, windblown dust and particulates from industrial emissions.

2.2.2 Radiosonde Data

Radiosonde data were obtained for Durban International Airport from the South African Weather Bureau for the period July to October 1997. Radiosonde soundings are performed twice daily at midnight and midday. This data set provides meteorological information at standard pressure levels, such as 1000, 925, 850, 700, 500, 400, 300, 250, 200, 150, 100, 70, 50, 30 and 20hPa, and at significant pressure levels where significant changes are detected in the temperature lapse rate. Standard pressure level data includes: pressure level in hPa, dry bulb temperature in °C, relative humidity, the height of the standard pressure level in geopotential meters above mean sea level, wind direction in degrees and wind speed in ms^{-1}. On the other hand, significant pressure level data includes: pressure in hPa, dry bulb temperature in °C and the height of the significant pressure levels in geopotential meters above mean sea level.

For the purpose of this study, radiosonde data from 1000hPa to 300hPa at both standard and significant pressure levels have been considered. Radiosonde data sets were utilised to plot the absolutely stable layers and temperature inversions in the atmosphere and to provide information on the vertical wind profiles for the case studies.

2.2.3 Surface Synoptic Charts

Surface synoptic charts for the selected case studies were obtained from the Daily Weather Bulletins published by the South African Weather Bureau. These synoptic charts were used to illustrate the atmospheric circulation over South Africa for the assessment of the synoptic situations during case studies.

2.2.4 Surface Meteorological Data

All surface meteorological data used in this study were collected from the automatic weather station (AWS) located at the Durban International Airport. Wind speed, direction and surface pressure data for the study periods in 1997 (July to October) were used in the assessment of the results presented in Chapter 5.

2.2.5 Trajectory Modelling

Trajectory modeling is a useful tool to monitor the long-range transport of airborne materials in the atmosphere in time and space (D'Abreton, 1996). Two methods, based on the Lagrangian advection principle, can be used to construct three-dimensional wind components; these are: the isentropic and kinematic approaches. Many workers have made comparisons between different trajectory computations (e.g. Kuo *et al.*, 1985; Fuelberg *et al.*, 1996). Fuelberg *et al.* (1996) and D'Abreton *et al.* (1996) have found that the kinematic trajectories undergo considerably greater vertical displacements than their isentropic counterparts.

The isentropic approach assumes that air parcels move on a sloping constant-potential temperature surface and the kinematic approach uses the observed wind velocity component to trace the three-dimensional movement of air parcels (D'Abreton *et al.*, 1998). The kinematic model is widely used, particularly when data from European Center for Medium-range Weather Forecast (ECMWF) are used.

The trajectory model used in this study is that used by the Climatology Research Group, University of Witwatersrand, Johannesburg. It is a kinematic model and was used by Tyson *et al.*(1998) in the construction of the air transport climatology for southern Africa. Ten-day backward trajectories for the selected case studies were captured. The model domains extended from 0-60°S and 90°W to 90°E.

The input wind data were obtained from ECMWF and consisted of data on a 2.5° latitude-longitude grid, at different standard pressure levels, such as 1000, 925, 850, 700, 500 and 300hPa. At each grid point of the trajectory, the wind components (horizontal and vertical) were interpolated in time and space. The trajectories were calculated from a point of origin – Durban (29°9'S; 30°9'E) at 12:00 UTC. A centered and 5-point trajectory grid around the starting point is then determined by interactive advection of air masses. However, only the centered trajectories are presented in this study.

2.2.6 Computer Packages

Computer packages used in this study include Corel Draw (version 5.0 and 6.0) and MS Office 97. Corel Draw was utilised to draw different figures and graphs in this study.

In addition, some customised computer programmes written in Turbo Pascal (version 6.0 and 7.0) have been used in this study. As mentioned earlier that the 'Hlidar.pas' program written by Kuppen (1992) has been utilised to calculate the number of return counts accumulated after every laser shot as a function of altitude. In addition, this programme displays the return counts and plots the graph of counts versus altitude to the screen. The 'Height.pas' program written by Frank Sokolic (1998) has been used to

calculate the height of pressure surfaces from the SAWB data. The 'Clean.pas' program written by Frank Sokolic (1999) was used to reformat all the raw SAWB data into a suitable format for MS Excel.

2.3 Data Limitations

During the data measurement period, a high signal return from 0 to 1km caused the photomultiplier to saturate. Since the photomultiplier is extremely sensitive, high light intensities can saturate it (Kuppen, 1992; 1996). As mentioned earlier, the laser beam interacts with molecules in the atmosphere and the back scattered light is detected by the photomultiplier. When the laser beam interacts with low-level altitude lights, such as city lights, it gives strong returns. If the photomultiplier is exposed to them, it will saturate and will show an increase in photon counts in the profile. Due to the strong returns from the low altitude, aerosol data between 0 to 1km has not been analysed in this study. Fortunately, the saturation was very low above ~1km and gave low (detectable) returns from higher altitudes (above ~1km) suitable for data analysis.

CHAPTER 3

A THEORETICAL PERSPECTIVE OF AEROSOLS

3.1 Introduction

Emissions of greenhouse gases, including carbon dioxide, methane, nitrous oxide and other gases have been rising steadily ever since the beginning of the Industrial Revolution (1750 – 1800), largely as a result of an increase in fossil fuel combustion. The relationship between an increase in greenhouse gases and increased infrared radiative fluxes to earth is well known, with the result that General Circulation Models (GCM's) predict a rise in the earth's mean temperature (Cahill, 1996). However, recently the predictions and validity of GCMs, based only on greenhouse gas changes, have been questioned due to the increasing recognition of the role of atmospheric aerosols in climate forcing (Andreae, 1995; Le Canut, 1996; Levine, 1990; Lindesay *et al.,* 1996; Rosenfeld, 1999; Russell *et al.,* 1999 and Qian e*t al.*, 1999).

Aerosols directly affect the planetary albedo by scattering and absorbing solar radiation. Scattering of shortwave radiation enhances the radiation reflected back to space, therefore increasing the reflectance (albedo) of the earth and cooling the climate. In addition, absorption of solar and longwave radiation affects the atmospheric heating rate, which in turn alters the atmospheric circulation. High concentrations of aerosol particles modify cloud properties, resulting in more cloud droplets, albeit smaller in size, that generally increase the albedo of clouds in the earth's atmosphere (Andreae *et al.*, 1995; Kirkman, 1998; Shaw, 1996 and Tyson *et al.*, 1996). Additional cloud properties, such as enhanced liquid water content and increased cloud lifetime, have also been observed under certain circumstances (Kemp, 1990). Finally, aerosol particles can have an indirect effect on heterogeneous chemistry, which in turn can influence climate by modifying the concentrations of climate-influencing constituents (such as greenhouse gases) (King, 1999). For all those reasons the study of aerosols has been receiving increasing attention.

Aerosols are usually defined as small suspended particles in the air. Each particle is a colloidal system of fine solid or liquid particles in the atmosphere (Stern, 1976). The shape of individual particles is generalized into spherical, cubical or irregular forms. Plate 3.1 shows photographs, taken through an electron microscope, of aerosols typical of clean rural air and aerosols from an urban, polluted environment.

Aerosols may be classified according to particle size (Preston-Whyte and Tyson, 1988; Stern, 1976). They range from the Aitken or nucleation particles (particle radius below 0.1μm), to large particles (between 0.1μm and 1.0μm) to giant particles (greater than 1.0μm). Particles between 0.1μm and 0.3μm form the accumulation mode (Lenoble, 1991; Warneck, 1988; Woods *et al.*, 1991).

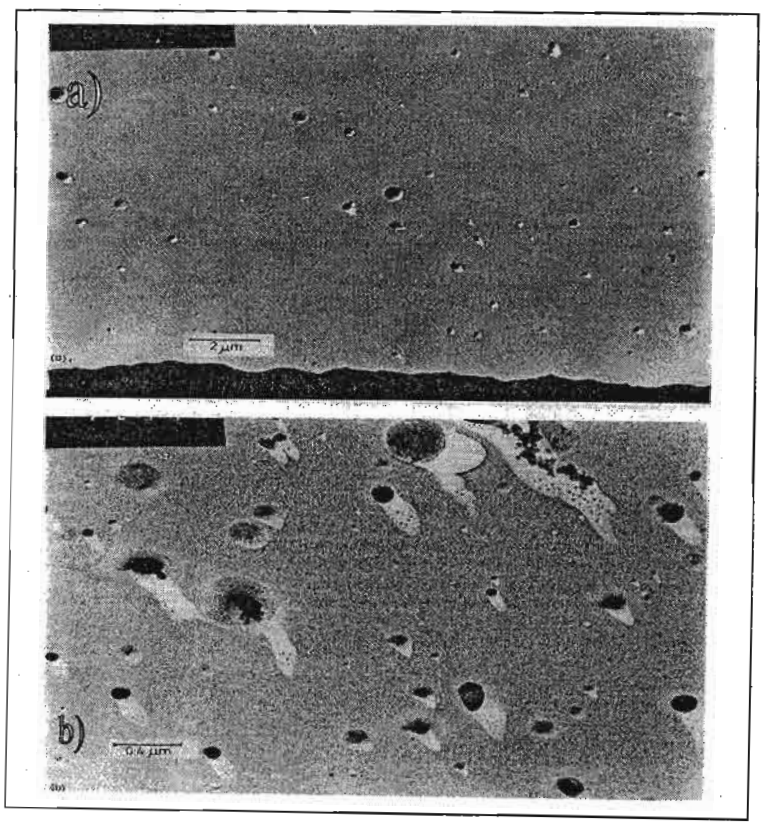

Plate 3.1 Photographs, taken through an electron microscope, of (a) a clean rural sampling and (b) an urban, polluted sampling of aerosol particles (Twomey, 1977).

Aerosols may also be classified as dispersion aerosols, which form when solid material breaks down or liquids atomize and the particulates are carried into suspension, or as

condensation aerosols which form when gases react with volatile or non-volatile solids (Preston-Whyte and Tyson, 1988; Stern, 1976). Table 3.1 shows the division of atmospheric aerosols into several classes, together with their sources and sinks and atmospheric lifetime.

Table 3.1: Different Classes of Atmospheric Aerosols

Designation	Aitken Nuclei	Large Aerosols	Giant Aerosols
Size (μm radius)	Below 0.1μm	0.1 - 1.0μm	Greater than 1.0μm
Sources	Combustion, gas to particle conversion.	Fly ash, sea-salt, pollens, coagulation of Aitken nuclei, cloud droplet evaporation.	Windblown dusts, industries.
Sinks	Coagulation, capture by cloud particles	Rain, snow.	Precipitation scavenging, dry fallout.
Lifetime	Less than an hour in polluted air or in clouds	Hours to days.	Minutes to hours.

Source: Preston-Whyte and Tyson, 1988.

3.2 Sources of Tropospheric Aerosols

Atmospheric aerosols originate from both natural and anthropogenic sources. Natural sources are principally sea salt, soil dust, particles from volcanic eruptions and forest fires. Anthropogenic sources consist of industrial and agricultural emissions. Their concentration, size distribution and chemical characteristics depend on the strength of their sources, climatic conditions and atmospheric dispersion and transport (Kaufman *et al.*, 1994; Rotstayn, 1999; Scholes *et al.*, 1996; Warneck, 1988). Figure 3.1 summarises the sources and types of atmospheric aerosols and Table 3.2 presents the estimated emissions of aerosol particles from both natural and anthropogenic sources.

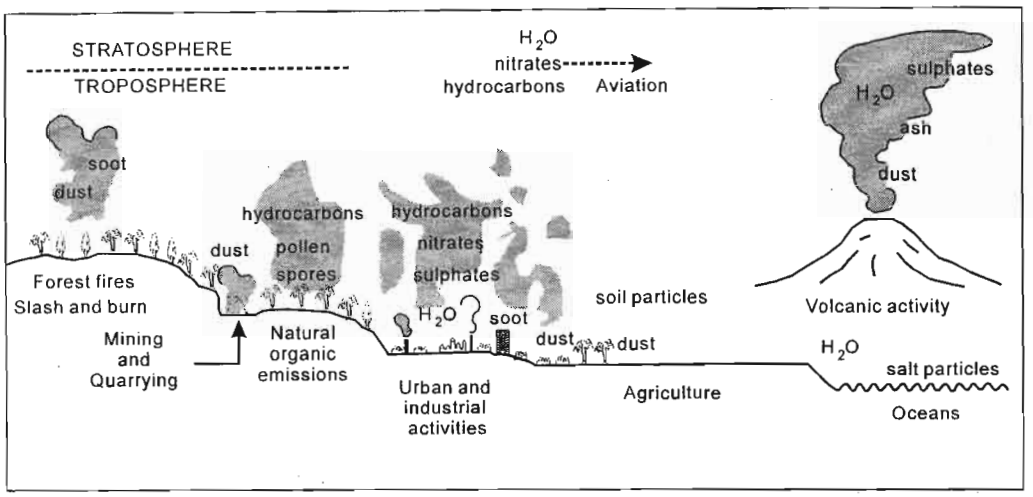

Figure 3.1: Sources and types of atmospheric aerosols (after Kemp, 1990).

Table 3.2: Worldwide Aerosol Particle Emissions by Major Source Category

Source		Emission Rate (Tg/yr)
Natural Particles	Soil and rock debris	1500
	Forest and slash fires	50
	Sea salt	1300
	Volcanic debris	33
	Gas-to-particle conversion: Sulphate from sulphur gases, Nitrate from NO_X, Organics (VOC) from plant exhalation and fire.	179
Subtotal		3062
Anthropogenic Particles	Direct or primary emissions	120
	Gas-to-particle conversion: Sulphate from S gas (SO_2 and H_2S) Nitrate from NO_X Organics (VOC)	266
Subtotal		386
Total		3450

Source: Andreae, 1995.

Four sources will be discussed here. They are: crustal or mineral; marine; anthropogenic or industrial sources; and biomass burning. Research on aerosol loading in South Africa conducted by Piketh *et al.* (1999) found that these sources are the key contributors to aerosol loading in the atmosphere.

3.2.1 Crustal or Mineral Sources

Deflation of soil and sediments at the earth surface is one of the major sources of atmospheric dust. The size distribution, residence time and transport of dust aerosols in the troposphere is governed by the theory of dust production outlined by Gillette and Goodwin (1974), which states that the first particles to be entrained as the wind speed increases over the threshold of erosion are those with radii between 20 and 50 μm.

These particles collide with other particles, dislodging and disaggregating smaller particles into the atmosphere. Particles larger than 20μm will settle back to the surface quickly when turbulence associated with the wind decreases, whereas smaller particles remain for days and weeks in the atmosphere (Gillette and Goodwin, 1974; Pinker *et al.,* 1997; Pinnick *et al.,* 1993; Pye, 1987; Warneck, 1998). The size distribution of tropospheric aerosols that are mainly soil derived has been found to range between radii of 10 and 100μm (Patterson and Gillette 1977). The soil texture determines particle size classes and the chemical composition of these aerosol particles in the atmosphere.

The world's arid and semi-arid regions contribute significantly to the concentration of crustal-derived aerosols in the atmosphere. In the recent decade, research in arid and semi-arid areas has increased with an attempt to calculate aerosol optical thickness, size distribution and the radiative effects. Pinnick *et al.* (1993) found that soil-derived aerosols contribute significantly to aerosol loading and absorption of radiation in the atmosphere in the southern United States. Similar results were found by Pinker *et al.* (1997) during an observational study initiated at the Jacob Blaustein Institute for Desert Research at Ben Gurion University, Israel.

3.2.2 Marine Sources

Oceans are the major source of atmospheric aerosols in the form of sea salt or crystal sodium chloride. These aerosols are found most abundantly in the air immediately above the marine boundary layer (MBL) (Pye, 1987; Shaw, 1996; Twomey, 1979; Warneck, 1988). Seawater contains sea salt to about 3.5 percent by weight, of which 85 percent is sodium chloride (Warneck, 1988). Sea salt is transferred to the atmosphere during cleaving, defined as the mechanical disruption of wave motions. Sulphate in the MBL is derived from the chemical process where sulphuric acid (H_2SO_4) is generated by oxidation of dimethyl sulphide, which is emitted by phytoplankton from the ocean surface (Raes, 1995; Detener *et al.,* 1996; Wolf *et al.,* 1997).

Marine aerosols affect the amount of solar energy absorbed by earth by both reflecting sunlight and influencing the cloud condensation nuclei (CCN) (Capaldo *et al.*, 1999). Due to the low concentration of CCN over the ocean, marine clouds have large droplets, which are relatively inefficient at scattering light (Pruppacher and Klett, 1980).

3.2.3 Anthropogenic or Industrial Sources

Anthropogenic or industrial emissions have long been recognized to play a major role in climate forcing (Mitchell *et al.,* 1995). Sources contributing large amounts of particulate matter to the atmosphere are electrical power stations, oil refineries, smaller factories and mine dumps and motor vehicles. Two types of aerosol are significant. They are: sulphate and black or elementary carbon (soot) (Haywood and Shine, 1995; Li, 1998). The presence of sulphate aerosols in the atmosphere is due to gas-to-particle conversion of gases that contain sulphur, where gas-to-particle conversion is defined as a process that builds up particles in the form of chains or aggregates. As a result, sulphuric acid and ammonium sulphates are produced. Soot is a by-product of fossil fuel burning (Haywood and Shine, 1995; Shaw, 1996; Connors *et al.,* 1991).

Studies that have been conducted on atmospheric sulphur and soot show that these aerosols enhance the planetary albedo and warm the atmosphere respectively (Haywood

and Shine, 1995; Li, 1998). From their study, Haywood and Shine (1995) estimate that sulphur produces a direct climate forcing between –0.28 to -1.3 Wm^{-2}.

3.2.4 Biomass Burning Sources

Biomass burning is undoubtedly a significant contributor of aerosols in the atmosphere. Biomass burning is both a natural and human induced phenomenon. Natural fires result from lighting strikes, while human induced fires result from land clearing for agricultural use, weed control and energy production for cooking and heating (Andreae, 1993; Levine, 1991; Meanut *et al.*, 1991).

Biomass burning emissions produce both solid and liquid particles of various shapes, sizes and chemical structure (Andreae, 1996; Lenoble, 1991). These particles contribute either directly or indirectly to the heat balance of the earth. The direct effect is caused by the scattering and absorption of sunlight by the particles themselves (Li., 1998). The indirect effect of aerosol particles on climate is caused by their interaction with clouds and their effect on cloud albedo (Twomey, 1977). In this process, aerosol particles act as cloud condensation nuclei. An increase in cloud condensation nuclei leads to an increase in cloud droplet concentrations. Since cloud albedo is determined by the cloud optical depth and is proportional to cloud droplet concentrations, that increase can make clouds more reflective of solar radiation (Andreae, 1988; Le Canut *et. al,* 1996; Russell *et al.*, 1999; Twomey, 1977).

According to Levine (1991), biomass burning has increased by about 50% since 1850. Human induced fires have made biomass burning the largest source of atmospheric trace gases and aerosols worldwide (Andreae, 1995; Levine, 1991; Woods *et al.*, 1991). Andreae (1995) pointed out that an area of 820 million ha is burned annually around the globe, resulting in the combustion of about 3400 to 3700Tg dm yr^{-1} (1Tg = 10^{12}g, dm: dry matter) of biomass. Emissions from savanna fires contribute significantly to atmospheric aerosols. About two-thirds of the world's savanna is found in Africa, and fires from African savannas account for about 75 percent of biomass burned annually

(Andreae, 1995; Piketh, 1996). African savannas are estimated to contribute 2000Tg dm yr^{-1} and the area exposed to fire each year is approximately 440 million ha (Hao, 1996).

3.3 The Effects of Particles in the Atmosphere

Atmospheric aerosols influence different atmospheric processes such as precipitation and radiative exchange, which in turn influence temperature and ozone concentration.

3.3.1 Aerosols and Precipitation

Aerosols play a major role in precipitation formation in the atmosphere. Under natural conditions, water droplets do not grow sufficiently under spontaneous nucleation of pure water if the atmosphere is subsaturated. Aerosols around which water droplets form are condensation aerosols which are formed when saturated or supersaturated vapors condense. These include Aitken and large nuclei. The condensation nuclei are able to form water droplets at low supersaturations. The larger the aerosols, the greater is their water solubility. The large aerosols have lower supersaturations than Aitken nuclei and hence serve as better condensation nuclei. Aerosol nuclei dissolve in water to form a solution droplet. The saturation vapor pressure of a solution droplet is less than that of a pure droplet, hence the solute effect enables them to grow at relative humidities that are lower than 100% (Boubel *et al.,* 1989; Preston Whyte and Tyson, 1988; Twomey, 1977).

Sulphate, nitrate, chloride and ammonium aerosols produced from industries allow condensation nuclei to form acid rain. Rain by nature is acidic, but the industrialized regions of Europe and North America often experience rainfall with very low pH values (Tyson *et al.*, 1988).

3.3.2 Aerosols and Radiative Exchange

Aerosols play an important role in climate and atmospheric chemistry on a global scale. The earth re-emits back to space the energy it absorbs in order to maintain an energy balance. Aerosol concentration in the atmosphere controls the amount of radiation intercepted, while the optical properties associated with size, shape and transparency of the aerosols determines whether the radiation is scattered, transmitted or absorbed (Russell *et al.,* 1999). The atmospheric energy balance will be unaltered if the aerosol particles are optically transparent. If aerosols are non-absorbing, but scatter or reflect radiation, they increase the albedo of the atmosphere and hence reduce the amount of solar radiation that reaches the earth's surface. On the other hand, absorbent aerosols will have the opposite effect. If aerosols absorb solar radiation, the upper atmosphere will be warmed, while the underlying surface remains cool. Aerosol's interaction with clouds and their effect on cloud albedo can make clouds more reflective of solar radiation (Twomey, 1977). The water droplets in clouds are very effective in reflecting solar energy back into space before it can become involved in the earth's atmospheric process. This ability of aerosols to change the path of the radiation through the atmosphere has the potential to change the earth's energy balance.

3.3.3 Aerosols and Temperature

The solar energy absorbed by the surface is used in part to heat the atmosphere and evaporate moisture (Twomey, 1977). Cloud reflectivity to solar radiation due to high aerosol concentration leads to less evaporation and a reduction in surface temperature. In an atmosphere with clouds, the heating rate is greatest at the cloud top and very small below the clouds (Andreae, 1995). This concept of a rapid earth's surface temperature decline due to aerosols has been used to explain the decline in global average temperature which occurred between 1940 and 1960 (Kemp, 1990). Lenoble (1991) observed a reduction in surface temperature between 1.5°C and 4°C as a result of smoke from a forest in Canada. The temperature in the mid-troposphere where smoke was concentrated increased by 2°C due to the absorption of radiation. During the 1982

eruption of El Chichon, high temperatures were observed in the stratosphere (Kemp, 1990). Engardt and Rodhe (1993) used a model to determine the effect of an increase in sulphate aerosol concentration over the industrial regions of Europe, North America and Asia from 1900 to 1980 and noted a marked cooling effect.

3.3.4 Aerosols and Ozone

Schoebel *et al.* (1993) and Chandra (1993) have measured a decline in ozone over the tropical and mid-latitude stratosphere. They have attributed a portion of this decrease to volcanic sulphate aerosols in the stratosphere that disturbs the radiation field, leading to a decrease in ozone. Large amounts of SO_2 released during the eruption react with OH to form sulphuric acid aerosols.

3.4 Distribution of Aerosols

3.4.1 Global Distribution of Aerosols

Aerosols do not spread across the globe as evenly as gases. Higher concentrations of aerosols tend to be found close to their sources. Two regions of high aerosol concentration exist, one at ground level and the other one in the lower stratosphere. Raindrops or gravitational fallout washes out large aerosols, whereas small aerosols can be coagulated and trapped by clouds. Only the very small aerosols can be injected into the stratosphere, besides the particles ejected by volcanic eruptions (Twomey, 1977).

Chandra (1993) and Cacciani *et al.* (1993) documented long distance transport of volcanic aerosols observed in the south pole from Mt. Pinatubo in Chile. Deshler and Hofman (1992) and Sheridan *et al.* (1992) observed 1 to 4km thick sulphate and carbonaceous aerosol layers at about 9 to 12km over Laramie, Wyoming. These aerosols were released to a height about 5km from the oil fires in Kuwait, transported by

the westerly winds to Central Asia, where they were convected to the upper troposphere and then transported by the jet stream to Laramie.

The global distribution of aerosol optical thickness derived from TOMS (Total Ozone Mapping Spectrometer) data is shown in Figure 3.2. High aerosol concentrations in India, China, Sahelian Africa and eastern South America which are most likely due to agricultural activities and desert dust storms. High concentrations of aerosols are also found in North America, western and eastern Europe and are associated with anthropogenic sources. Compared to Europe, there is less evidence of major aerosol production from anthropogenic sources in the Southern Hemisphere. Aerosol loading in the tropical atmosphere over the continents, particularly South America and Africa, is dominated by two main sources: production from forest vegetation and human-induced biomass burning.

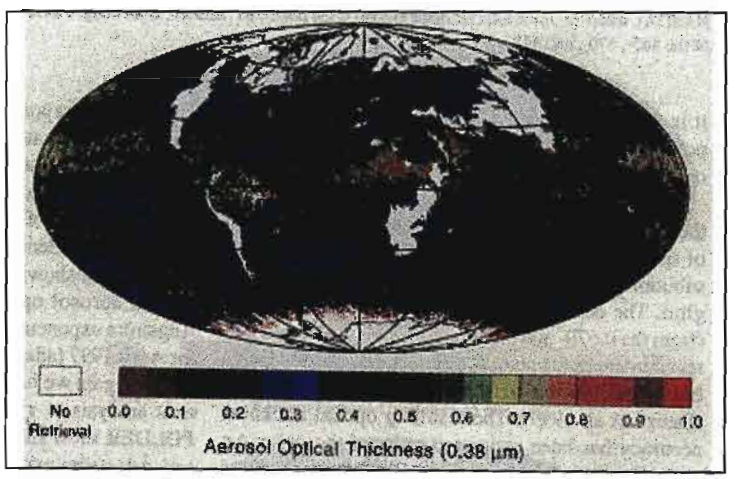

Figure 3.2: Aerosol optical thickness from TOMS data (0.38μm) in April 1997 (King, Kaufman, Tanre' and Nakajima, 1999).

3.4.2 Aerosol Distribution over Southern Africa

Atmospheric research on tropospheric aerosol properties south of the equator has increased in the last decade. The first and largest international experiment was the Southern African Fire-Atmosphere Research Initiative (SAFARI-92), which was a component of the STARE (Southern Tropical Atlantic Regional Experiment)

programme, conducted between August and October 1992. SAFARI-92 investigated the relationship between fires and savanna ecology and the atmospheric impacts of biomass burning emissions over southern Africa (Lindesay *et al.*, 1996). This experiment was conducted in the Kruger National Park, South Africa and some field sites in Namibia and Zimbabwe, in addition to aircraft campaign over the whole of southern Africa. From the studies of fire behavior, trace gas and aerosol emissions and their impact on atmospheric chemistry and the meteorology over this region, it was concluded that vegetation fires account for a substantial amount of photochemical oxidants and haze over southern African region and contribute strongly to the ozone balance in the remote atmosphere over the southern tropical Atlantic region (Hao *et al.*, 1996; Lindesay *et al.*, 1992, 1986; Thompson *et al.*, 1996).

A follow-up experiment to SAFARI-92 was the Southern African Atmosphere Research Initiative (SA'ARI-94) conducted during May 1994 (Helas *et al.*, 1996). SA'ARI-94 investigated the concentrations and physical characteristics of tropospheric aerosols and trace gases over southern Africa outside the biomass burning season (Helas, 1995). From SA'ARI-94, measurements indicated a persistent layer with an enhanced burden of trace components in the upper part of the mixed layer over most of the southern African subcontinent (Helas *et al.*, 1995). From June 1995 to January 1997 the Ben MacDhui High Altitude and Trace Gases Transport Experiment (BHATTEX) was undertaken (Piketh *et al.*, 1999). The results from BHATTEX highlighted the long-range aerosol transport patterns over South Africa. The most recent and ongoing experiment is the Aerosol Recirculation and Rainfall Experiment (ARREX) that has been initiated to investigate the physical and chemical properties of aerosols, their impact on cloud microphysics processes and their transport over the southern African region (Swap and Annegarn, 1999).

SAFARI-92 and SA'ARI-94 studies have emphasized the impact of biomass burning aerosol particles on climate. The contribution of biomass burning emissions to total aerosol loading has been found to be seasonal in South Africa (Le Canut *et al.*, 1996; Menaut *et al.*, 1996; Piketh *et al.*, 1999a and 1999b). The maximum concentration of biomass burning aerosols in the atmosphere occurs during the burning season, usually

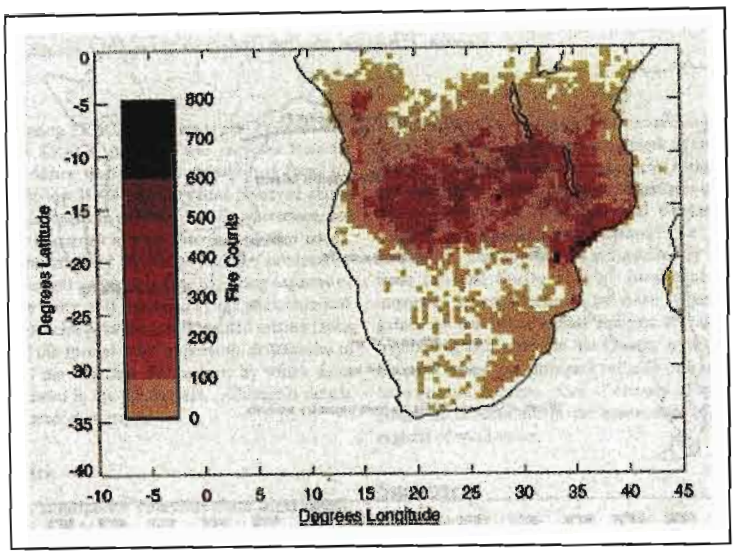

Figure 3.3: AVHRR depiction of fires over southern Africa for September-October (Fishman *et al.*,1996).

from August to October, in South Africa. Figure 3.3 illustrates the burning pattern during September-October, 1992 over southern Africa. Figure 3.4 shows the composite of active fires for the period August 16 to October 15, 1989 over central and southern Africa.

However, Piketh *et al.* (1999) argue that biomass burning is not the major source of tropospheric aerosols over South Africa and that mineral dust and industrial emissions contribute many more aerosols to the total atmospheric aerosol burden. Furthermore, Piketh (1999a and 1999b) found that soil-derived aerosols are the major contributors to aerosol loading in the dry winter periods over the plateau of South Africa. His studies showed that regardless of seasonal variations in aerosol composition, soil-derived aerosols dominate the composition of aerosol loading throughout the year. Along with soil-derived aerosols, the contribution of marine aerosols to aerosol loading has been found to be significant along the marine boundary layer in South Africa for both summer and winter (Piketh *et al.*, 1999a). The strong southwesterly winds in summer and northwesterly winds in winter along the west coast, ensure that marine aerosol contributes significantly to the total aerosol loading in South Africa (Piketh *et al.*, 1999a).

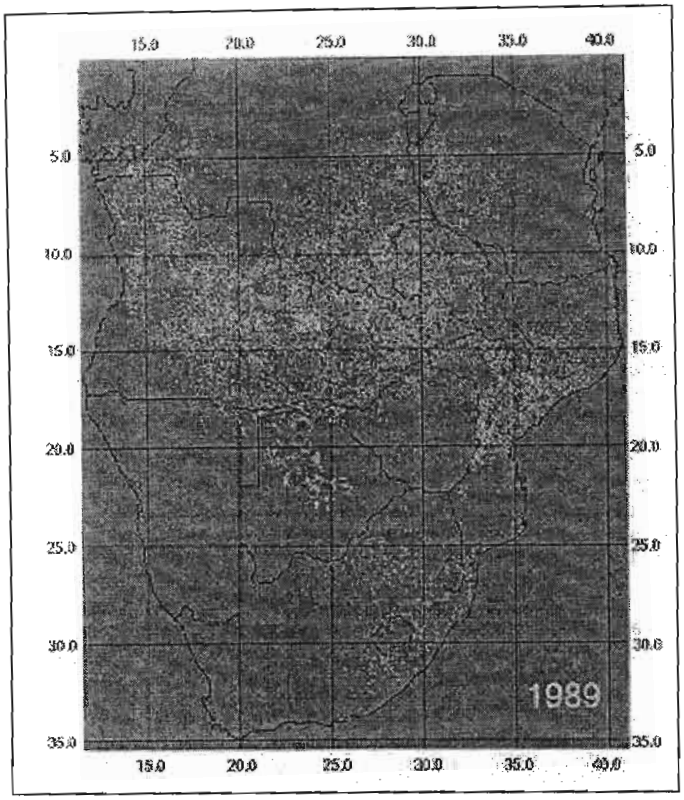

Figure 3.4: Composite of active fires detected for the period August 16 to October 15, 1989 (Justice *et al.*, 1996).

The sulphur aerosols derived from industries are very significant in aerosol research in South Africa due to the large industrial base in the Highveld region. Their contribution varies little throughout the year and the maximum loading is found in the fine fraction of the total aerosol concentration (Piketh *et al.*, 1999a and 1999b). Table 3.3 shows the estimated source concentration to the total (inorganic and organic) sampled atmospheric aerosol load from ten different sites in the southern African region from 1992 to 1997 (Piketh *et al.*, 1999)

After the success of SAFARI-92, SAFARI 2000 will build upon its scientific legacy, and identify the key linkages among the physical, chemical, biological and anthropogenic processes underpinning the functioning of the biogeophysical and biogeochemical systems of southern Africa (Swap and Annegarn, 1999). This initiative will act as a platform to explore and study the relationships between land-atmosphere processes, principally the biogenic, pyrogenic and anthropogenic emissions occurring in

this region. In addition, emission transport and transformations in the atmosphere, their influence on regional climate and meteorology, their eventual deposition and effects on the functioning of the eco-systems of this region will be considered (Swap and Annegarn, 1999).

Table 3.3: Estimated Source Concentrations to the Total (Inorganic and Organic) Sampled Atmospheric Aerosol Load.

Designation		Source			
		Aeolian Dust	Industrial	Biomass Burning	Marine
Site	Season	Mean Estimated Concentrations, $\mu g\ m^{-3}$			
Ben MacDhui	Summer	2.1	1.9	0.5	0.1
	Winter	3.2	0.9	0.8	0.2
Ulusaba	Summer	1.4	1.1	0.6	2
	Winter	6.6	1.8	1.6	0.5
Misty Mountain	Summer	1.2	0.5	1.0	0.4
	Winter	4.1	1.5	1.2	-
Elandsfontein	Summer	-	-	-	-
	Winter	8.9	1.5	1.2	-
Brand se Baai	Summer	0.5	0.7	-	2.1
	Winter	1.4	0.8	-	2.1

Source: Piketh et al., 1999.

Aerosols will be one of the core program elements of SAFARI 2000 (Swap and Annegarn, 1999). Several key issues related to aerosols will be investigated, such as:

1. Aerosol composition, concentration and source characterization.
2. Aerosol optical and radiative properties.
3. Aerosol deposition and resultant impacts on biogeochemistry.
4. Formation of secondary organic aerosols.

By exploring the relationship between and integrating the range of single-discipline studies on aerosols, SAFARI 2000 will produce a better understanding of the influence of the regional atmospheric dynamics on the functioning of southern and central African ecosystems (Swap and Annegarn, 1999).

CHAPTER 4

ATMOSPHERIC CIRCULATION AND WEATHER OVER SOUTH AFRICA

4.1. Introduction

The climate of South Africa is influenced by four main factors. These are: latitudinal position; distance from the sea and ocean currents; the presence of the escarpment and general atmospheric circulation. South Africa is located between 22°S to 35°S, and as such is situated approximately in the centre of the sub-tropical high pressure belt. Due to its latitudinal extent, this region is affected by weather systems prevailing in both the tropics to the north and the temperate latitudes to the south. Moreover, the region is also dominated by the sub-tropical high pressure cells centered at ~30°S (Fig. 4.1).

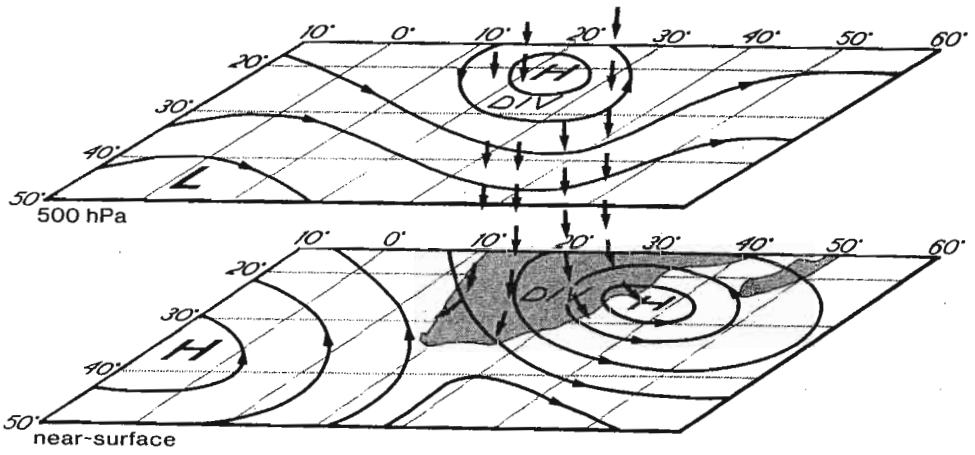

Figure 4.1: A schematic representation of the near surface and 500hPa fine-weather circulation associated with high pressure systems over southern Africa (after Preston-Whyte and Tyson, 1988).

The atmospheric circulation and weather phenomena over southern Africa have been examined extensively and are well documented (e.g. Tyson and Preston-Whyte, 2000; Swap and Tyson, 1999; Taljaard, 1953). The discussion in this chapter will concentrate

on those aspects of atmospheric circulation that are important for the dispersion of air pollutants in the southern Africa region, particularly on the east coast of South Africa. In essence, the topographic setting and the weather and climate of an area determine the air pollution climatology. Under favourable meteorological conditions, the atmosphere possesses a number of efficient mechanisms for the dispersion and removal of pollutants (Diab, 1975). At other times, particularly during the presence of inversions or stable layers and light winds, pollution tends to accumulate and concentrations rise. The dispersion of pollution generally consists of vertical motion that is governed by atmospheric stability and horizontal transport that is a function of wind speed and direction. Each of these will be discussed in turn.

4.2. Vertical Dispersion and Stability Characteristics

4.2.1 Atmospheric Stability

Vertical dispersion is a function of the buoyancy present in the atmosphere, being least under stable conditions and greatest under unstable conditions. Stability is defined by comparing the temperature lapse rate of the environment with the temperature of a rising or sinking parcel of air. Diab (1975) defined stability as a condition of equilibrium, where stable equilibrium is referred as a condition in which a mass of air, uplifted by some outside force, tends to return to its original position, and unstable equilibrium is referred to as a condition in which a mass of air given an upward or downward impetus will continue to rise or sink of its own accord.

When the temperature increases with elevation, the change of air temperature with height can be defined as an inversion. Surface based inversions are usually nocturnal features caused by the radiational loss of heat from the earth's surface. The development of strong inversions is favoured under calm and cloud-free conditions. Pollution emitted into the atmosphere below the top of a surface inversion becomes trapped and spreads horizontally because of the wind velocity and the atmospheric stability. High ground level pollution concentrations may occur, until the inversion is able to dissipate completely (Preston-Whyte and Diab, 1995).

Elevated inversions or upper air inversions are caused by large-scale subsidence of air or in association with frontal boundaries between air masses. This type of inversion occurs at different heights above the surface. The closer the inversion base to the surface, the greater the air pollution potential (Diab, 1995). Elevated inversions act as a barrier to the upward dispersion of pollutants by keeping the mixture of air and pollutants in a limited volume. Elevated inversions are known to be potentially more serious than surface inversions because they are not destroyed rapidly after sunrise (Diab, 1995). In general, inversions are often accompanied by low wind speed; hence there is limited horizontal and vertical dispersion during inversions. This upper limit to vertical mixing is termed the mixing height and the layer within which the mixing occurs is termed the mixing depth (Diab, 1975). Maximum mixing depths are a key indicator of the expected amount of vertical diffusion of pollution in the atmosphere. The maximum mixing depth varies during the day as well as from season to season.

4.2.2 Stability Structure over South Africa

The stability structure of the atmosphere over southern Africa has long been known to control the local accumulation and dispersion of atmospheric pollutants. Early work on the occurrence of surface and upper level inversions over South Africa was undertaken by Diab (1975), Tyson *et al.* (1979) and Preston-Whyte *et al.* (1977). More explicit links to pollution accumulation were discussed in papers by Diab (1976; 1978); Preston-Whyte, 1975; and Preston-Whyte and Diab (1980; 1995). More recently, the focus has been on the occurrence of absolutely stable layers rather than inversions. Stable layers are defined as layers where the environmental lapse rate is less than the saturated adiabatic lapse rate (Cosijn and Tyson, 1996).

Results from SAFARI-92 (Southern African Fire-Atmosphere Research Initiative) first reported the presence of stable discontinuities in the troposphere over southern Africa (Garstang *et al.*, 1996). During this study, it was noted that the vertical movement and horizontal transport of aerosols between the surface and the troposphere was governed more by these stable discontinuities. The presence of absolutely stable layers observed during the SAFARI period is illustrated in Figure 4.2.

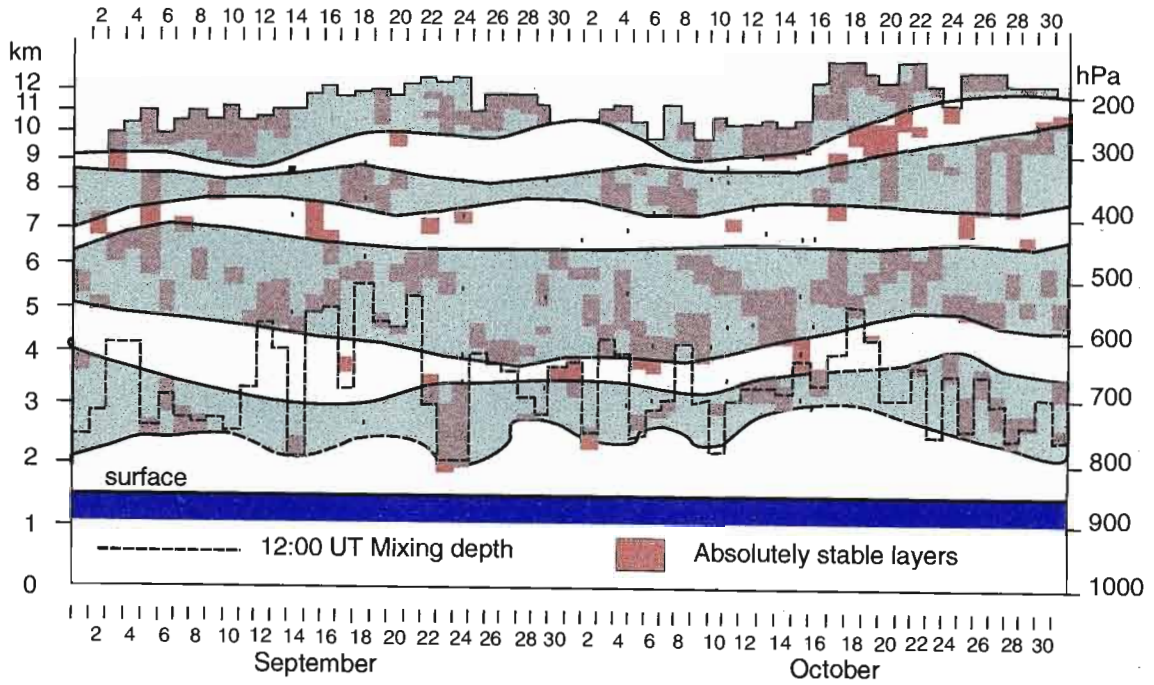

Figure 4.2: Absolutely stable layers at Pretoria during the SAFARI-92 period. The absolutely stable layers on each day are shaded (after Garstang *et al.*, 1996).

Subsequent analysis of data over a much longer time period, in fact 2925 fine-weather South African rawinsonde observations over the period 1986-1992, confirmed the presence of stable discontinuities (Cosijn and Tyson, 1996). Persistent layers at the 700, 500 and 300hPa levels, together with an additional layer based at the 850hPa level for the coastal area, were identified (Cosijn and Tyson, 1996). They were shown to be persistent throughout the year and under a variety of different circulation systems. On average, the layers were observed on about 3 out of 4 days in winter and on around 2 out of 3 days for the year as a whole over most of South Africa. According to Garstang *et al.* (1996) the stable layers are both spatially and temporarily persistent across the sub-continent. This result also corresponds well with the base levels of the first elevated inversions reported by Diab (1975) and Preston-Whyte *et al.* (1977). Figure 4.3 shows the occurrence of absolutely stable layers over South Africa.

The ~850, ~ 700 and ~500hPa absolutely stable layers vary slightly in mean base height and depth during the year (Cosijn and Tyson, 1996). According to Cosijn and Tyson

(1996), the ~850hPa stable layer has a mean base of 842hPa along the coastal areas, a mean depth of 51hPa and a 70% frequency of occurrence. In KwaZulu-Natal, this layer terminates against the Drakensberg escarpment creating a bounded airspace, referred to by Preston-Whyte (1990) as the Natal 'airshed'. Any pollution emitted into this fixed air space will remain until the stable layer dissipates. On the western coastal areas, this stable layer increases in height with distance from the sea and gradually merges with the ~700hPa layer.

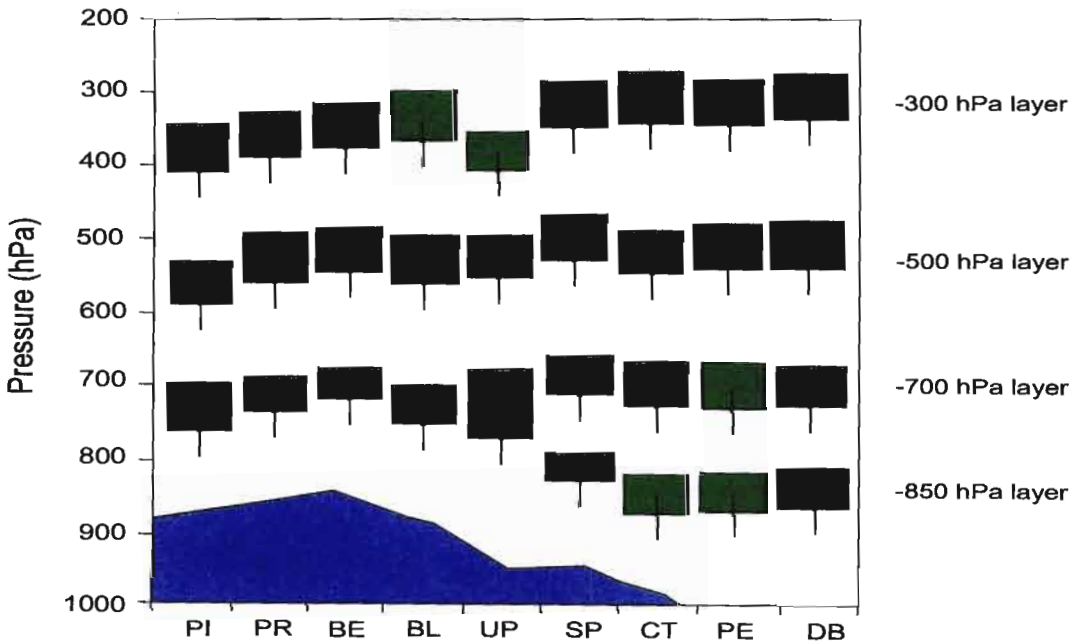

Figure 4.3: The occurrence of absolutely stable layers over South Africa, where absolutely stable layers are indicated by block shading (after Cosijn and Tyson, 1996).

The ~700hPa layer, varies in height between 720 and 700hPa, and is observed most frequently in winter. The mean depth of this layer is 57hPa with a 74% frequency of occurrence throughout the year (Cosijn and Tyson, 1996). This layer marks the top of the boundary layer and is disrupted frequently by the passage of westerly waves. Figure 4.4 shows the spatial extent of the ~700hPa stable layer over southern Africa on October 6, 1992.

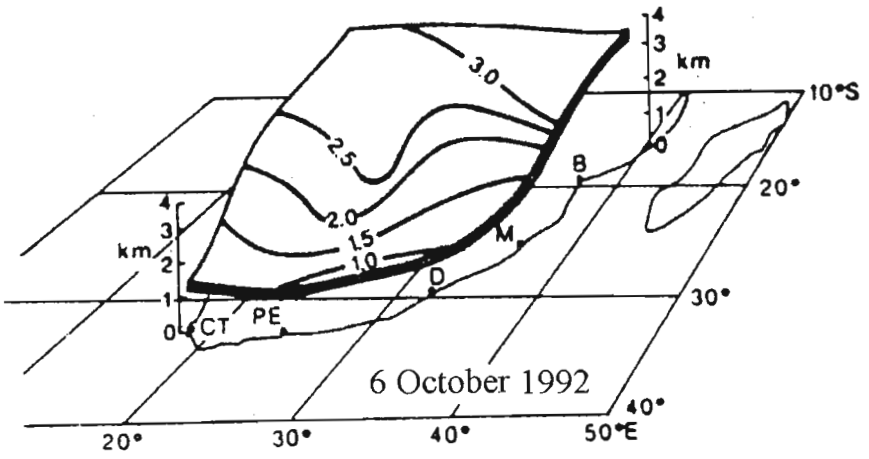

Figure 4.4: The spatial extent of the 3km absolutely stable layer over southern Africa on October 6, 1992 (after Garstang *et al.*, 1996).

The ~500hPa absolutely stable layer is the most persistent of all the layers and is the prime determinant of the haze layer over southern Africa. This layer varies little in base height over South Africa. The depth is around 65hPa and it has high frequency of occurrence (~80%). This layer is associated with subsidence in the subtropical anticyclonic circulation (Cosijn and Tyson, 1996). According to Swap and Tyson (1999), this stable layer is not easily or frequently disrupted, particularly in the winter half of the year, when it may prevail for about six weeks without a break. Over much of the year, surface derived dust, urban industrial pollution, biomass burning products and aerosols are trapped in a dust pall beneath the ~500hPa stable discontinuity to form the pronounced haze layer (Tyson and Preston-Whyte, 2000). This layer blankets the whole subcontinent from South Africa to northern Zambia and beyond during no-rain days, particularly during winter.

The highest upper tropospheric stable layer at ~300hPa has a frequency of occurrence of 85%, with an estimated depth of around 66hPa. However, the top of this layer grades into the stable layer associated with the tropopause, and as a result it is difficult to determine its actual depth. In general, this layer is very persistent and shows the largest seasonal change in height, being highest in winter and lowest in summer (Cosijn and Tyson, 1996).

4.2.3 Inversions and Mixing Depth Characteristics over South Africa

Anticyclonic circulation over South Africa and the clear skies produce favourable conditions for the development of surface inversions. The frequency and strength of surface inversions are highest in the winter season, particularly during June and July, under clear skies, lowered humidity and weak winds. Mean early morning winter surface inversions over this region generally vary between 3°- 11°C in strength and 100 - 400m in depth (Diab, 1975). Very strong surface winds and rainy conditions will prevent surface inversions developing at night (Preston-Whyte *et al.*, 1977). Surface inversions during summer and spring are neither as intense nor as deep as those in the winter season due to higher surface temperatures, greater wind speeds and the reduced period of nocturnal cooling (Tyson *et al.*, 1979). The frequency of surface inversions declines to less than 40% in spring when strong winds are common (Preston-Whyte and Diab, 1995).

Adiabatic warming of subsiding air in high-pressure systems is the primary cause of subsidence or elevated inversions over southern Africa (Preston-Whyte *et al.*, 1977). This inversion occurs over South Africa throughout the year, although it varies considerably in intensity and height above the surface, with a frequency in excess of 70% from August to December. Over KwaZulu-Natal, the mean base of the subsidence inversion occurs at about 1500m, with a mean depth between 400 and 500m and an average temperature intensity between 2 and 3°C (Diab, 1975). The subsidence inversion shows little diurnal variation and always caps the midday mixing layer (Tyson *et al.*, 1979). The height of the subsidence inversion is influenced by the passage of eastward moving weather producing systems, which cause the subsidence inversion to be situated closer to the surface ahead of frontal disturbances (Preston-Whyte and Diab, 1980). Frequently, the mixing depth does not reach the subsidence inversion, since the height of the midday winter mixing depth is about 1000m. Thus, it is likely that over time a trapping layer will develop beneath the subsidence inversion. The mixing depth varies in association with the passage of low-pressure systems along the coast. Usually the maximum mixing depth contracts beneath the lowered elevated inversion and expands immediately following the passage of the low. Generally, maximum midday

mixing depths vary between 1000m to 2000m above ground level in winter and may exceed 2500m in summer over the interior plateau (Diab, 1975).

4.3 Horizontal Transport over South Africa

The horizontal component of atmospheric dispersion is a function of wind speed and direction. The greater the wind speed, the greater the capacity of atmosphere to disperse pollutants and hence to decrease the pollutant concentrations. However, very strong winds may cause 'stack downdrafting' which can increase the ground level concentration of pollutants (Preston-Whyte and Diab, 1996). On the other hand, light wind speeds in a stable atmosphere can transport pollution for considerable distances from the sources of pollutants with little or no dispersion taking place. There is thus a direct relationship between wind speed and horizontal dispersion and an inverse relationship between wind speed and pollution concentration.

The nature of the transport and circulation over the southern African region has been reviewed in detail by Tyson *et al.* (1996). Cosijn and Tyson (1996) used four dominant circulation types to assess the variation in the stable layers with change in the circulation type. The four major circulation patterns, occurring with different frequencies throughout the year, are: semi-permanent sub-tropical continental anticyclonic circulation centred over the eastern part of South Africa, transient ridging anticyclones in the westerlies, barotropic semi-stationary easterly waves with trough lines over the western interior and travelling disturbances associated with baroclinic westerly waves and the passage of a cold front.

The semi-permanent south Atlantic anticyclone, the continental anticyclone over this region, and also south Indian anticyclone, have a dominating effect on all transport patterns of trace gases and aerosols. Stable layers at 500hPa and 850hPa over coastal areas appear to be of greatest significance in controlling both horizontal and vertical transport of pollutants.

Large-scale recirculation of air over this region occurs on a sub-continental and regional scale (Tyson *et al.*, 1996). Garstang *et al.* (1996) identified three major and dominant circulation types over southern Africa. These are: a combined continental and ridging anticyclone class, combined westerly waves/troughs and cutoff lows and easterly wave disturbances. Based on this study, Garstang *et al.* (1996) were able to highlight five different transport patterns for trace gases, particularly aerosols and ozone, in the atmosphere. Those are either direct easterly or westerly transport or westerly transport, easterly or westerly advection out of an initially anticyclonic circulation or anticyclonic recirculation (Fig. 4.5). These have subsequently been summarised into two major pathways: the Natal plume to the east and the Angolan plume to the west. There is also substantial recirculation of air over the subcontinent. Recirculation produces complex atmospheric chemistry in terms of mixing of different air masses from marine, biomass burning, crustal and industrial sources (Tyson *et al.*, 1996; Tyson *et al.*, 1999).

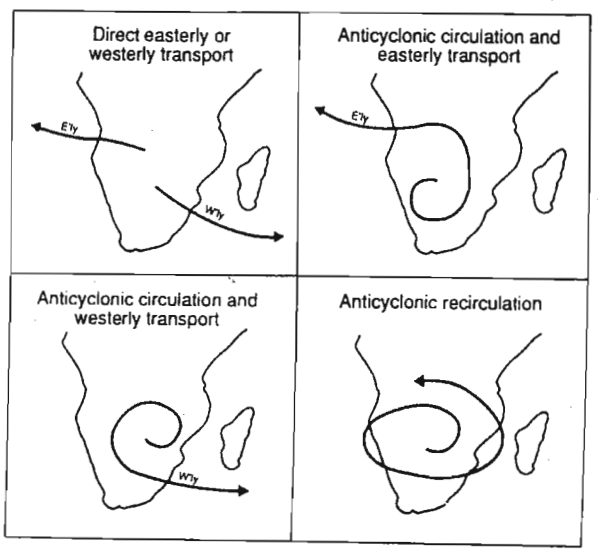

Figure 4.5: Schematic representation of major low-level transport trajectory modes likely to result in easterly or westerly exiting of material from southern Africa or in recirculation over the subcontinent (after Garstang *et al.*, 1996).

The dominant anticyclonic circulation over the subcontinent is responsible for inhibiting the dispersion of pollutants in the troposphere. The troposphere becomes stratified and pollutants are retained in the lower part of atmosphere. After the recirculation and

accumulation of the pollutants the material can be ejected either via the Angolan plume to the Atlantic Ocean or via the Natal plume to the Indian Ocean. Recirculated air moves into this region from the west at lower levels than the direct transport to the east via the Natal plume. However, air moves from the west at a higher level than the direct transport to the west via Angolan plume (Tyson *et al.*, 1996). Figure 4.6 shows the generalised atmospheric transport pathways over southern Africa.

Figure 4.6: A schematic representation of dominant transport pathways over southern Africa, the southern African plume to the Indian Ocean and recirculation pathways (after Tyson and Preston-Whyte, 2000).

4.4 Influence of Synoptic Weather on Stability Characteristics and Transport Patterns

The goal of synoptic climatology is to identify the relationship between the atmospheric circulation over a region and local climate. The synoptic features influencing transport of trace gases over this region have been reviewed in detail by Tyson *et al.* (1996). Synoptic-scale influences are particularly evident on the east coast when a coastal low moves north-eastward along the Natal coast, followed by a south-westerly flow.

Diab *et al.* (1991) identified three distinct synoptic categories for the KwaZulu-Natal region, each with different effects on the accumulation or dispersion of pollution. These

are the established high-pressure system, the pre-frontal situation and the post-frontal situation.

4.4.1 Established High Pressure System

Under this high-pressure condition, the weather is typically fine with clear skies, low wind speed and no rainfall. Because of the existence of an upper air subsidence inversion, this situation is characterised by low mixing depths (Diab and Preston-Whyte, 1995). Cloudless skies also favour the development of nocturnal surface inversions. Thus, there is great stability and very little vertical dispersion is possible. As a result, due to the poor dispersion capacity of the atmosphere, air pollution potential is moderate to high. Pollution becomes trapped below the subsiding air and within the surface inversion. Figure 4.7 shows the first synoptic situation, the established high-pressure system.

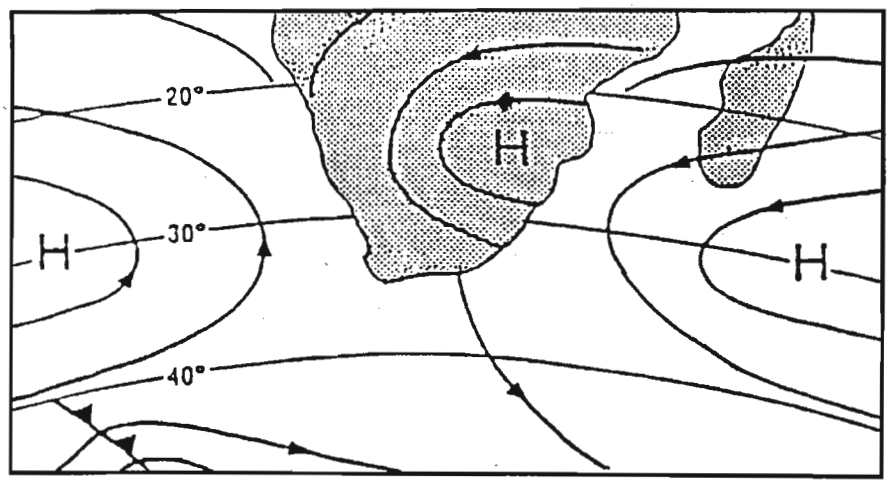

Figure 4.7: Established high-pressure system (after Diab and Preston-Whyte, 1995).

4.4.2 Pre-frontal System

This situation occurs just prior to the passage of a coastal low or cold front and is associated with a north-easterly wind direction. Under this situation, the air pollution potential is high due to the dipping of the subsidence inversion towards the surface (Diab and Preston-Whyte, 1995).

The coastal low is associated with uplift and general instability causing drizzle and mist, with warm offshore flow of air ahead and cool onshore flow behind the low pressure cell. In winter, the prefrontal situation is sometimes characterised by Berg winds. They blow from the interior towards the coast and are characterised by high positive temperature departures caused by general subsidence and by additional adiabatic heating of dry air descending from the plateau to coast (Preston-Whyte and Tyson, 1988). Berg winds can blow for several days or only a few hours and are associated with poor atmospheric dispersal and high air pollution potential. Figure 4.8 shows the second synoptic regime, the pre-frontal condition.

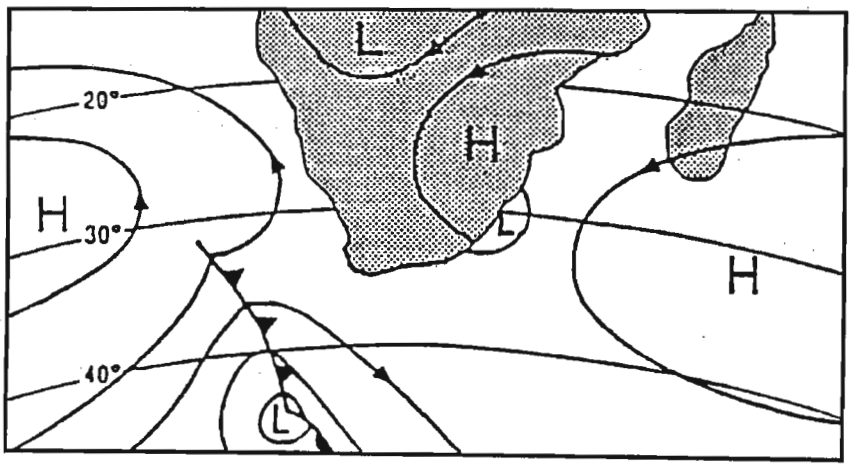

Figure 4.8: Pre-frontal conditions (after Diab and Preston-Whyte, 1995).

4.4.3 Post-frontal System

This situation occurs after the passage of the cold front and is characterised by moderate to strong south-westerly winds. The subsidence inversion is either lifted or dissipated completely. This situation creates unstable air with cloud cover and precipitation. The combination of rain along with the rapid dispersion of pollutants gives rise to low air pollution potential conditions. Figure 4.9 shows the final synoptic regime, the post-frontal condition.

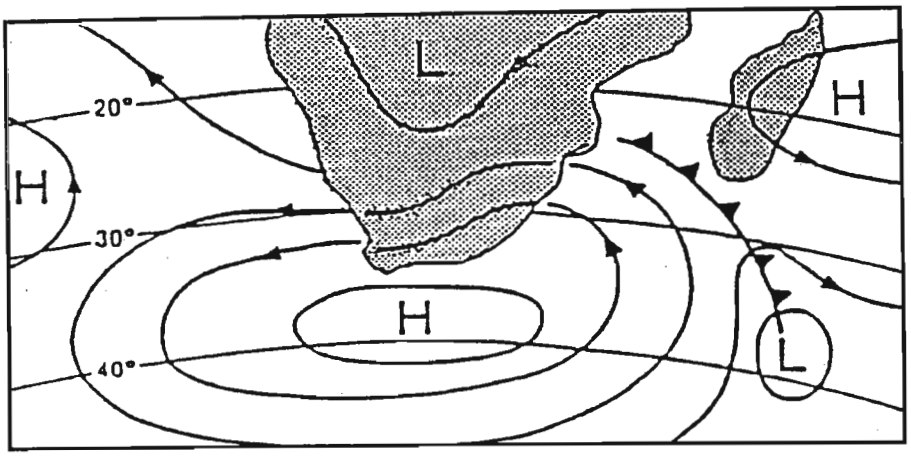

Figure 4.9: Post-frontal conditions (after Diab and Preston-Whyte, 1995).

4.5 Mesoscale Circulation

Mesoscale circulation systems such as land and sea breezes and topographically induced winds, including the regional mountain-plain and plain-mountain wind systems, are important controlling factors on atmospheric pollution dispersion over KwaZulu-Natal. Whilst the influence of these mesoscale wind systems is predominantly confined to the boundary layer, their influence at a larger scale is experienced through their role in recirculating pollutants in the boundary layer leading to greater accumulation. When suitable synoptic weather situations prevail, contaminated boundary layer air is then moved to higher levels in the atmosphere. Differences in wind velocity and stability govern the horizontal transport and vertical movement of atmospheric pollutants.

4.5.1 Land-Sea Breezes

Most of the work on land and sea breezes was undertaken in the 1960s and 1970s by Preston-Whyte (e.g. Preston-Whyte, 1968; 1969; 1970; 1974; Preston-Whyte *et al.*, 1977; 1980 and 1988).

Land breezes are best developed under calm, cloudless anticyclonic conditions which dominate during the winter months. This stable, offshore north-westerly flow creates an ideal situation for the transportation of pollutants. As a result, contaminated air is

moved seawards by the land breeze at night and the pollutants can be carried a considerable distance from the source and then returned to the land the following morning by the returning sea breeze (Preston-Whyte, 1970).

Sea breezes strengthen the prevailing north-easterly gradient winds, which are associated with the South-Indian anticyclonic circulation over the Agulhas Current, and favour the dispersion of pollutants under unstable atmospheric conditions (Diab, 1995). Sea breezes are known to move pollutants generated at the coast around 60km inland (Preston-Whyte, 1969; Tyson and Preston-Whyte, 2000). Although the sea breeze is a stronger circulation than the land breeze, the land breezes combines with regional topographically induced mountain-plain winds to produce a deeper and more significant wind system.

4.5.2 Mountain-plain and Plain-mountain winds

Mountain-plain winds, which are essentially non-turbulent winds, occur on a much larger scale together with the land-sea breezes as the part of the local circulations over KwaZulu-Natal. This wind blows away from the Drakensberg towards the coastline at night. It is dominant and strongest in winter when cooling effects are most pronounced (Preston-Whyte, 1988). Together with the land breeze, the mountain-plain wind produces a very stable layer (Diab and Preston-Whyte, 1995). Such conditions may cause pollutants, such as aerosols and trace gases, to be carried over distances up to 200km or more toward the coast with little dispersion occurring due to the stable conditions prevailing. However, during the day, the reverse transport occurs and allows pollutants to be recirculated over the land by the plain-mountain winds (Diab and Preston-Whyte, 1995; Tyson and Preston-Whyte, 2000) (Fig. 4.10).

Plain-mountain winds produce an opposite flow and are associated with instability. They develop during the day and blow toward the interior, but are not well developed due to the presence of dominant synoptic winds during the day (Diab and Preston-Whyte, 1995). Pollutants emitted into the Natal 'airshed' can be transported seaward by

mountain-plain winds and landwards by plain-mountain winds (Diab and Preston-Whyte, 1995) (Fig. 4.11).

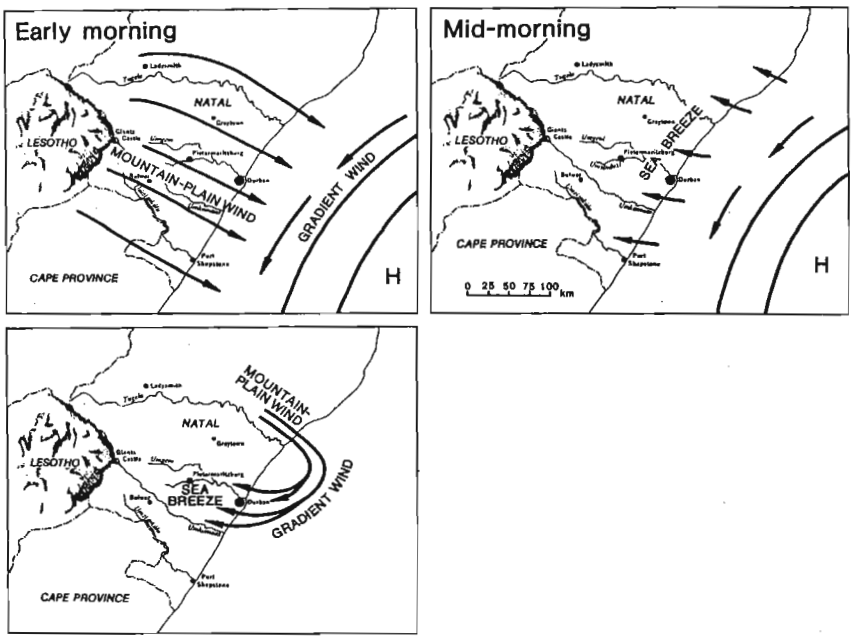

Figure 4.10: Recirculation of pollution by early morning and gradient winds over KwaZulu-Natal (after Preston-Whyte and Tyson, 1988).

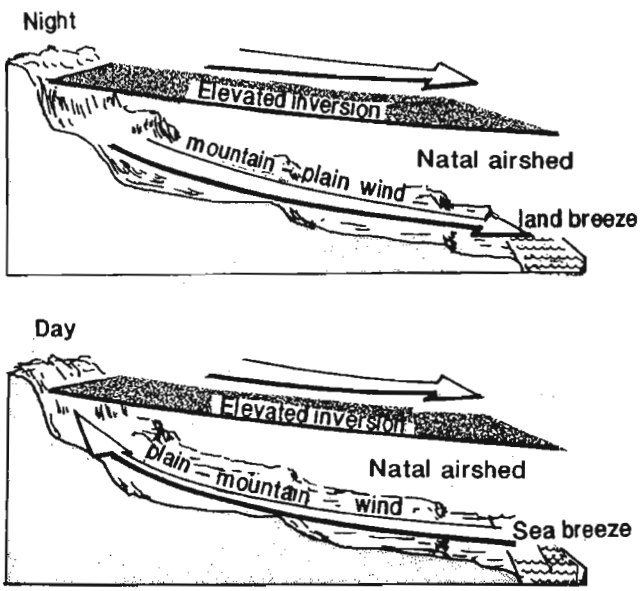

Figure 4.11: The KwaZulu-Natal 'airshed' contained by the Drakensberg escarpment to the west and an elevated inversion above (after Preston-Whyte, 1990).

*****

As mentioned earlier, this region is more or less in the centre of the sub-tropical high pressure belt. The presence of high pressure over this region can be stated as the rule rather than the exception. Such anticyclonic conditions facilitate the formation of absolutely stable layers in the atmosphere (Tyson *et al.*, 1996).

The most prominent stable layer at 500hPa act as a barrier to the vertical transport and dispersal of trace gases. Recirculation has the major influence on the transport patterns of trace gases and aerosols over the sub-continent. During the process of recirculation, trace gases and aerosols are trapped beneath absolutely stable layers over South Africa. When westerly or easterly winds occur, pollutants may move as far as Amsterdam Island (5000km to the south-east) and Ascension Island (4000km to the north-west) respectively (Tyson *et al.*, 1996).

CHAPTER 5

DATA PRESENTATION AND ANALYSIS

5.1 Introduction

As mentioned earlier, the objective of this study is to investigate the vertical distribution of aerosols in relation to atmospheric stability structure and horizontal transport of air masses. In addition, the influence of synoptic weather conditions and related meteorological variables, such as wind speed and direction and surface pressure will be studied. In this chapter, six case studies of the vertical distribution of aerosols will be analysed. The results are plotted as aerosol profiles, where the values on the y-axis represent height (km) and the values on the x-axis represent the number of aerosol particles (number of counts recorded by the photomultiplier). Absolutely stable layers as determined from the radiosonde data have been superimposed on each profile. Accompanying each profile is the relevant surface synoptic weather chart, surface wind and pressure variations, the vertical wind profile and 10-day back trajectory analyses. The results are presented first as case studies and thereafter are combined to highlight the major features.

5.2 Characteristics of Vertical Distribution and Horizontal Transport Patterns of Aerosols

5.2.1 Case Study 1 (July 3, 1997)

The aerosol profile presented in Figure 5.1a shows a sharp discontinuity in aerosol concentrations at 5km. Relatively high aerosol concentrations are found in the lower layer, with the highest aerosol concentrations occurring at 4km. This lower layer is characterised by marked stratification, with photon counts varying between approximately 100 and 250 photons. The atmosphere is comparatively clean between 5

and 10km, after which aerosol concentrations increase with height to a photon count of ~100.

Absolutely stable layers are observed at approximately 1, 3 and 5km (Fig. 5.1a). Aerosol peaks are noted to occur in the intervening layers, being trapped by the stable layers above and below.

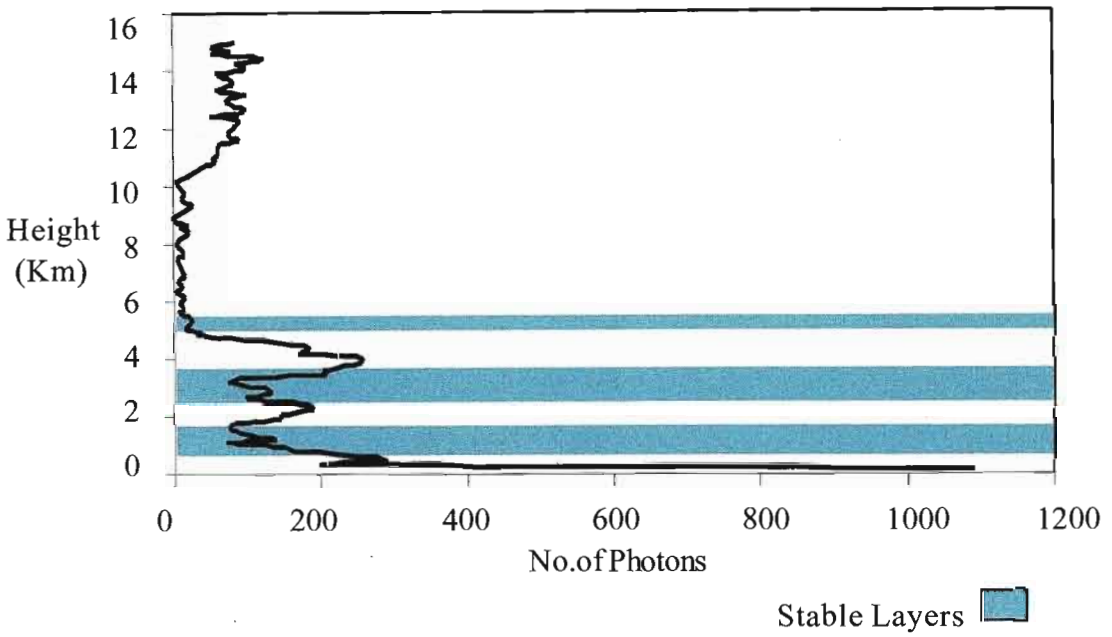

Figure 5.1a: Aerosol Profile for July 3, 1997. The occurrence of absolutely stable layers is indicated by shading.

Large scale circulation over southern Africa on this day is shown in Figure 5.1b. The circulation is anticyclonic and is characterised by light surface winds (generally less than $4ms^{-1}$). At night surface winds are NW, blowing from the interior to the coast as expected, and during the day they back to NE (Fig. 5.1c). Wind speeds in the 5-10km layer are relatively stronger than at other levels (Fig. 5.1e), which could be a factor contributing to the low aerosol concentrations detected in that layer. Speeds peak at $25ms^{-1}$ at 10km.

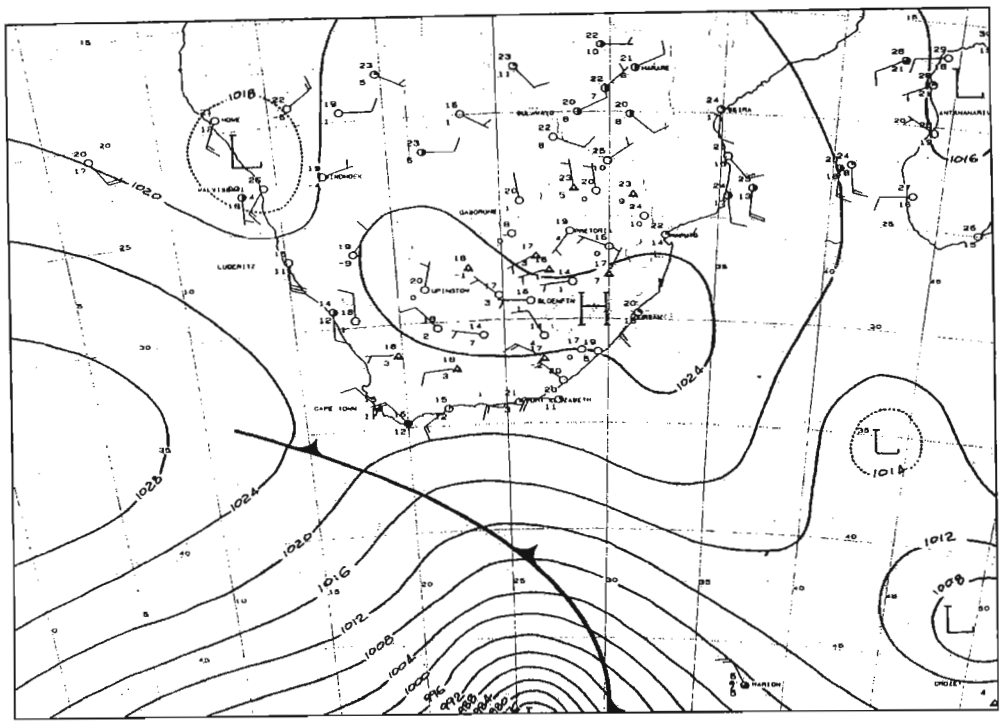

Figure 5.1b: Surface synoptic chart over southern Africa generated at 14:00 (Daily Weather Bulletin, SAWB) showing the circulation patterns for July 3, 1997.

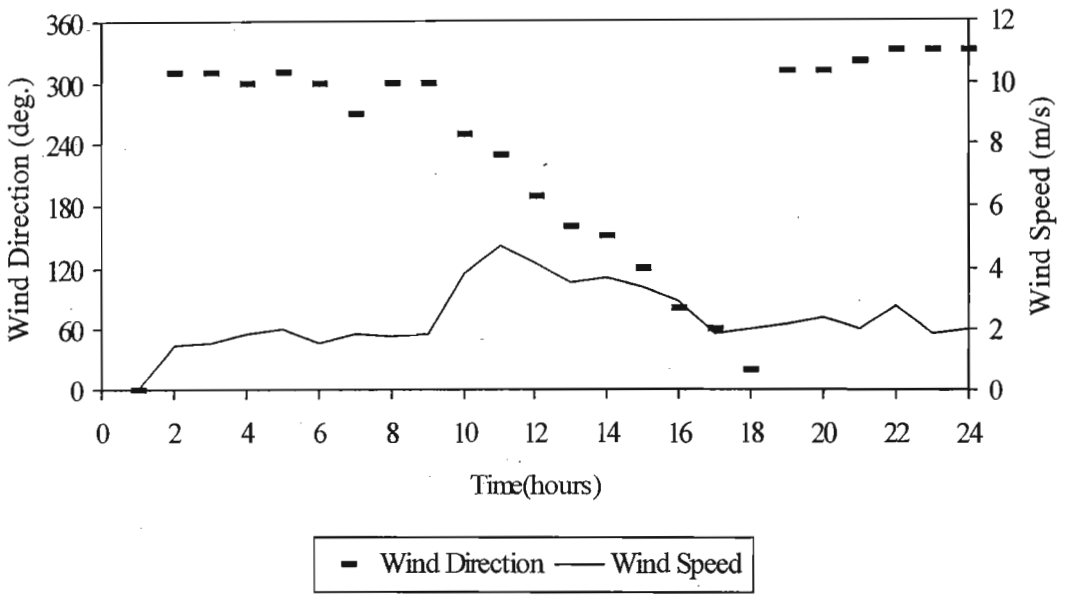

Figure 5.1c: Surface wind speed and direction for July 3, 1997.

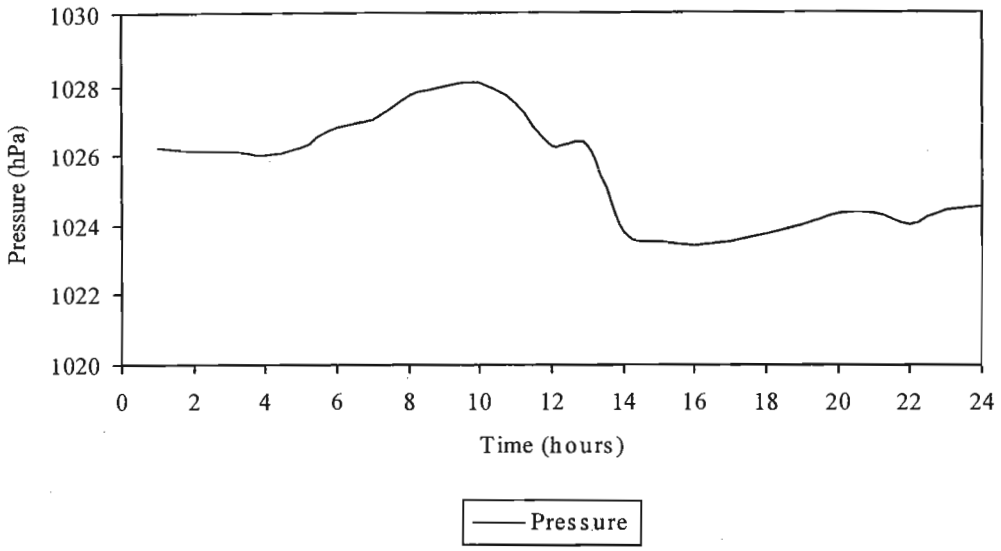

Figure 5.1d: Surface pressure for July 3, 1997.

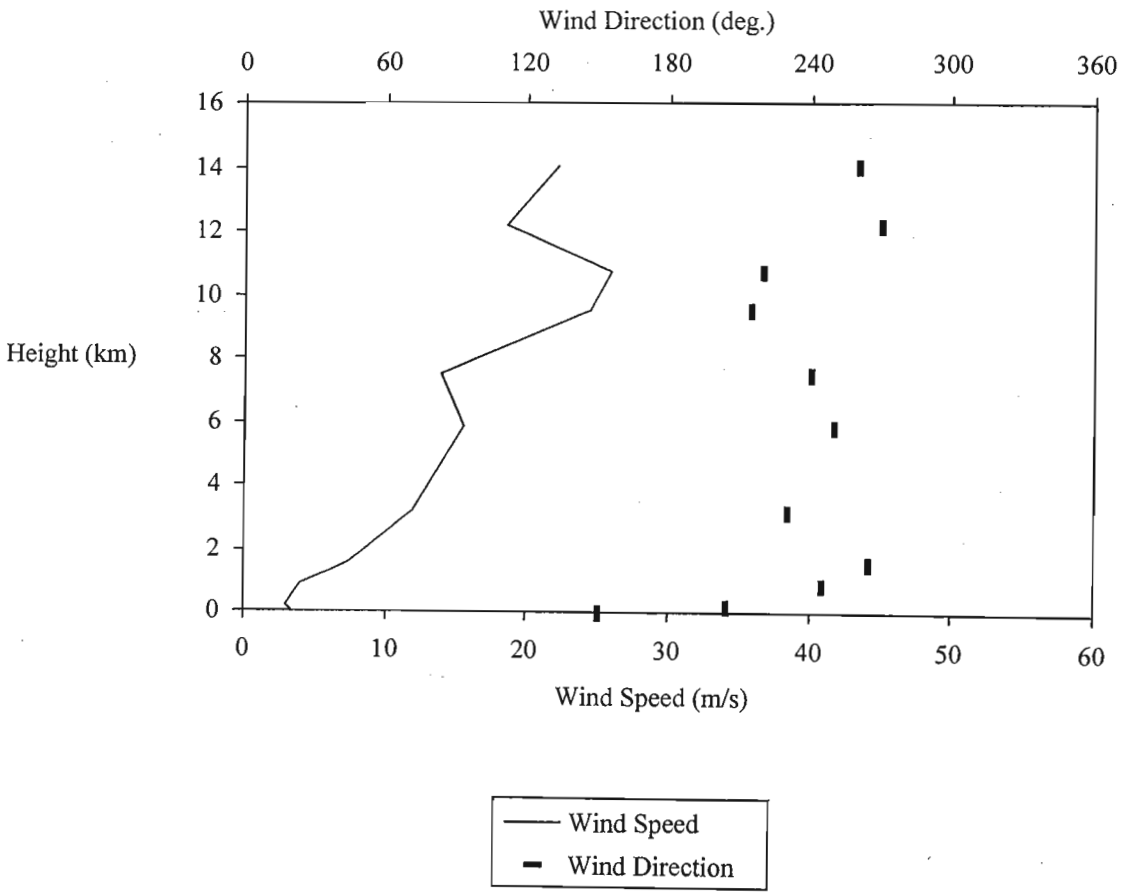

Figure 5.1e: Vertical wind profile on July 3, 1997.

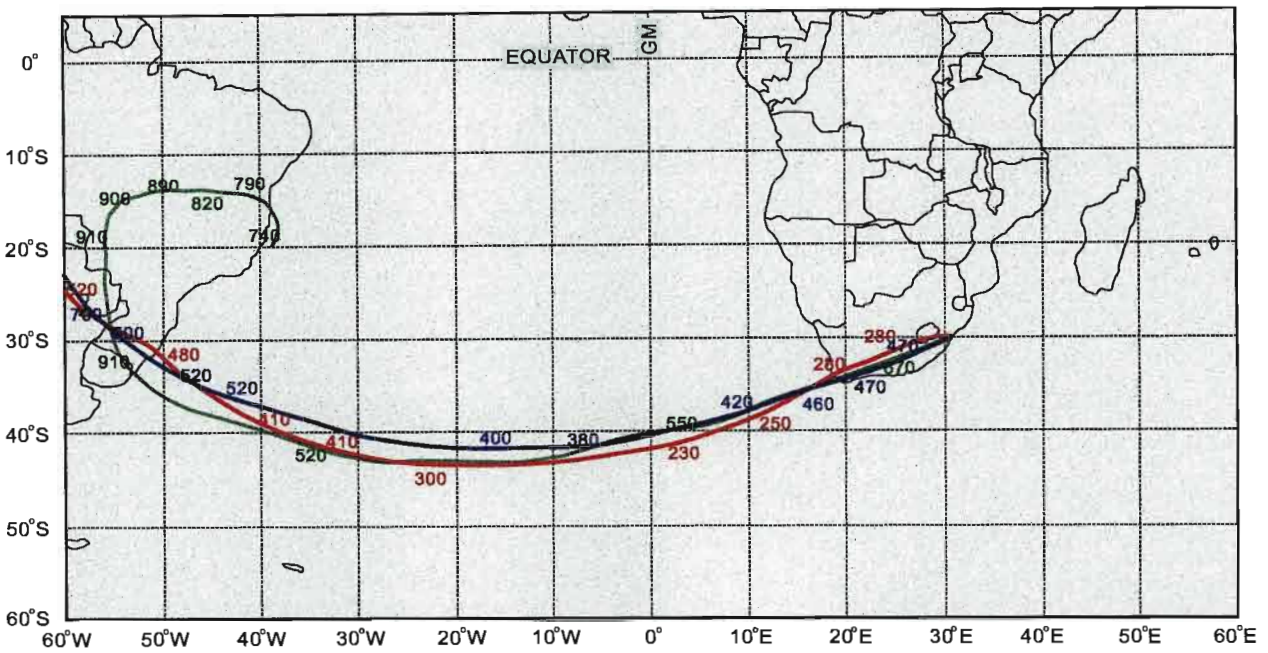

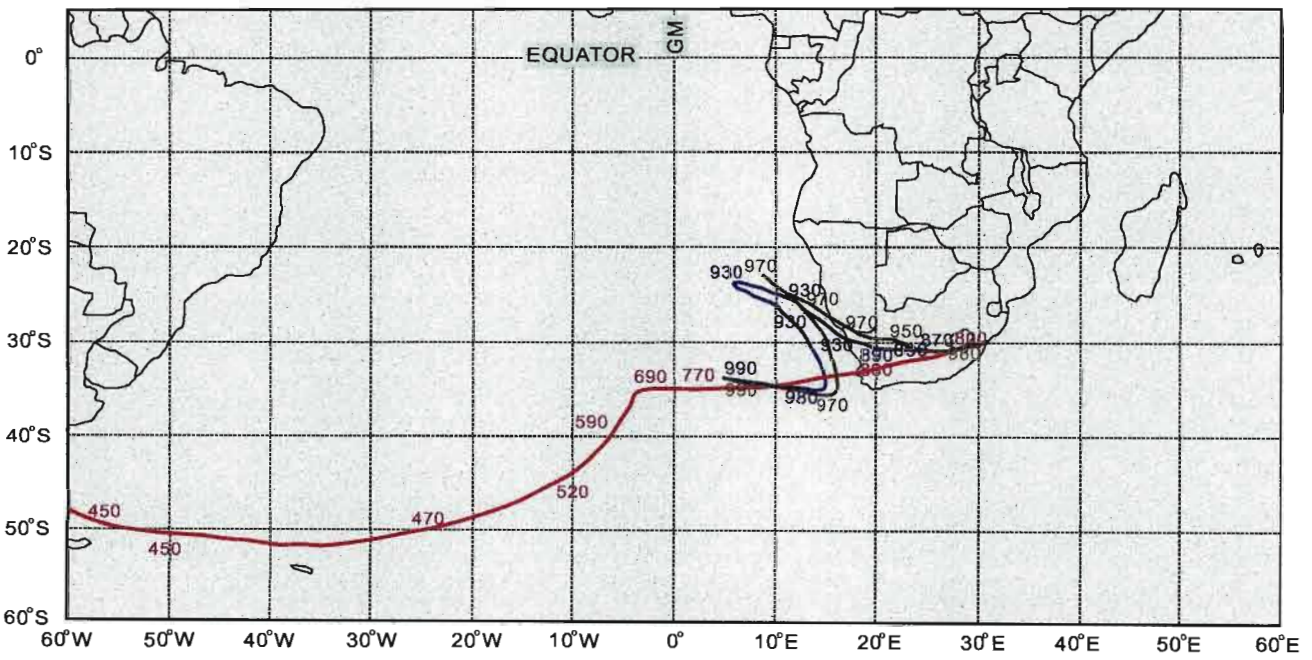

Figure 5.1f: Ten-day Backward Trajectories for July 3, 1997.

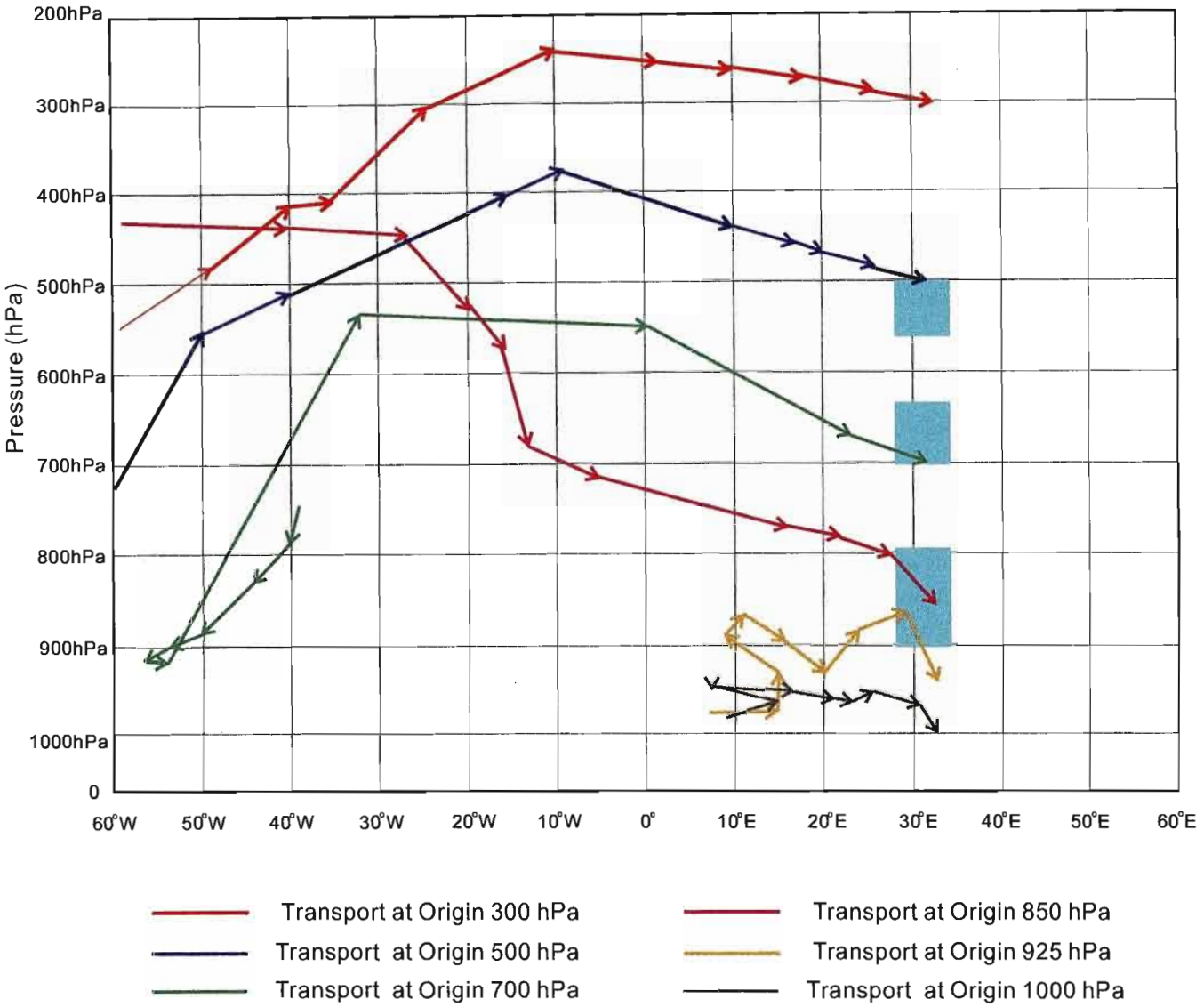

Figure 5.1g: Vertical cross-section showing transport of aerosols originating at selected pressure levels. The occurence of absolutely stable layers is indicated by shading for July3,1997.

Figure 5.1f shows the backward trajectories from Durban at selected pressure levels. The origin of air masses at the 300, 500, 700 and 850hPa levels was from South America, whereas those at 925 and 1000hPa originated in the South Atlantic Ocean approximately 1600km off the coast of southern Africa. It is evident that there was a northward movement up the coast, followed by a return movement over the continent towards the SE.

Figure 5.1g shows the back trajectories plotted as a function of height. After exiting South America air parcels at 300, 500 and 700hPa are lifted vertically, possibly in the strong convective activity found at these latitudes. The 700hPa trajectory displays initial subsidence and anticyclonic turning before being entrained into the convective uplift that characterise the region. At approximately 10°W and further south of their original location (40°S) they encounter the region of anticyclonic subsidence and sink over the South Atlantic Ocean and adjacent subcontinent. Back trajectories at the lower layers (925 and 1000hPa) exhibited very little vertical movement and much less horizontal transport due to the lower wind speeds. The 1000hPa back trajectory in particular was trapped below the first stable layer.

Comparing Figures 5.1a, f and g, it is evident that, the aerosol peak just below the first stable layer is due to transport of marine aerosols from the South Atlantic Ocean combined with aerosols generated over the continental areas and transported to Durban at the 1000 and 925hPa levels. The aerosol peaks 2km and 4km are due either to the high aerosol loading of the maritime air masses or to aerosols that originated over South America. Uplift in convective storms could be responsible for transporting surface generated aerosols, most likely from biomass burning, to the upper levels where they are transported long distance areas over the Atlantic Ocean. Above 5km the low aerosol loading of the atmosphere is clearly a function of the stability structure of the atmosphere rather than the origin of trajectories. Both 500 and 300hPa trajectories are very similar, yet above 5km (~500hPa) the atmosphere is very clean. The high aerosol loading in the lower atmosphere is a function of recirculation and trapping by the stable layers.

5.2.2 Case Study 2 (July 23, 1997)

The aerosol profile of the second case study (Fig. 5.2a) shows a similar sharp discontinuity at 5km to that observed in the first case study (Fig. 5.1a). Aerosol concentrations in the lower layer are characterised by marked stratification and slightly higher concentrations, varying from photon counts of 180 to 350. Above 5km, aerosol concentrations increased gradually with height, to about 150 photons.

Four absolutely stable layers were present at ~1, 3, 4.5 and 7km (Fig. 5.2a). The deepest and strongest layer coincided with the discontinuity in the aerosol profile. Peak aerosol concentrations occurred in the intervening layers between the stable layers.

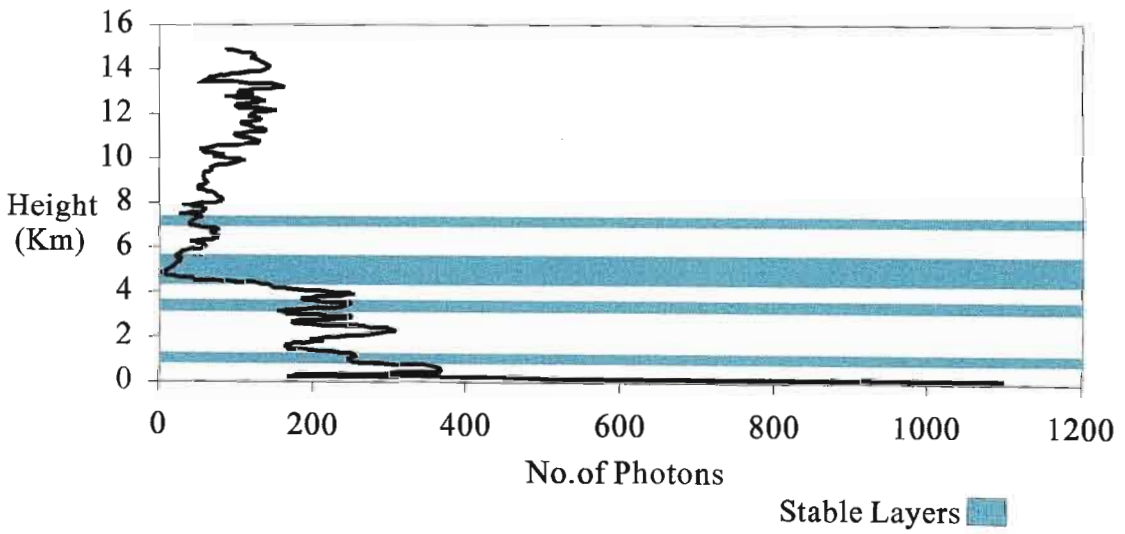

Figure 5.2a: Aerosol Profile for July 23, 1997. The occurrence of absolutely stable layers is indicated by shading.

The surface synoptic chart (Fig. 5.2b) shows that fine and mild to warm weather conditions prevailed over the northern and eastern regions of South Africa. The frontal system was moving in a northeasterly direction from Cape Town. Temperatures along the coast were higher than the previous case study. A typical diurnal pattern in surface wind direction is noted with NW winds prevailing during the night (land breeze) and NE winds during the day (large scale anticyclonic gradient flow and sea breeze) (Fig. 5.2c). Wind speeds in the lower troposphere were very light (Fig. 5.2e), most likely contributing towards the high aerosol concentrations in this layer.

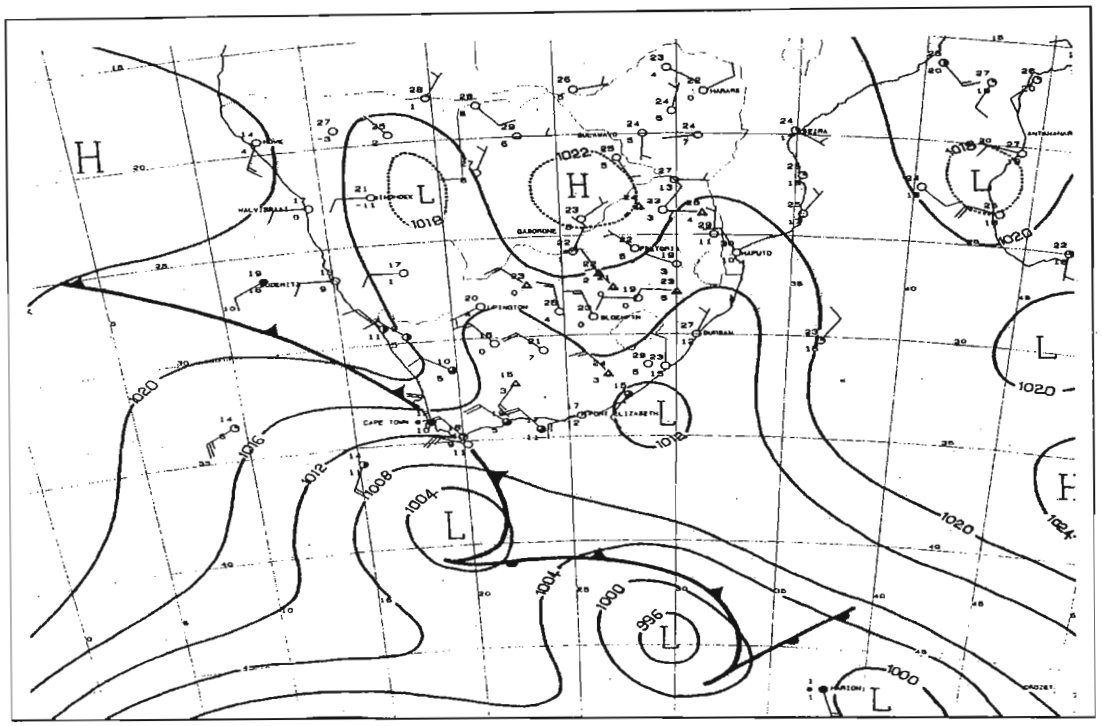

Figure 5.2b: Surface synoptic chart over southern Africa generated at 14:00 (Daily Weather Bulletin, SAWB) showing the circulation patterns for July 23, 1997.

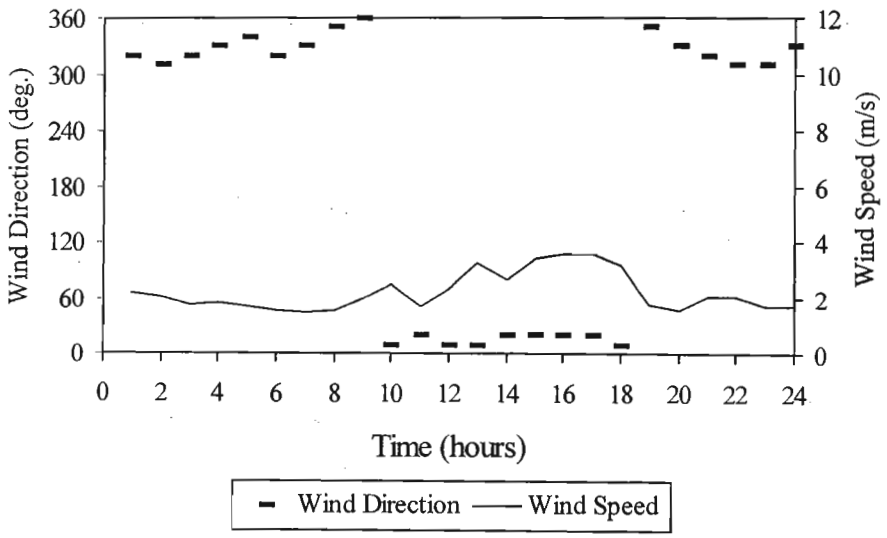

Figure 5.2c: Surface wind speed and direction for July 23, 1997.

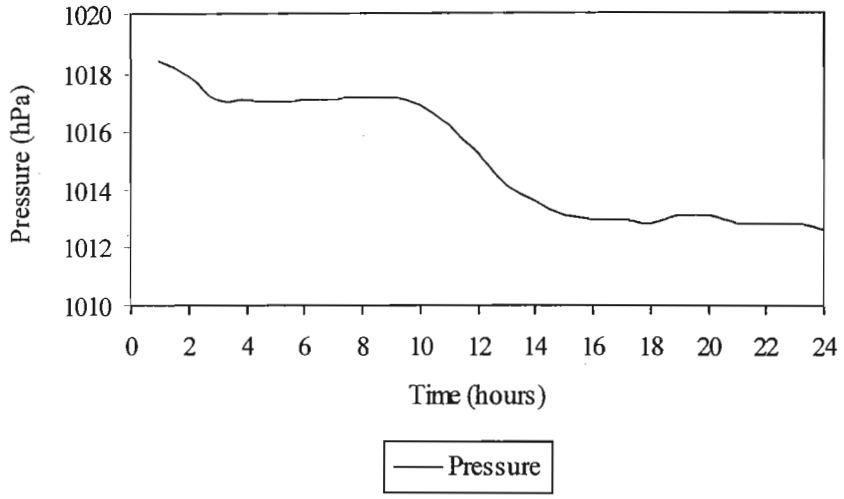

Figure 5.2d: Surface pressure for July 23, 1997.

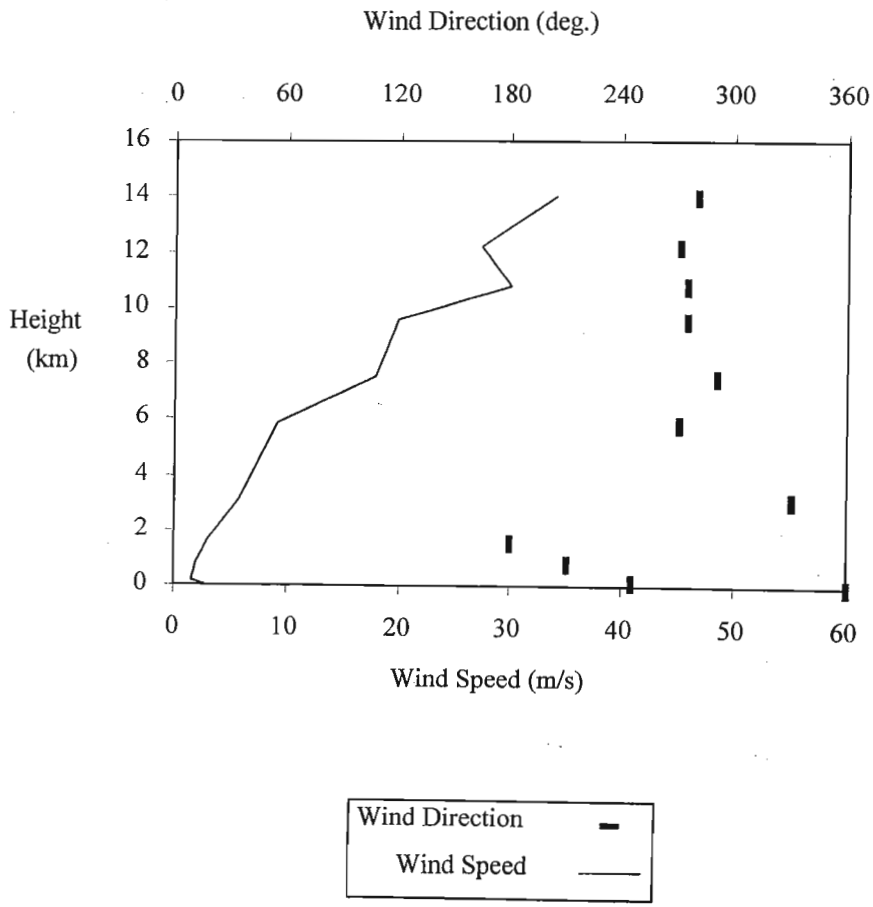

Figure 5.2e: Vertical wind profile on July 23, 1997.

It can be seen from Figure 5.2f that in the mid-troposphere, the 300, 500 and 700hPa level trajectories originated from a due westerly direction over South America, while trajectories between 850 and 1000hPa originated at higher latitudes to the south-west of the African subcontinent. However, there was an anticyclonic turning of these latter trajectories near the continent, such that they approached Durban from a NE direction.

Figure 5.2g shows the back trajectories as a function of height, and indicates westward transport at 850, 925 and 1000hPa and eastward transport at 300, 500 and 700hPa. The recurving air moving in from the east at a low level is constrained by the stable layer situated between 900 and 850hPa. Again, the presence of stable layers caused the air to sink as it entered into the stable atmospheric situation. In the upper layer (700–300hPa), the trajectories are initially characterised by rising motion, followed by sinking motion from about 10°E. Those trajectories originating further south (1000-850hPa) exhibit sinking motion characteristic of the anticyclonic circulation at those latitudes.

From a comparison of Figures 5.2a, f and g, it is clear that low level aerosol peaks (<1km and 2km) are due to transport of marine aerosols from the Indian Ocean. There is also a possibility that continentally derived aerosols that were transported offshore is the Natal plume that is known to exist (Tyson *et al.*, 1996) could be recirculated ahead of the passage of the cold front.

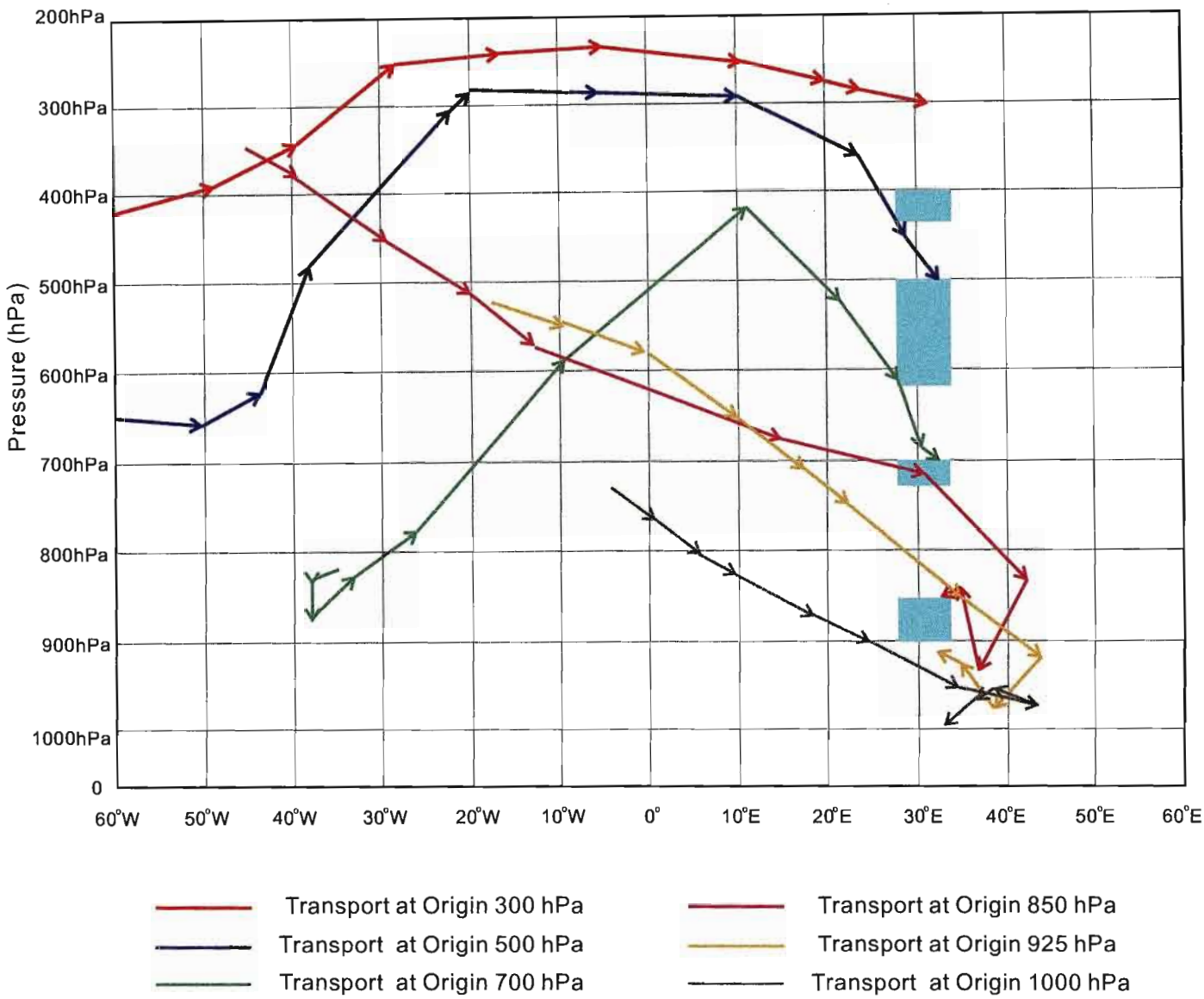

Figure 5.2g: Vertical cross-section showing transport of aerosols originating at selected pressure levels. The occurence of absolutely stable layers isindicated by shading for July 23,1997.

5.2.3 Case Study 3 (August 8, 1997)

The vertical distribution of aerosols on August 8, 1997 (Fig. 5.3a) is again characterised by the aerosol discontinuity at 5km. Aerosol concentrations in the lower layer are characterised by marked stratification, as in the previous two case studies, but photon counts are slightly lower, varying between approximately 150 and 200 photons. Above 5km, aerosol concentrations increased gradually with height, to about 150 photons.

Absolutely stable layers are observed at approximately 3, 5 and 9km (Fig. 5.3a). The 5km stable layer is particularly strong and deep (> 2km deep) and coincides with the marked aerosol discontinuity.

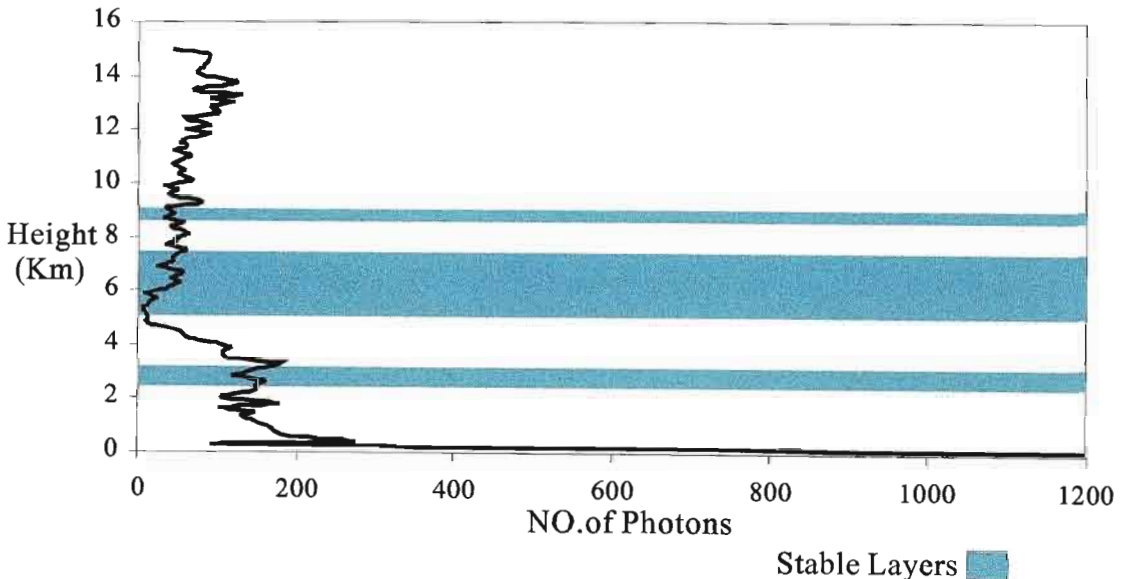

Figure 5.3a: Aerosol Profile for August 8, 1997. The occurrence of absolutely stable layers is indicated by shading.

Synoptic weather conditions were again characterised by a typical anticyclonic circulation as shown in Figure 5.3b. Surface winds were light and exhibited the same diurnal pattern as the previous case studies (Fig. 5.3c). This high-pressure system is responsible for poor dispersion and the accumulation of aerosols in the lower layer

5.2.4 Case Study 4 (August 21, 1997)

The aerosol profile (Fig. 5.4a) recorded on August 21, 1997 is dramatically different from the other profiles considered in this study. The atmosphere on this day depicted a very low photon count (<50) from 2km throughout the troposphere. Below 2km there was a peak of 200 photon counts at ~1km and then a gradual decline to the consistently low aerosol loadings observed in the rest of the troposphere. There was also a marked absence of the stratification that characterised the aerosol profiles in the previous three case studies.

Distinguishing features on this day were the passage of the coastal low depicted in Figure 5.4b. The passage of the coastal low during the afternoon is clearly indicated in the surface wind and pressure records (Fig. 5.4c and 5.4d). The surface wind direction changed from NE to SW and the pressure minimum observed at 14:00 was followed by an increase in pressure as the low passed. The aerosol profile, which was recorded at 20:00, was therefore characteristic of a post-coastal low situation. Another distinguishing feature on this day were the strong winds (>50ms^{-1}) observed in the upper troposphere (Fig. 5.4e). They would have contributed to the tropospheric aerosol reduction observed on this day.

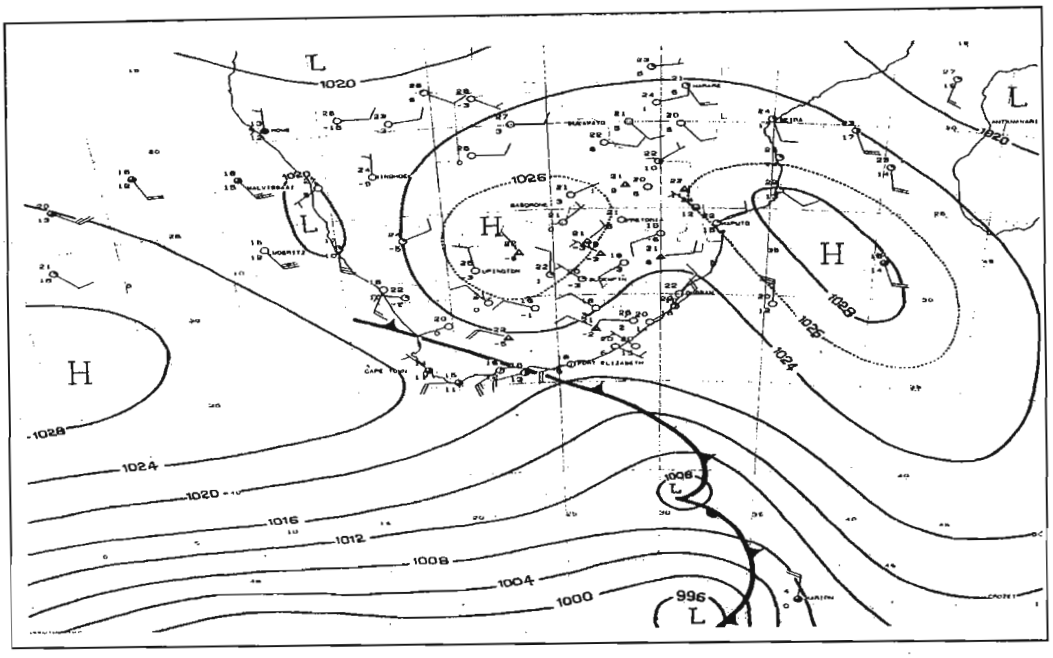

Figure 5.3b: Surface synoptic chart over southern Africa generated at 14:00 (Daily Weather Bulletin, SAWB) showing the circulation patterns for August 8, 1997.

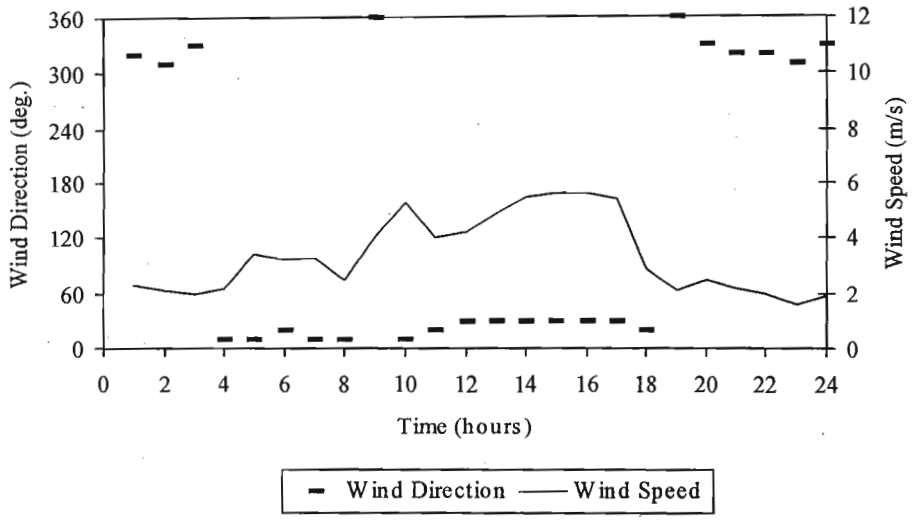

Figure 5.3c: Surface wind speed and direction for August 8, 1997.

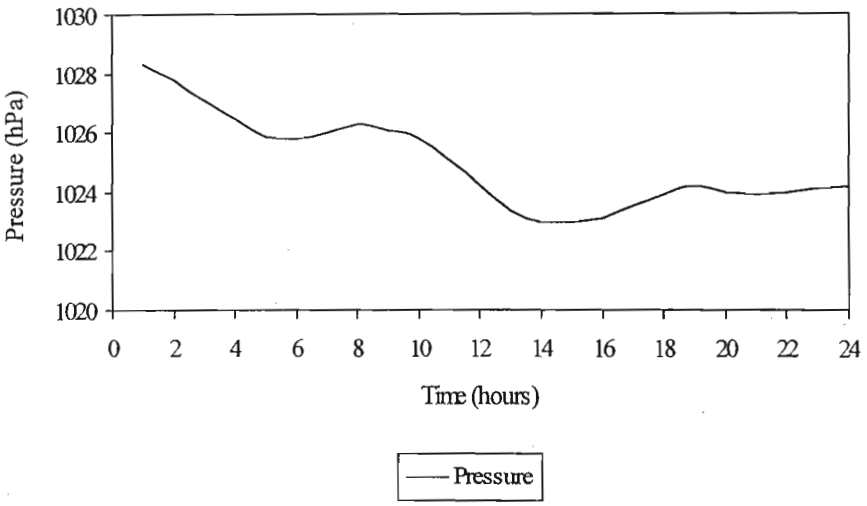

Figure 5.3d: Surface pressure for August 8, 1997.

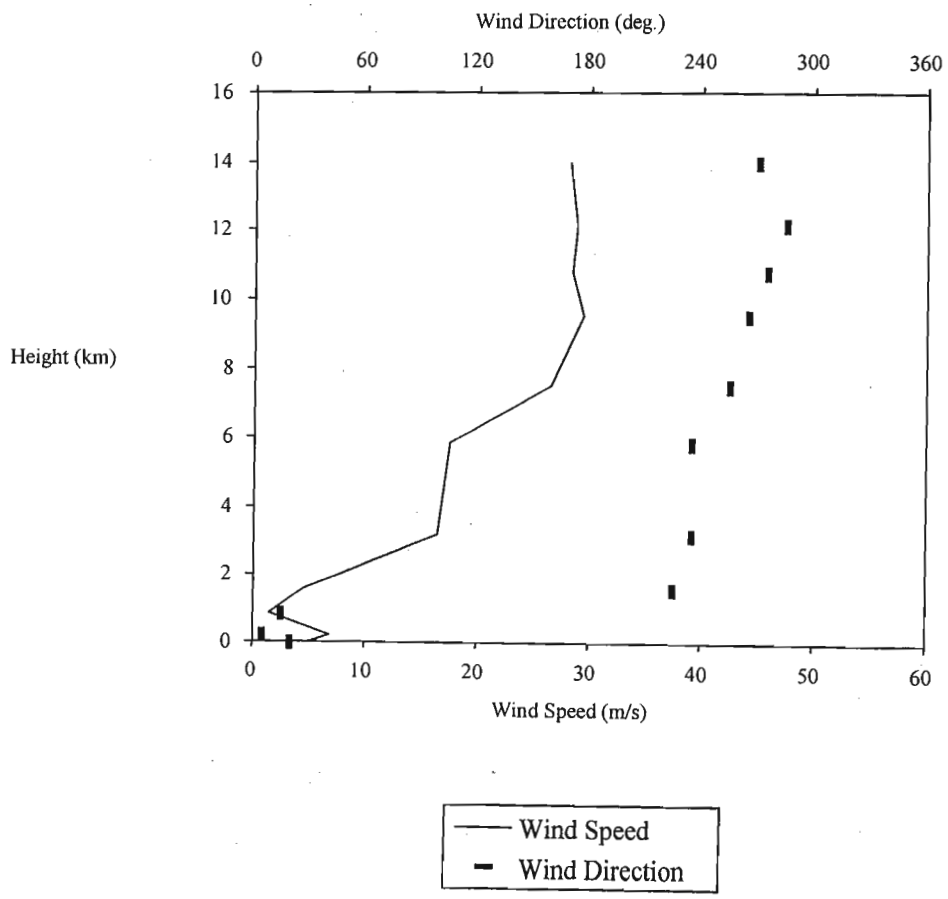

Figure 5.3e: Vertical wind profile on August 8, 1997.

Significant variations in the origin of air masses were observed in the ten-day back trajectory analysis (Fig. 5.3f). The origin of the 300hPa back trajectory was from a due westerly direction over South America. This trajectory was characterised by minimal vertical movement (Fig. 5.3g) as it originated too far south to experience the convective uplift that dominates the lower latitudes of South America. The 500hPa trajectory originated from the West African region and again shows little vertical movement. In contrast, the 700hPa trajectory, which originated over Zambia is characterised initially by strong vertical uplift, followed by subsidence as it encounters the anticyclonic circulation over southern Africa (Fig. 5.3f). In the lower layers, the 925hPa trajectory was entrained into the anticyclonic circulation, having originated over Mozambique/ Zimbabwe, whereas the 1000hPa trajectory originated south of the subcontinent (Fig. 5.3f). Very little vertical movement was evident in the lowest layer (Fig. 5.3g).

If Figures 5.3a, f and g are compared, it is noted that with the exception of the 1000hPa trajectory, the aerosols below 4km are largely of continental origin (Mozambique and Zimbabwe). It is significant that the photon counts are lower (~200) than for air masses of marine origin. The presence of the strong 5km stable layer plays a major role in confining the vertical movement of low-level trajectories to < 500hPa.

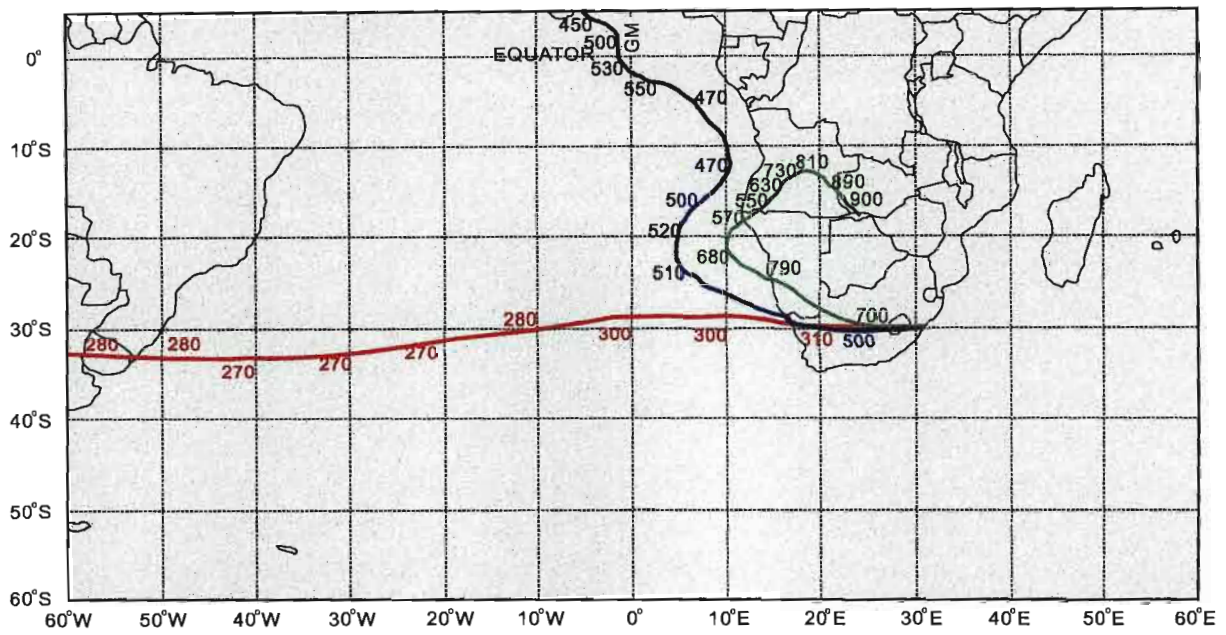

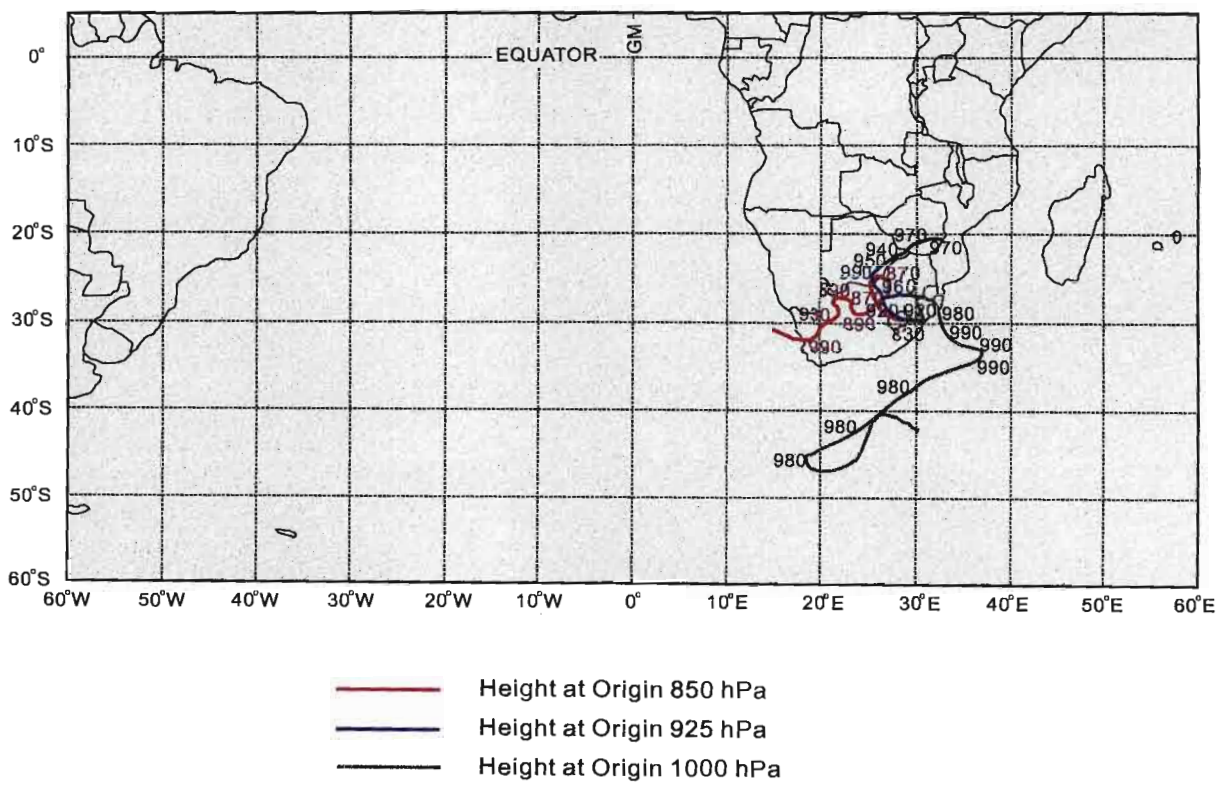

Figure 5.3f: Ten-day Backward Trajectories for August 8, 1997.

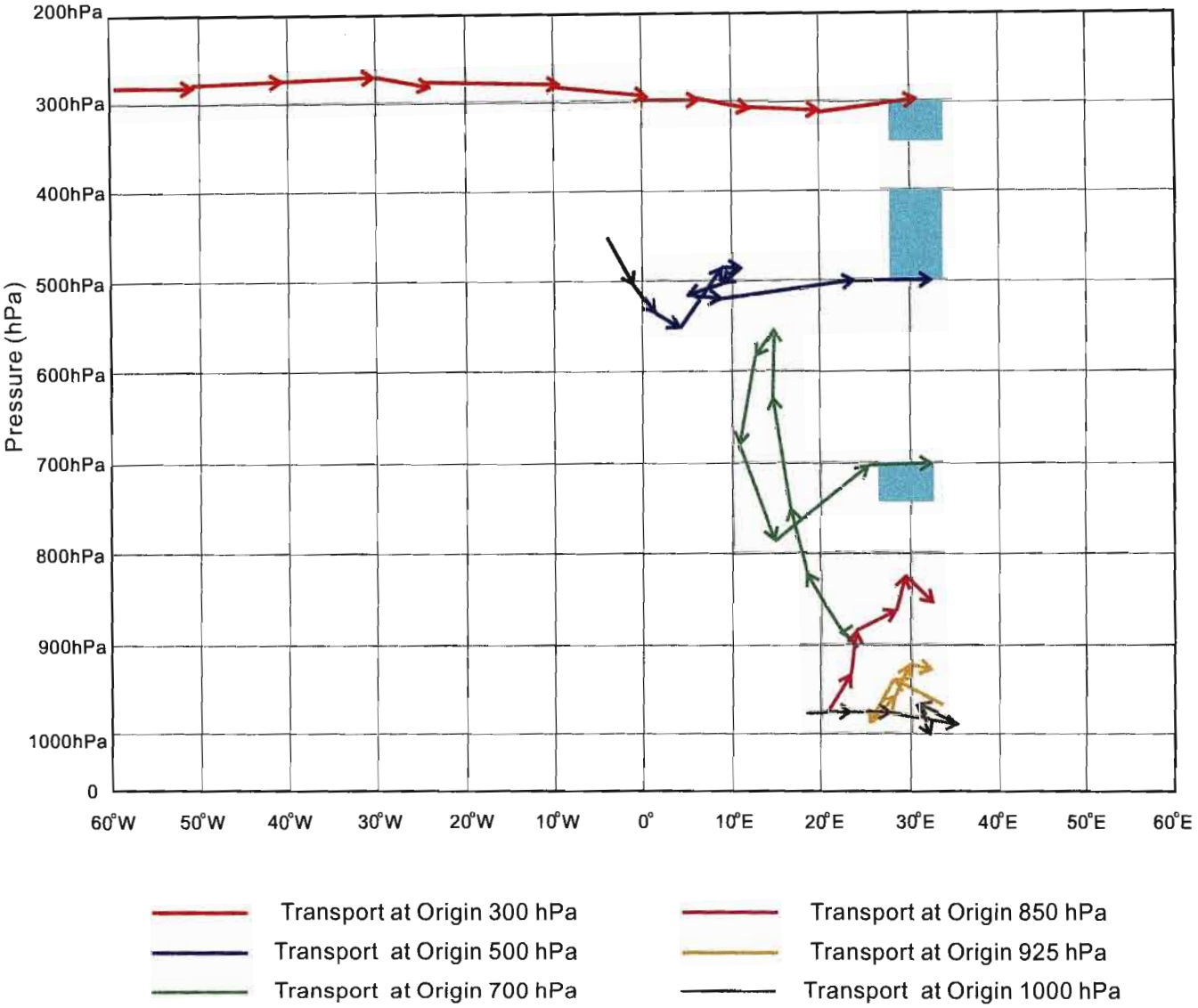

Figure 5.3g: Vertical cross-section showing transport of aerosols originating at selected pressure levels. The occurence of absolutely stable layers is indicated by shading for August 8,1997.

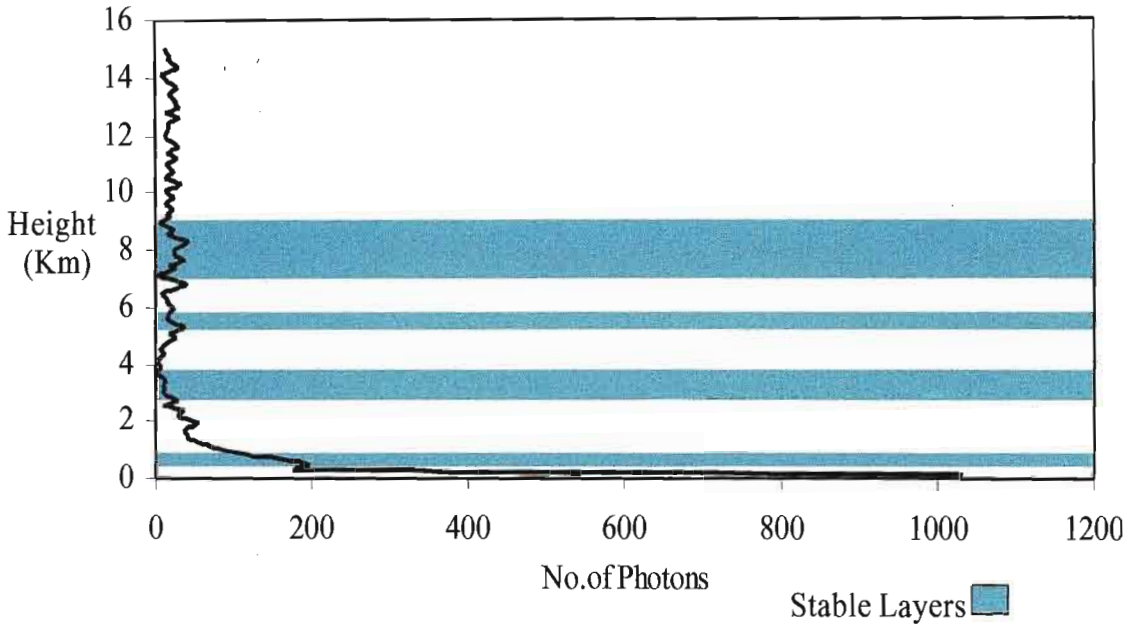

Figure 5.4a: Aerosol profile for August 21, 1997. The occurrence of absolutely stable layers is indicated by shading.

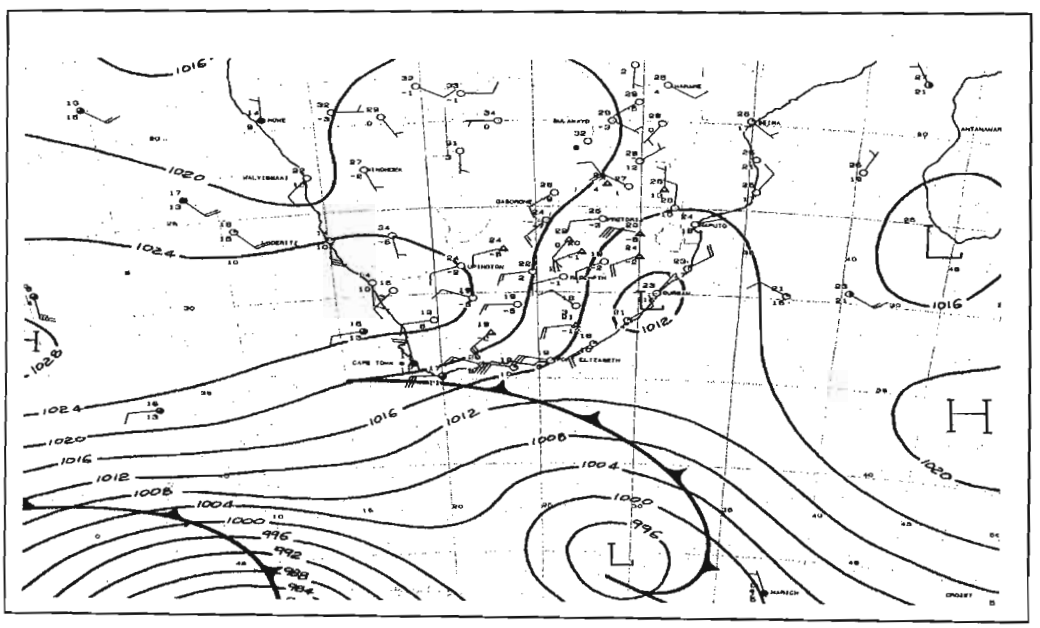

Figure 5.4b: Surface synoptic chart over southern Africa generated at 14:00 (Daily Weather Bulletin, SAWB) showing the circulation patterns for August 21, 1997.

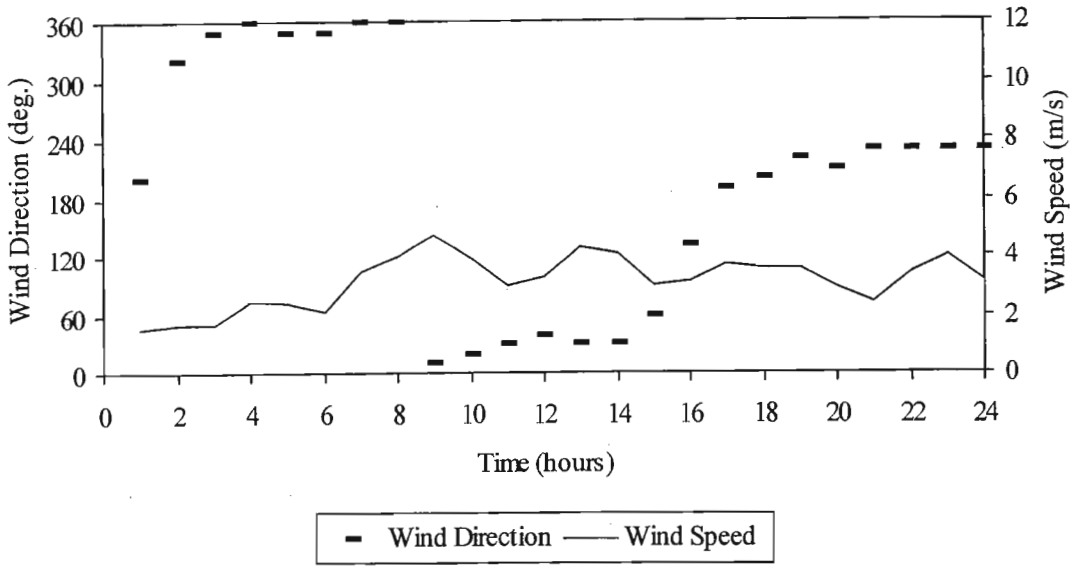

Figure: 5.4c: Surface wind speed and direction for August 21, 1997.

The ten-day back trajectory analysis was based on data that characterise the atmosphere prior to the passage of the coastal low and therefore do not reveal a typical post-coastal low situation. Ten-day back trajectory analysis showed that at 300 to 700hPa, the origin of the air parcels was over South America (Fig. 5.4f). The 850hPa trajectory originated over the Atlantic Ocean and revealed strong sinking over the subcontinent (Fig. 5.4g). At the 925 and 1000hPa levels the anticlockwise circulation was associated with the continental anticyclone. The air was also trapped below the first stable layer.

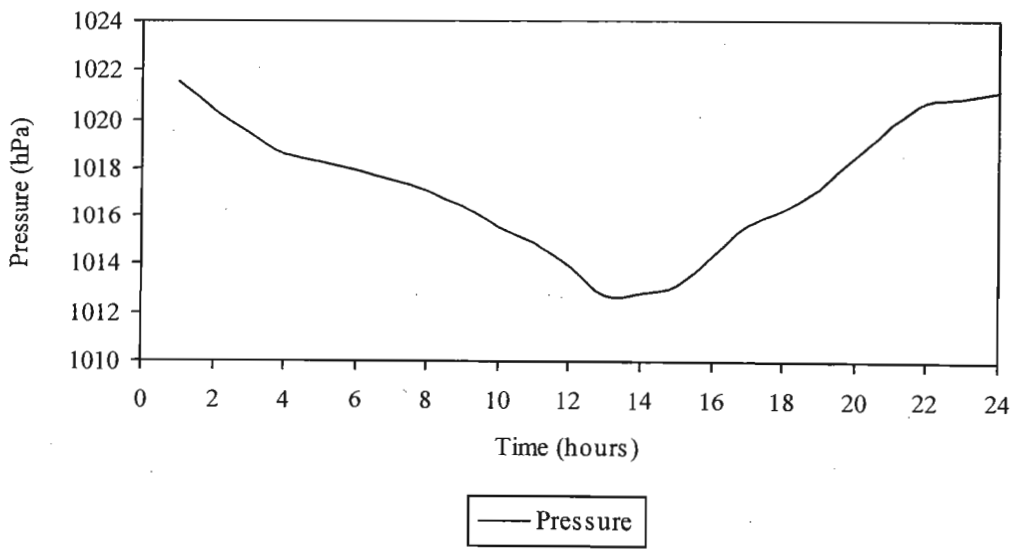

Figure 5.4d: Surface pressure for August 21, 1997.

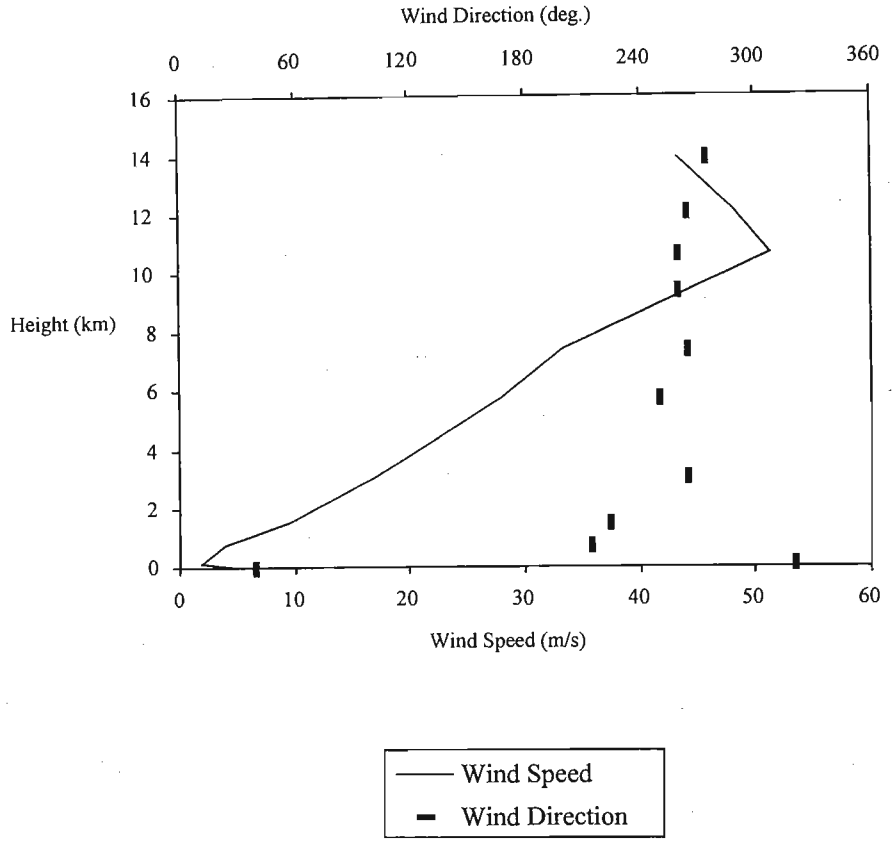

Figure 5.4e: Vertical wind profile on August 21, 1997.

From an examination of Figures 5.4a, f and g, it is noted that the aerosol peaks at 925 and 1000hPa originated from Mozambique curving anticyclonically into Durban accounting for the aerosol peak just below 1km. In contrast, in the upper troposphere, the concentration of aerosols declined rapidly most likely because of the rapid transport of Atlantic marine air over the continent and the lack of opportunity to entrain continentally derived aerosols.

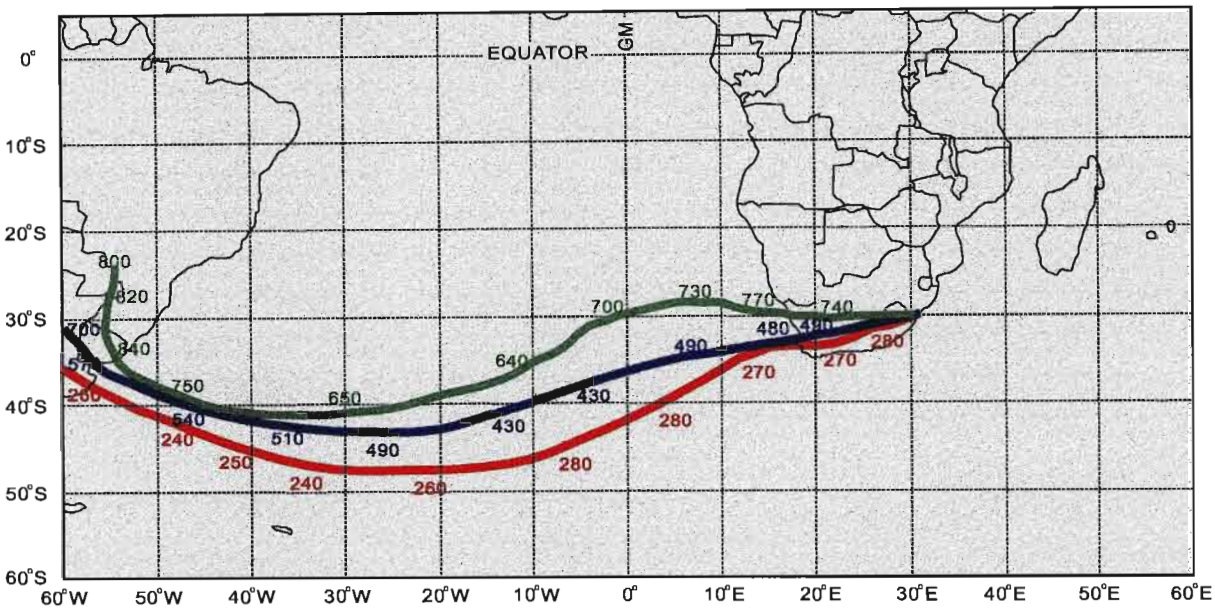

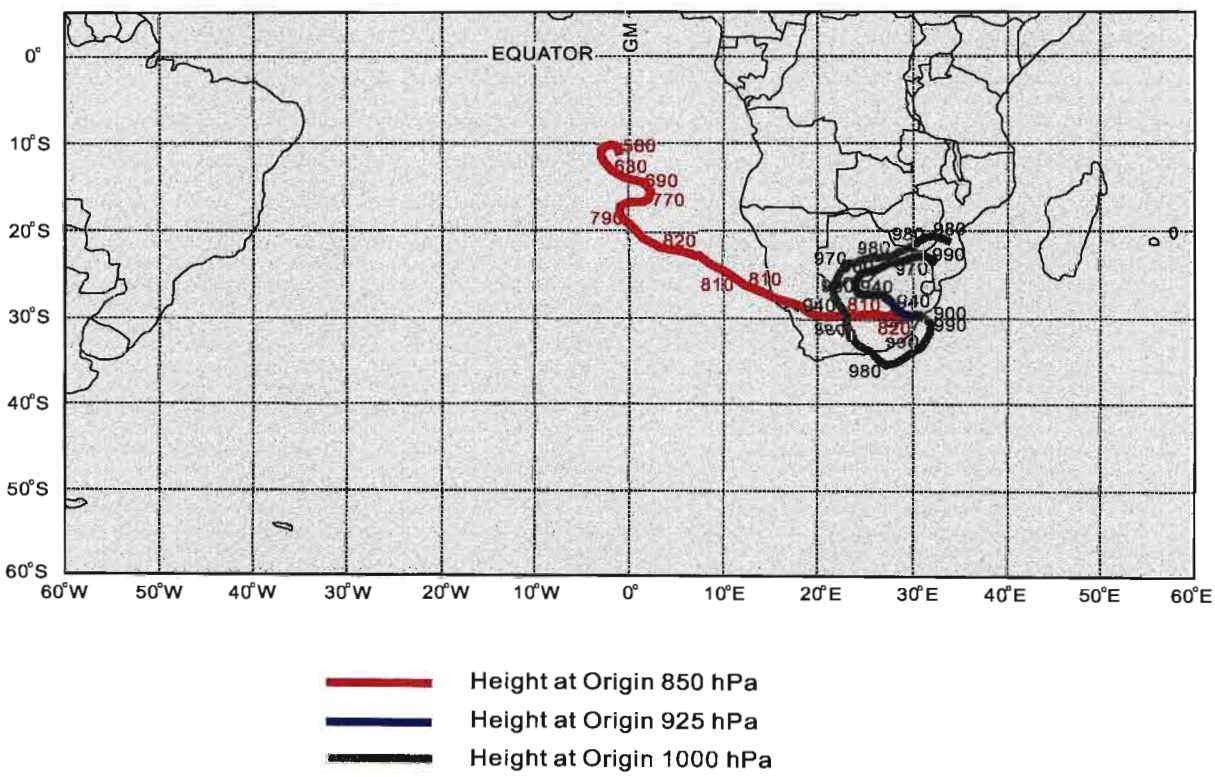

Figure 5.4f: Ten-day Backward Trajectories for August 21, 1997

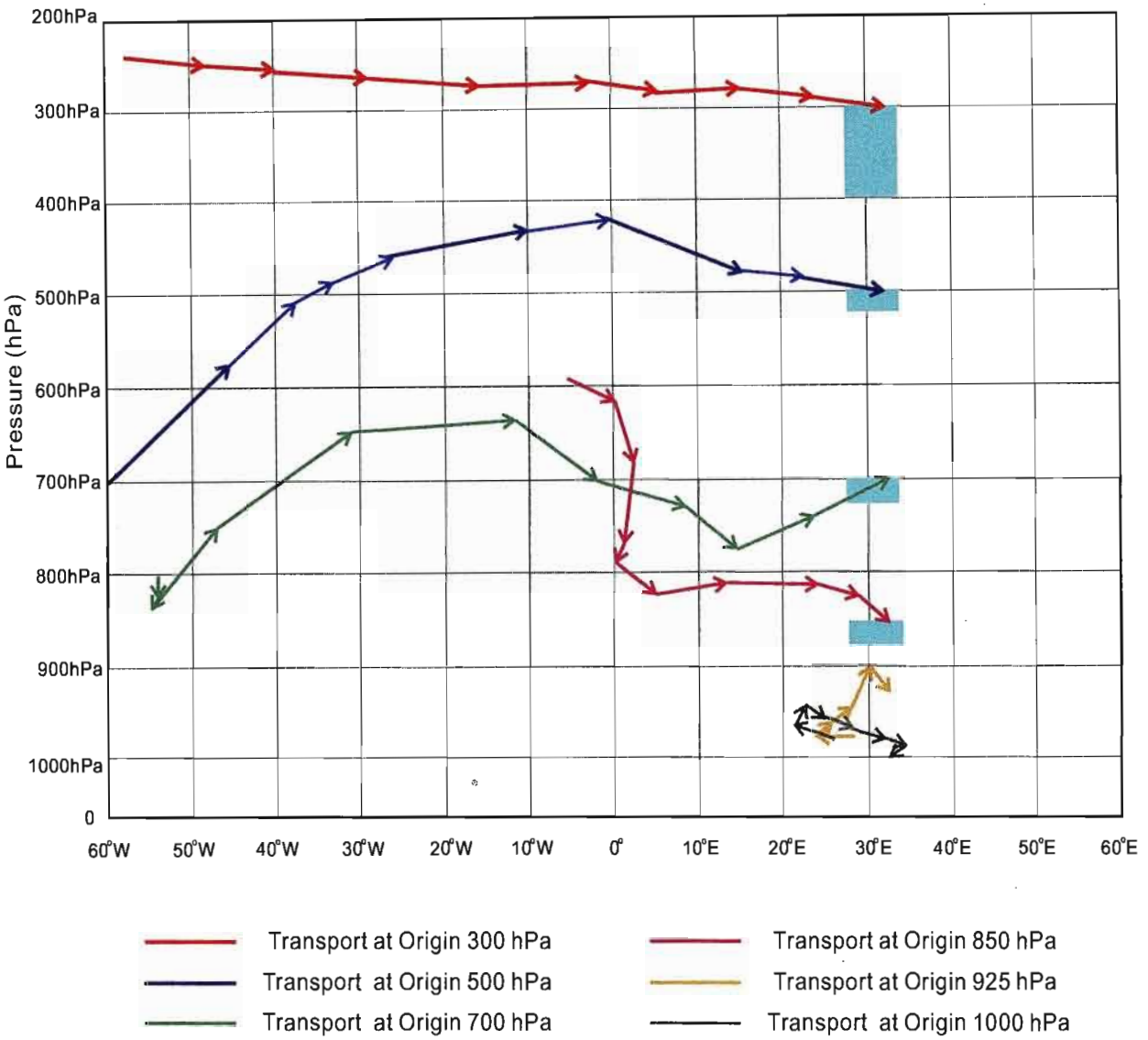

Figure 5.4g: Vertical cross-section showing transport of aerosols originating at selected pressure levels. The occurence of absolutely stable layers is indicated by shading for August21,1997.

5.2.5 Case Study 5 (September 26, 1997)

The aerosol profile presented in Figure 5.5a again shows a sharp discontinuity in aerosol concentration at 5km, which coincides with the presence of a shallow stable layer. Relatively high aerosol concentrations are found in the lower layer, with the highest aerosol concentrations occurring at 3km. This lower layer is again characterised by marked stratification, with photon counts varying between approximately 150 and 250 photons. Above 5km, aerosol concentrations vary between approximately 70 and 150 photons.

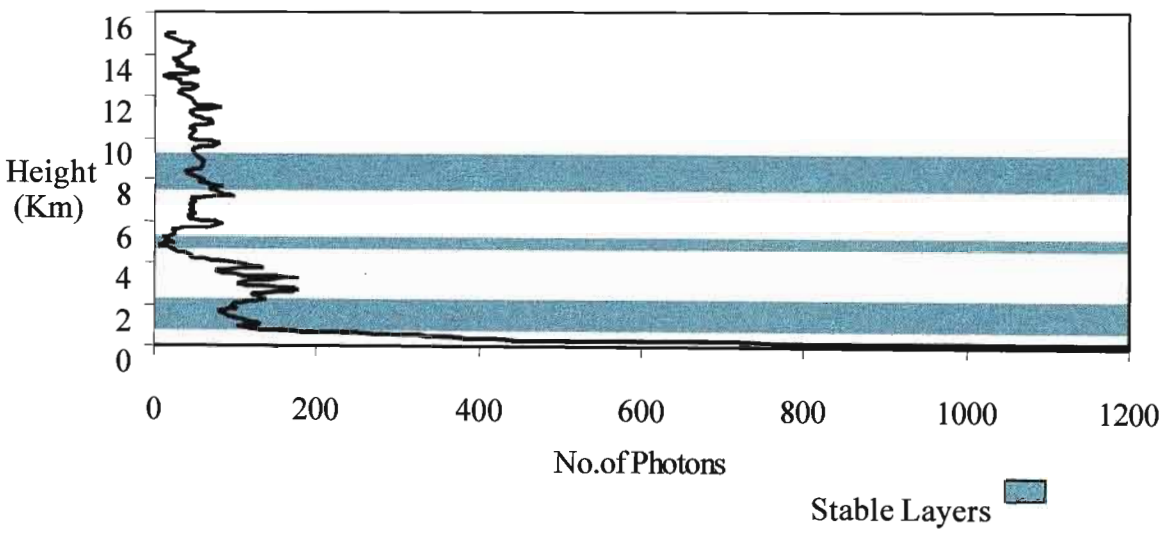

Figure 5.5a: Aerosol Profile for September 26, 1997

Absolutely stable layers are observed at approximately 1, 5 and 7km (Fig. 5.5a). Peaks are noted to occur in the intervening layers, being trapped by the stable layers above and below. Surface wind speeds on this day were far higher (up to $10ms^{-1}$) than in previous case studies and remained strong and NE into the night (Fig. 5.5c). Strong wind shear was evident at ~2km. Below this level, winds were NE, whereas above 2km they were W (Fig. 5.5e). Possibly this could account for the dip in aerosol concentrations at 2km (Fig. 5.5a).

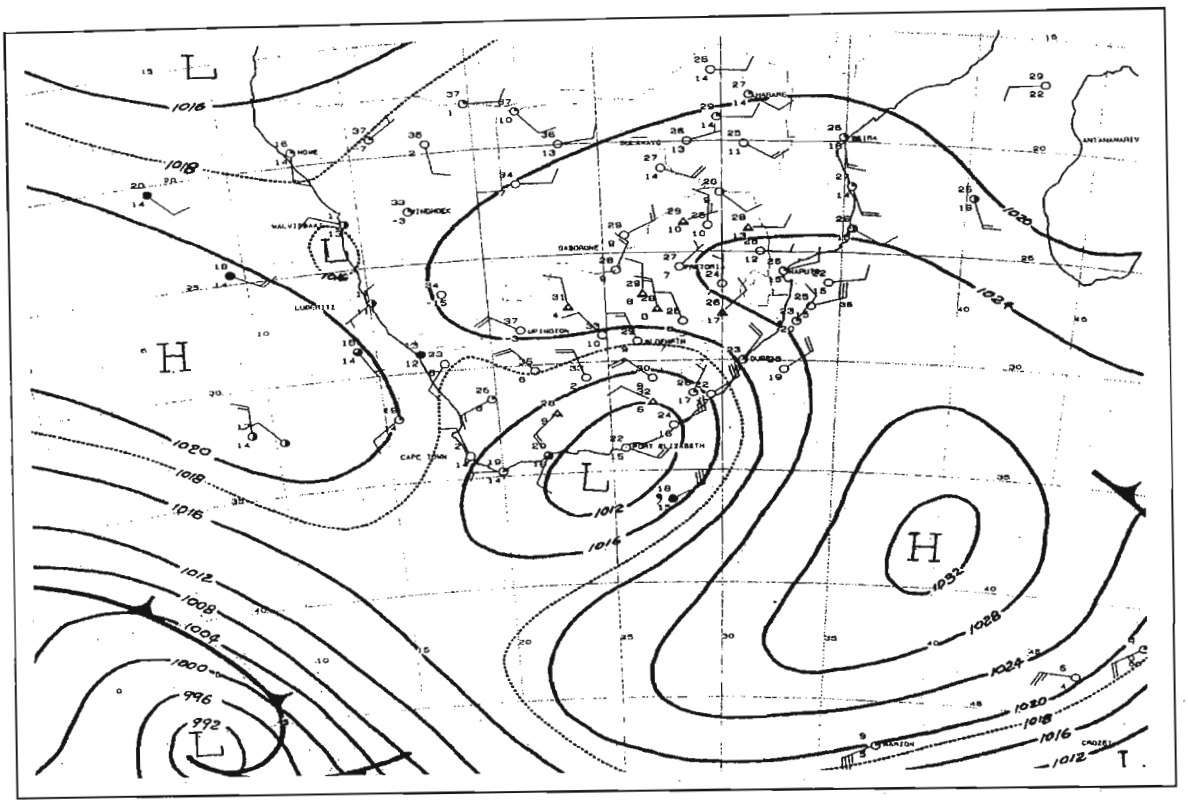

Figure 5.5b: Surface synoptic chart over southern Africa generated at 14:00 (Daily Weather Bulletin, SAWB) showing the circulation patterns for September 26, 1997.

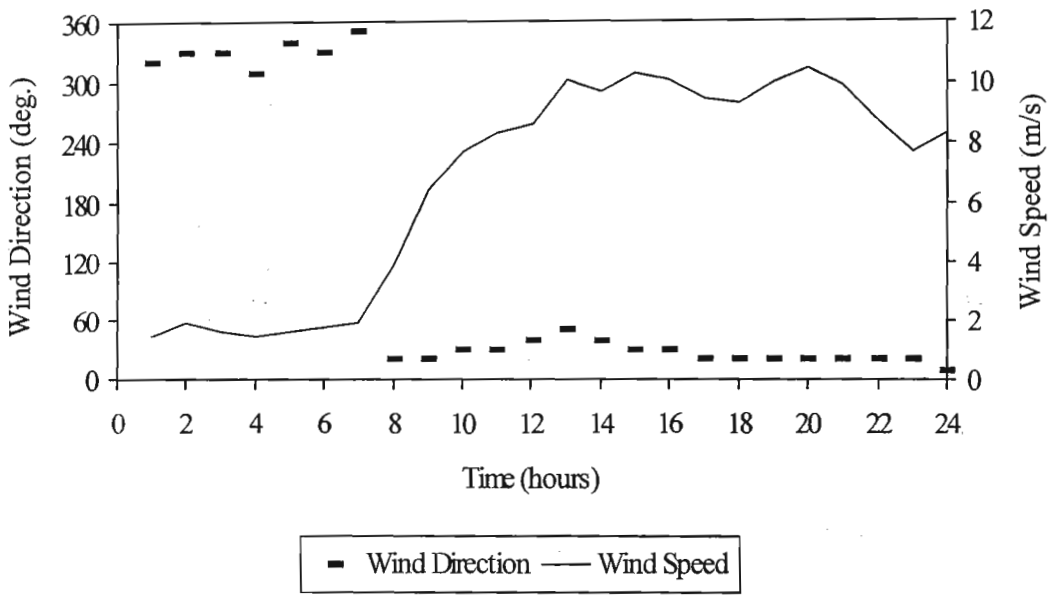

Figure 5.5c: Surface wind speed and direction for September 26, 1997.

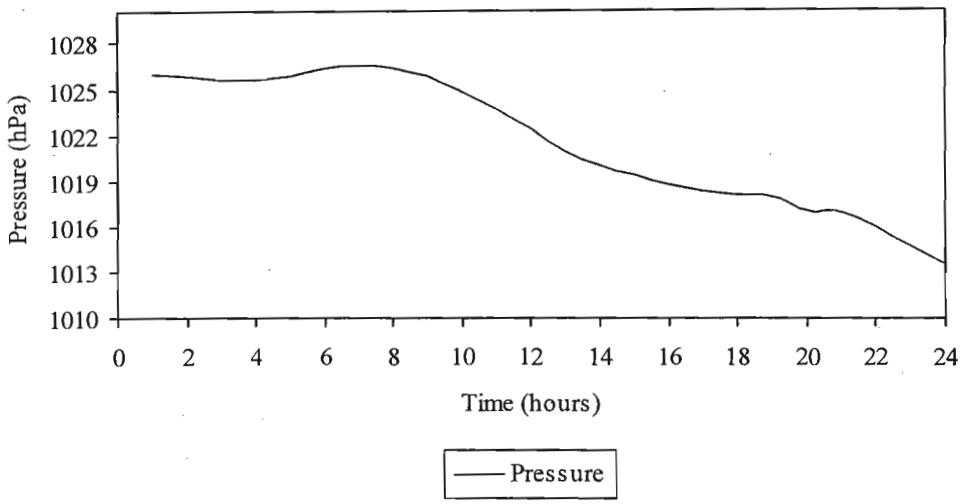

Figure 5.5d: Surface pressure for September 26, 1997.

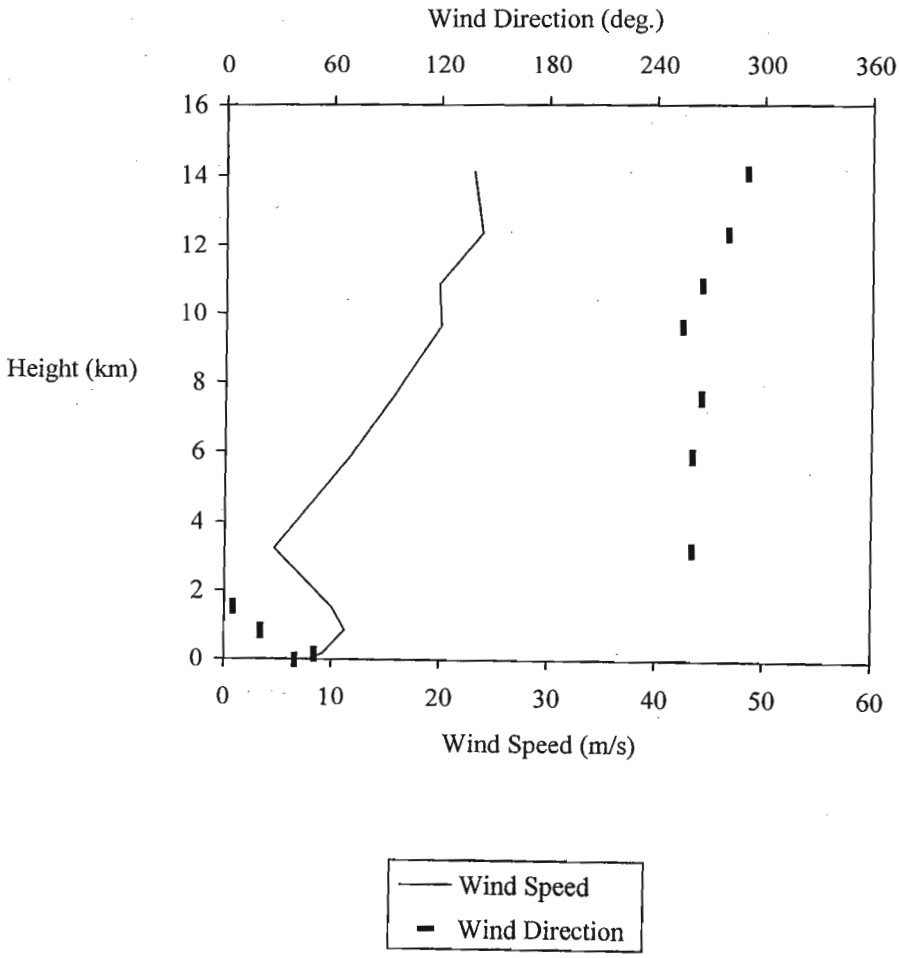

Figure 5.5e: Vertical wind profile on September 26, 1997.

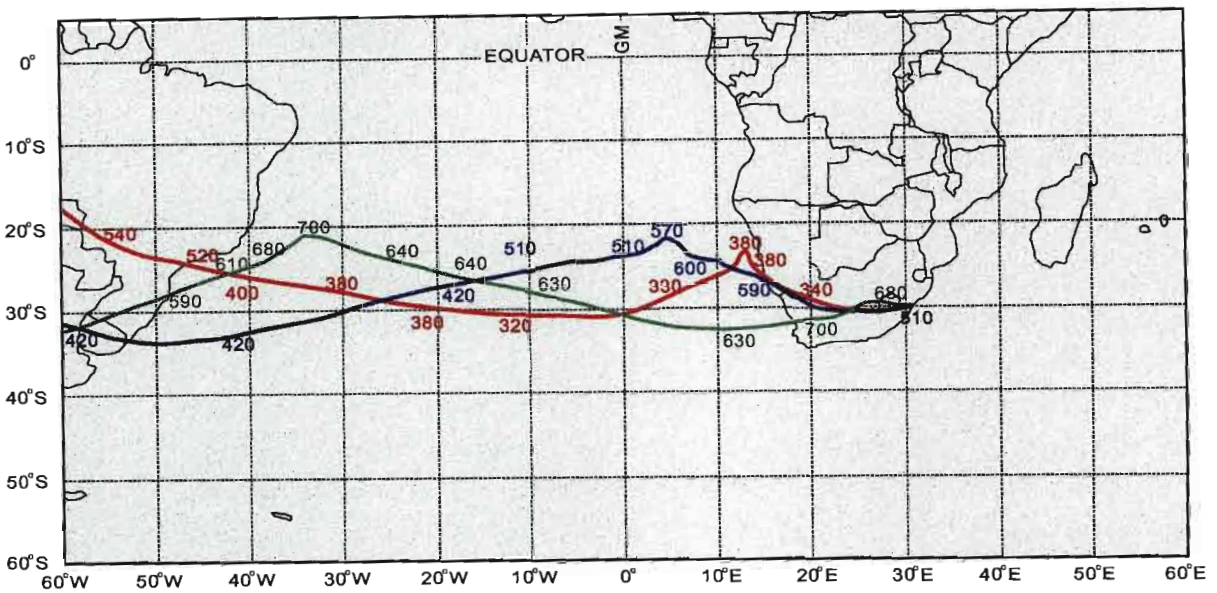

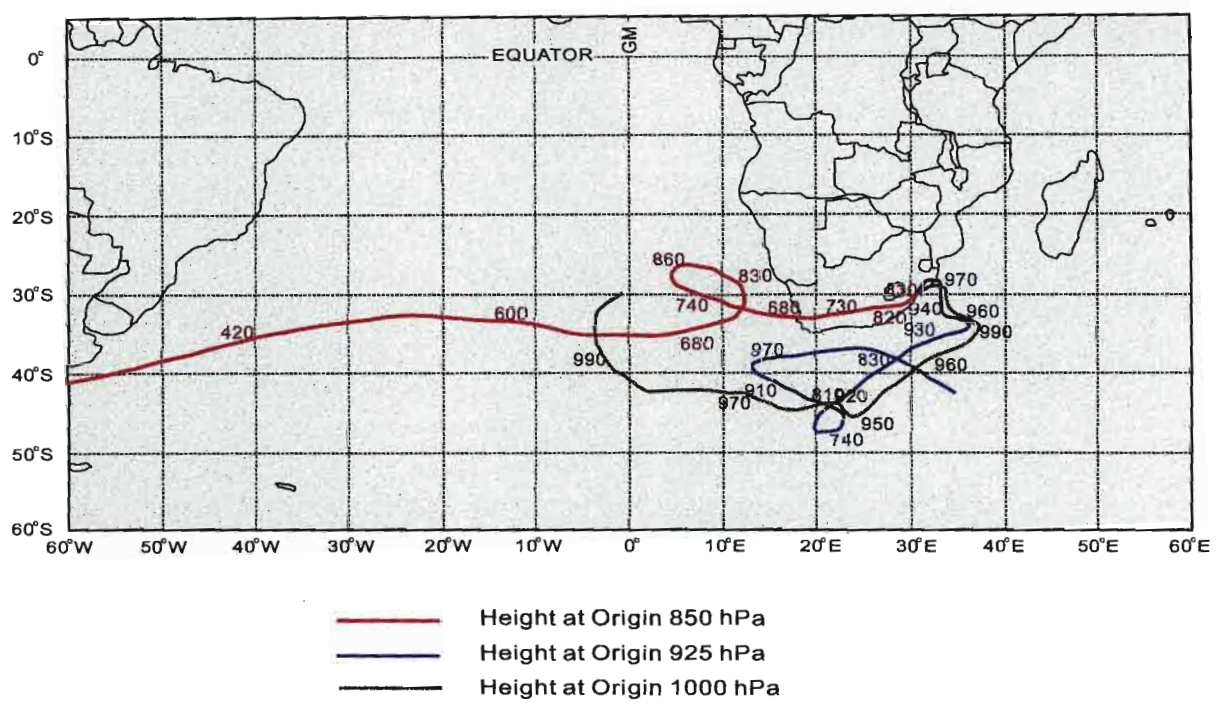

Figure 5.5f: Ten-day Backward Trajectories for September 26, 1997.

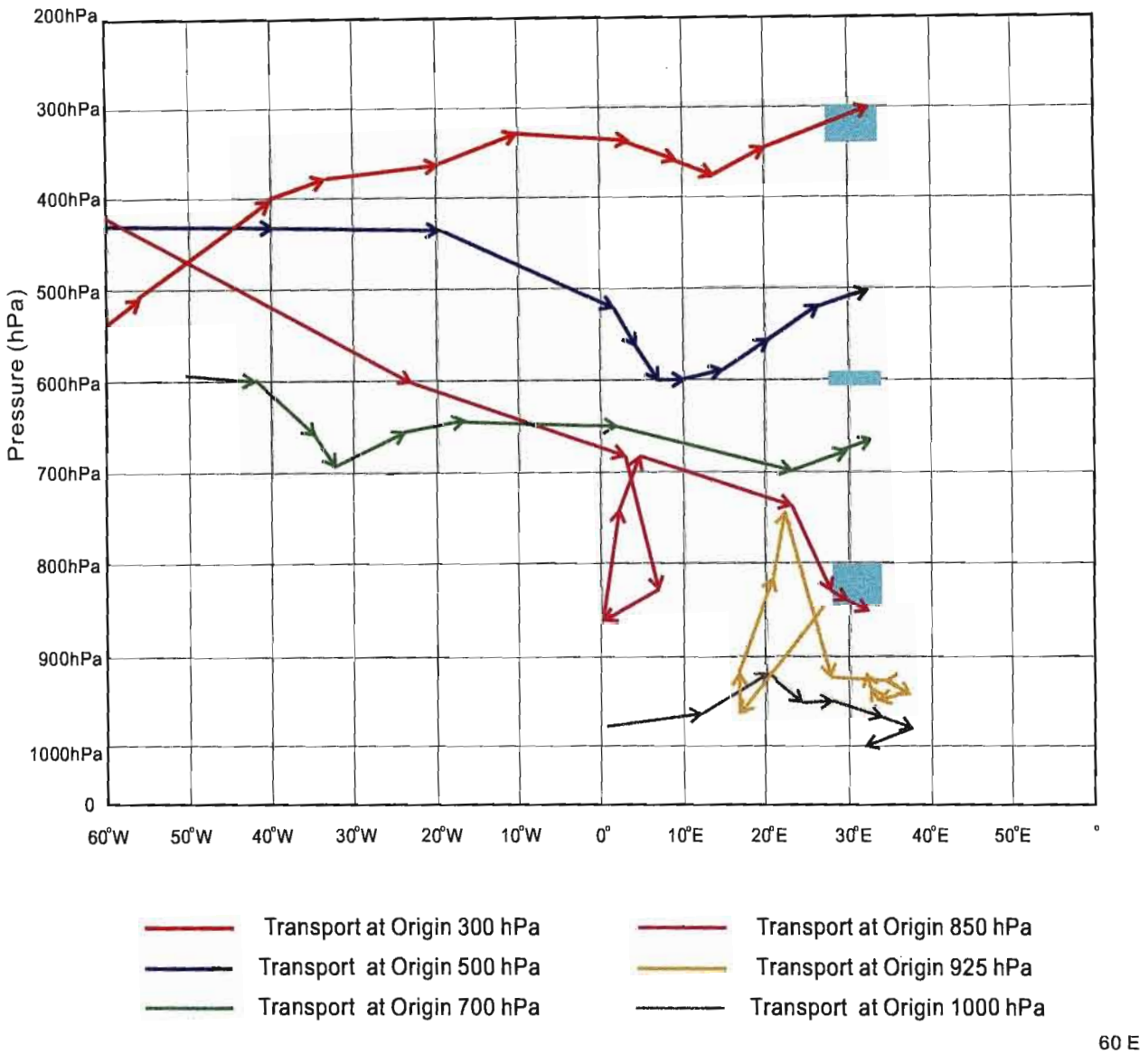

Figure 5.5g: Vertical cross-section showing transport of aerosols originating at selected pressure levels. The occurence of absolutely stable layers is indicated by shading for September26,1997.

Figure 5.5f shows the backward trajectories from Durban at selected pressure levels. The origin of air masses at the 300, 500, 700 and 850hPa levels was from South America. Air parcels at 925hPa originated in the Indian Ocean approximately 2000km off the east coast of southern Africa and at 1000hPa originated in the South Atlantic Ocean approximately 2200km off the west coast of southern Africa. Anticyclonic recurvature was evident at both the 925 and 1000hPa levels.

Figure 5.5g shows the back trajectories as a function of height. Sinking motion over the continent is indicated in both the 925 and 850hPa trajectories. Very little vertical motion is evident in the 1000hPa trajectory.

Comparing Figures 5.5a, f and g, it is evident that the lower tropospheric peak (2-4km) originates from the west, comprising aerosols of both continental and marine origin. Below 2km, the air is relatively clean, and it is noted here that trajectories originate at south of the continent.

5.2.6 Case Study 6 (October 20, 1997)

The aerosol profile (Fig. 5.6a) recorded on 20 October shows a marked minimum which extends from 5-6.5km. Aerosol concentrations in the lower layer are characterised by two strong peaks at approximately 1 and 3km. Photon counts of 400 in the lower peak are the highest observed in the case studies analysed. The peak is located below the first absolutely stable layer. Above 6km aerosol concentrations increased with height to about 150 photons and showed a similar structure to most of the previous case studies.

Two absolutely stable layers were present at 1 and 7km (Fig. 5.6a). The aerosol peak observed just below 3km is unrelated to the presence of a stable layer and is difficult to explain at this stage.

From an examination of the synoptic weather situation (Fig. 5.6b), it is clear that a well established high-pressure system persisted on this day. A coastal low was evident along the Cape south coast. Although at the surface, the winds revealed a diurnal pattern typical of a dominant high pressure system (Fig. 5.6c), there is evidence from the

vertical wind profile (Fig. 5.6e) that southerly winds prevailed above the surface. This would account for the absence of the 5km stable layer.

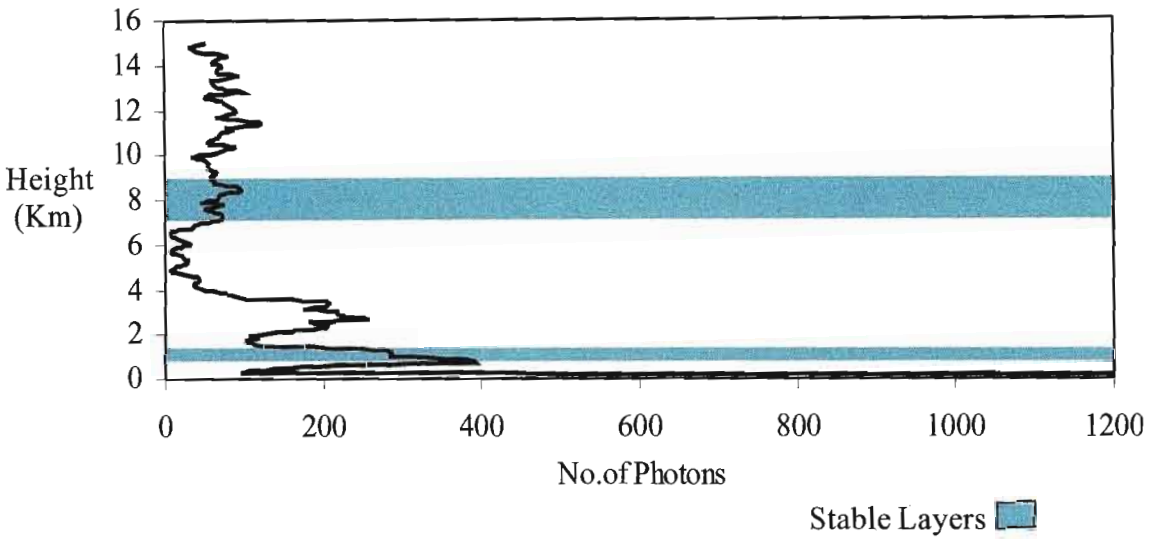

Figure 5.6a: Aerosol Profile for October 20, 1997. The occurrence of stable layers is indicated by shading.

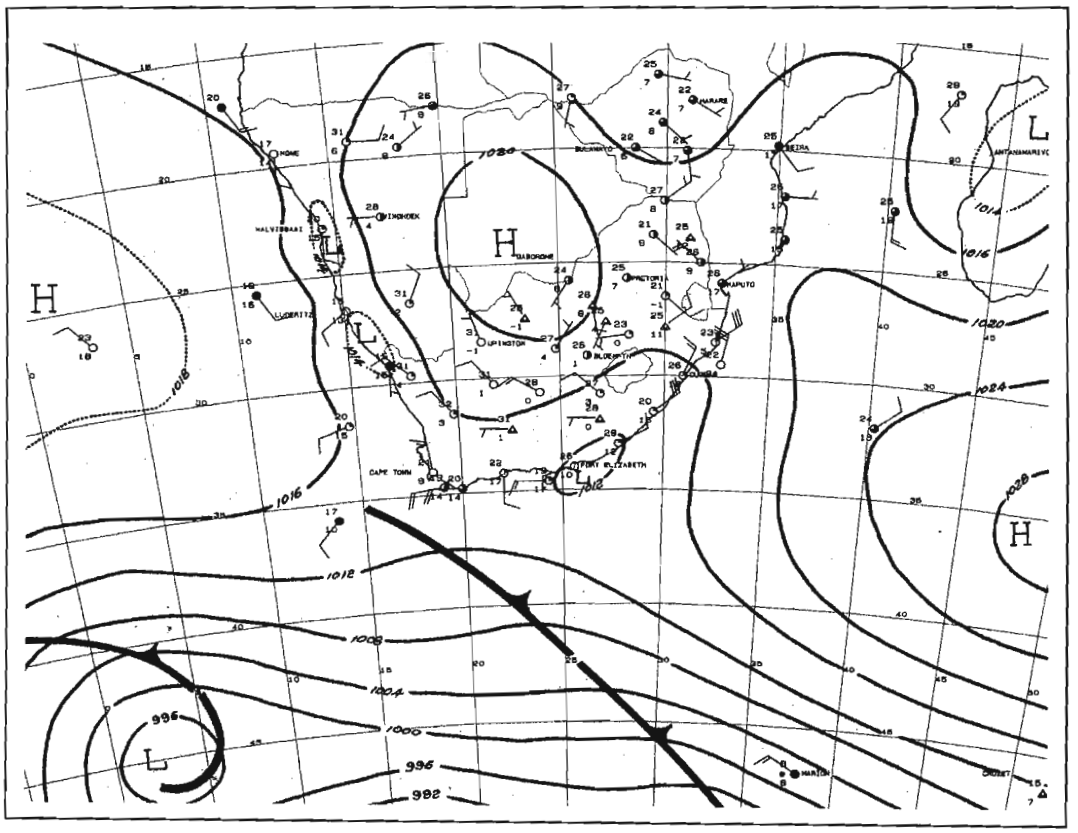

Figure 5.6b: Surface synoptic chart over southern Africa generated at 14:00 (Daily Weather Bulletin, SAWB) showing the circulation patterns for October 20, 1997.

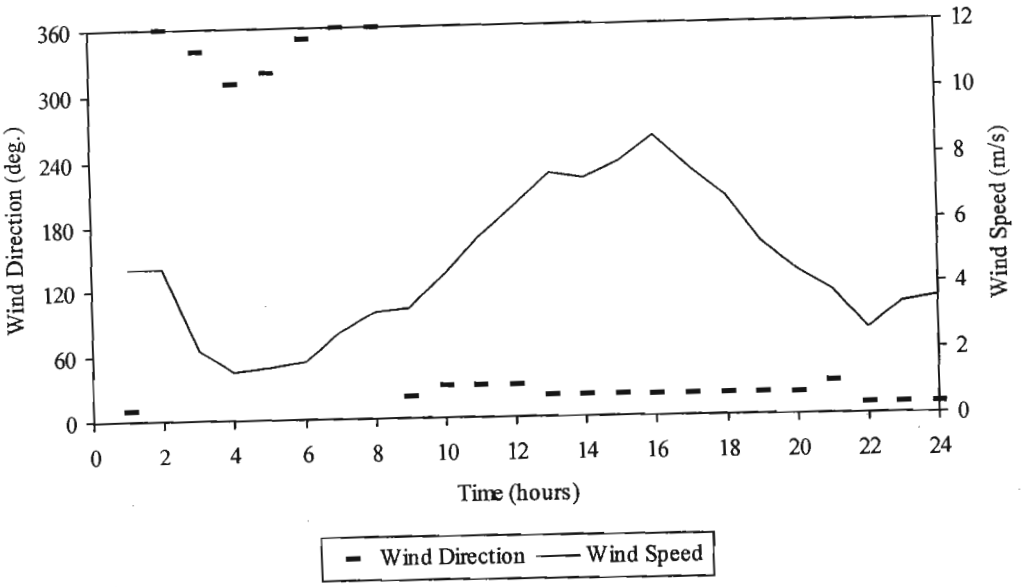

Figure 5.6c: Surface wind speed and direction for October 20, 1997.

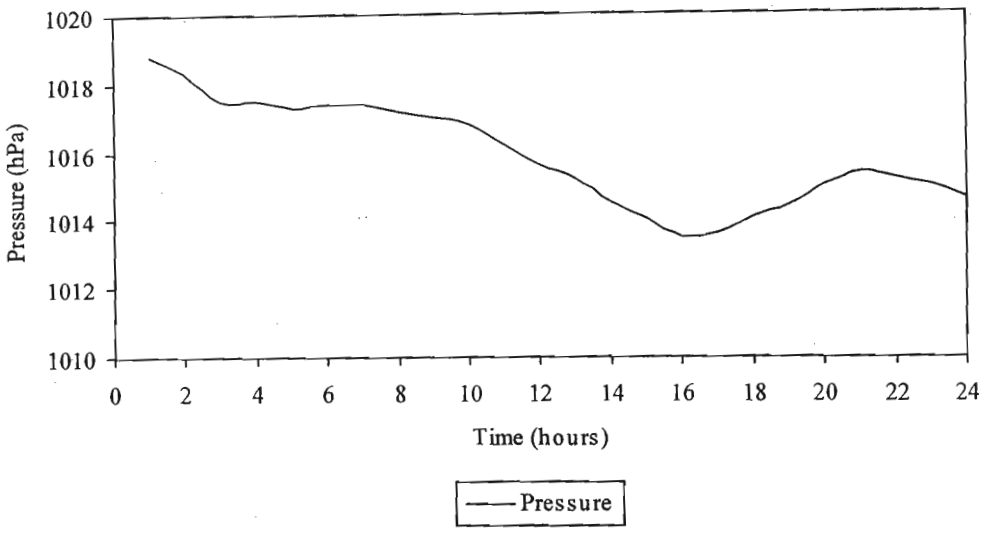

Figure 5.6d: Surface pressure for October 20, 1997.

Ten-day back trajectory analysis indicated that with the exception of the 700hPa trajectory, whilst they all originated in the W or SW of the subcontinent they approached from the E and SE (Fig. 5.6f) and were characterised by particularly strong subsiding motion (Fig. 5.6g) over the African continent. Vertical transport of mid to upper-tropospheric aerosols to the lower layers is responsible for the exceptionally high aerosol peaks observed at 3km (Fig. 5.6a). These aerosols could either be of continental origin (Africa) having being trapped in the upper layers over Africa for a long period of

time or could originate from the South American continent where they were transported vertically and then eastwards to Africa.

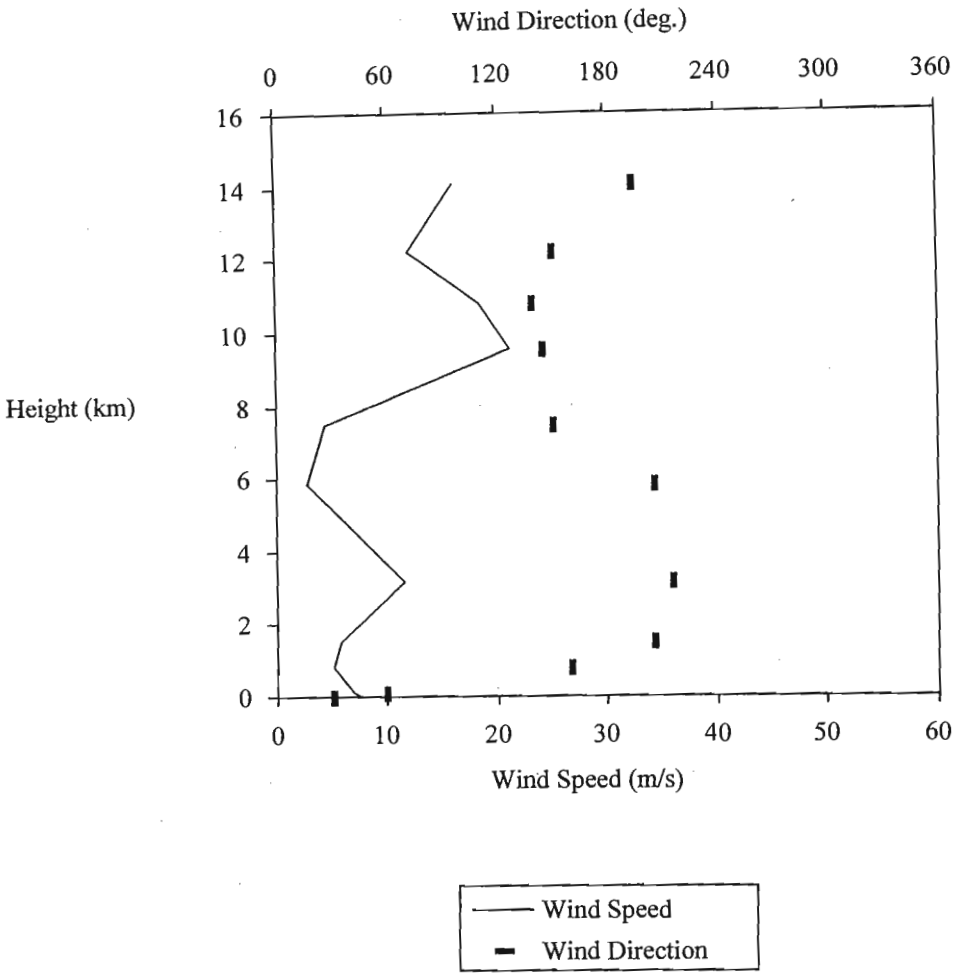

Figure 5.6e: Vertical wind profile on October 20, 1997.

The high aerosol concentrations in the lower atmosphere on this day are also associated with air of a maritime origin (925 and 1000hPa) from the south and south-east of the subcontinent. The peak at ~1km is most likely due to aerosols transported from the east. As noted in case study 2, the approach from the east is significant in accounting for the high aerosol loading of the lower atmosphere.

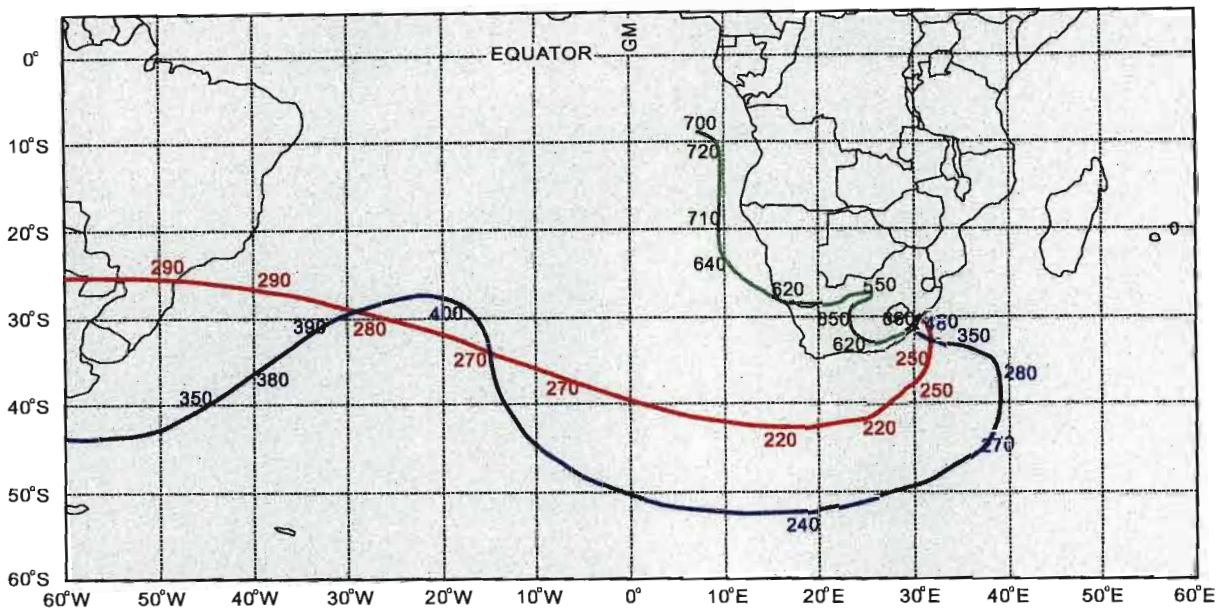

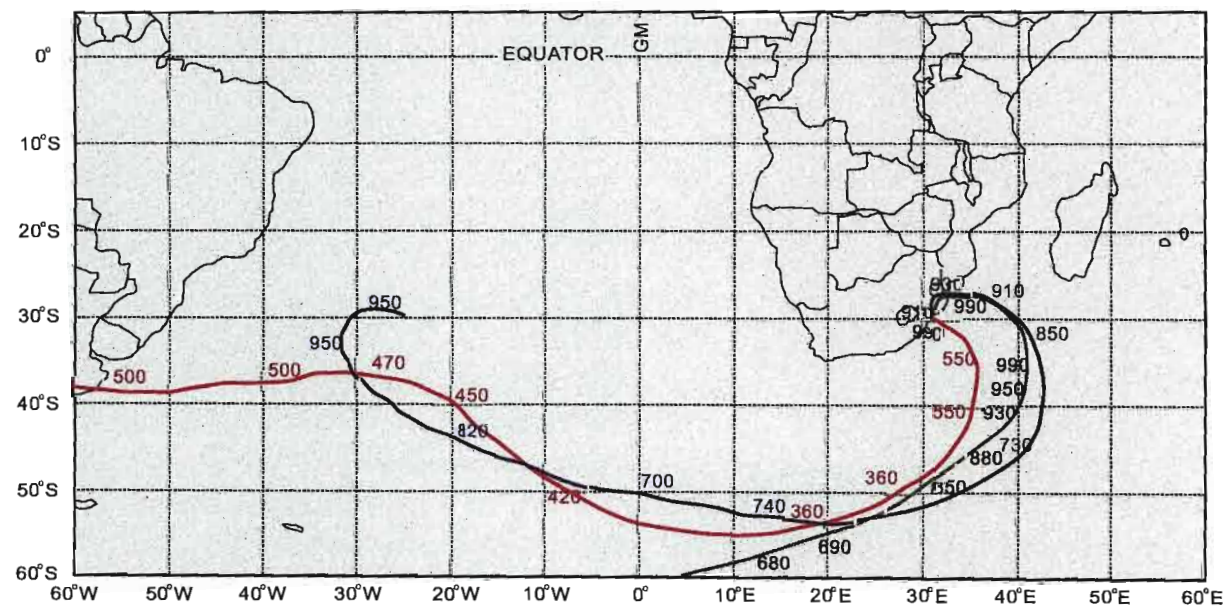

Figure 5.6f: Ten-day Backward Trajectories for October 20, 1997.

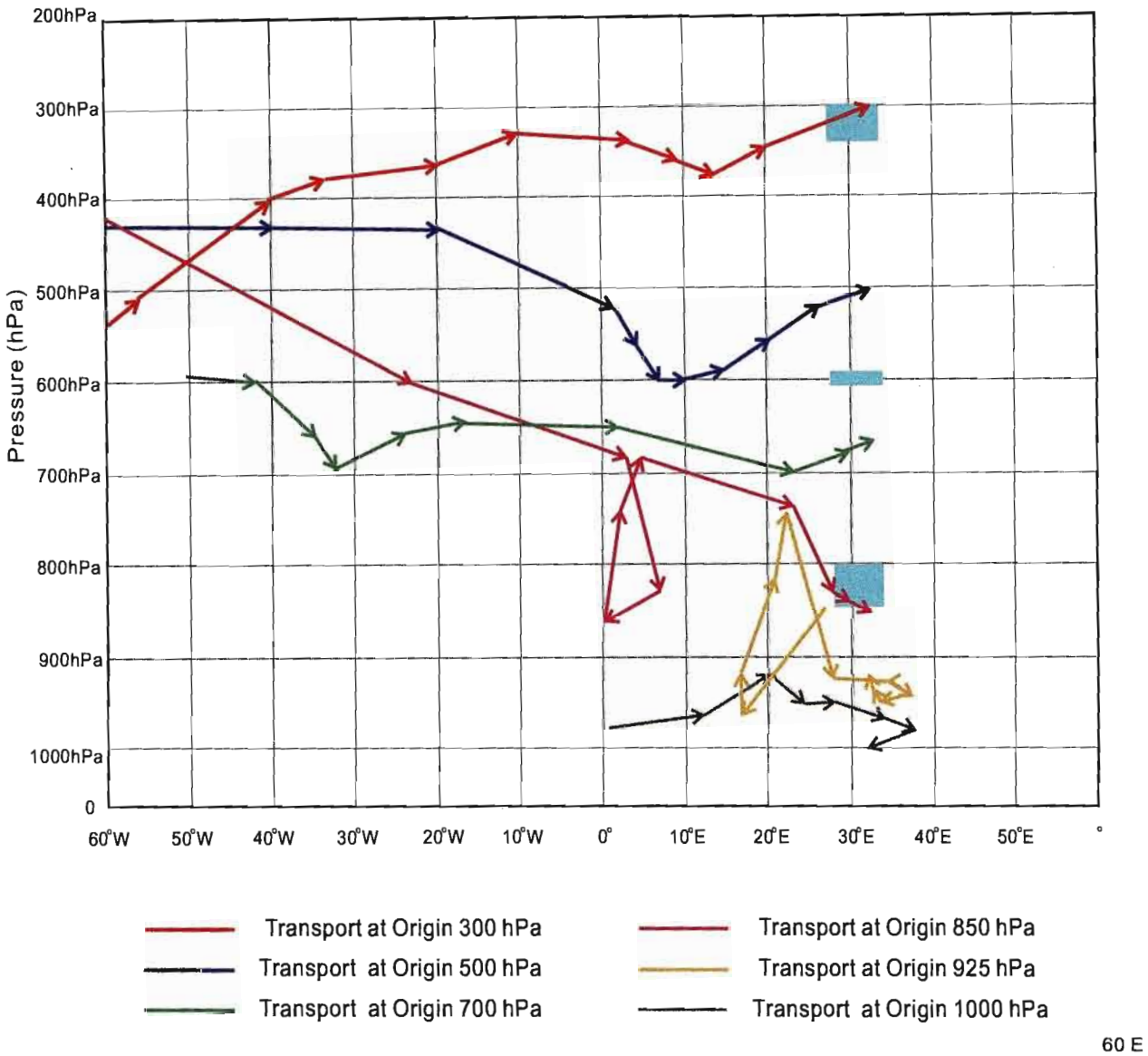

Figure 5.5g: Vertical cross-section showing transport of aerosols originating at selected pressure levels. The occurence of absolutely stable layers is indicated by shading for September26,1997.

5.3 Major Findings

1. With the exception of case study 4, all aerosol profiles were characterised by a sharp discontinuity at 5km. In all cases (except case study 6) the discontinuity was accompanied by an absolutely stable layer, which was frequently very shallow, but most pronounced in case study 3. The work of Cosijn and Tyson (1996) drew attention to the persistence and dominance of the 5km stable layer over the whole of southern Africa. They noted the effectiveness of this stable layer in preventing the upward and downward convective mixing of aerosols. It acts as a barrier between the lower troposphere and upper layers and according to Tyson and Preston-Whyte (2000), aerosols and trace gases trapped below this layer form a pronounced haze layer over the whole subcontinent from South Africa to northern Zambia and beyond. The results of this study endorse the significant trapping role played by the 5km stable layer and show clearly the influence on the shape of the vertical aerosol profile.

2. Aerosol concentrations in the lower troposphere (<5km) were higher than in the upper troposphere. They ranged between 150 and 450 photon counts, whereas in the upper troposphere, photon counts of 100 to 150 were recorded. The lower troposphere was also characterised by a marked stratification, typical of patterns observed by other authors for anticyclonic conditions (e.g. Diab *et al.,* 1996; Tyson *et al.*, 1996).

3. Particularly high aerosol concentrations in the lower layer (<5km) were observed when air parcels approached Durban from a NE direction (e.g. case study 2 and 6). Recirculation was observed with the occurrence of transient ridging anticyclones during those two days. The high aerosol contributions of the lower atmosphere are therefore due either to the onshore transport of marine aerosols in ridging anticyclones from a warm ocean current or to the recirculation of aerosol laden air of continental origin back over the land. Recently Piketh *et al.*, (1999) argued that the contribution of marine aerosols to the aerosol loading along the coast was significant. During their experiment a high concentration of marine aerosols (54% of

total aerosol loading over east coast) was detected when ridging anticyclonic circulation prevailed over the east coast (Piketh *et al.*, 1999).

4. Relatively high aerosol values were depicted throughout the troposphere in all cases except case study 4. The pattern that emerged from the analysis of case studies is that, aerosol concentrations were high (case study 1, 2, 3, 5, and 6) in the period prior to the passage of a coastal low and cold front, whereas low aerosol concentrations (case study 4) occurred after a frontal passage. The high concentration of aerosols was favoured by the high temperature, low wind speed and recirculation that occurred under anticyclonic situations. The atmosphere became much cleaner as the coastal low moved north-eastwards along the east coast, followed by a southwesterly flow (Diab *et al.*, 1995). Strong upper air winds observed during case study 4 caused better dilution of polluted air by rapidly mixing with unpolluted air, whereas the weak wind speeds observed in the five other case studies had less of diluting effect. The influence of frontal systems along the east coast of this region on the accumulation of pollutants was also observed by other authors (Diab *et al.*, 1995).

5. Back trajectory analysis in the upper troposphere (300, 500 and 700hPa) indicated that generally, the air masses originated over South America or W and SW of the African subcontinent. In most cases, trajectories exhibited marked vertical uplift due to strong convection over the Atlantic Ocean before descending towards the surface as they came under the influence of the stable discontinuities that characterise the anticyclonic circulation over the southern African region. These results are consistent with those of Swap *et al.*, (1996) and Tyson *et al.*, (1996).

6. Lower level trajectories (850, 925 and 1000hPa) indicated diverse origins. Transport at these lower levels was considerably less than the upper levels due to the lower wind speeds. Trajectories originating over continental areas to the north generally exhibited anticyclonic curvature and very little vertical movement. Trajectories which may have originated over the Atlantic Ocean but which approached Durban

from the east were generally characterised by highest aerosol loadings (e.g. case studies 2 and 6).

7. It is clear that most of the aerosols are recirculating in the semi-permanent anticyclone over southern Africa in the lower troposphere and might exit the subcontinent to the southeast over the Indian Ocean. Recirculation has been shown to control/ influence on the accumulation of aerosols over this region.

8. The aerosol peak at the near-surface is due to the transportation of marine aerosols from the Indian Ocean. However, in several case studies, transportation of aerosols originating from Mozambique and Zimbabwe also caused high concentration of aerosols at certain levels. In addition, the peak at around 3 to 4km is due to transport of aerosol mid-tropospheric air circulating over South Africa.

CHAPTER 6

CONCLUSION

The main objective of this dissertation was to examine the vertical distribution of aerosols over Durban in relation to the vertical stability characteristics and horizontal transport of air masses. A comprehensive literature review on aerosols and atmospheric circulation over southern Africa was given. The analysis of six aerosol profile case studies presented in this study has revealed a clear relationship between the distribution of aerosols and the observed atmospheric circulation and its associated dynamics. Indeed, the passage of a coastal low was found to have a marked influence on the vertical aerosol distribution. The low aerosol concentrations observed endorsed the cleaning role of a frontal passage that has been highlighted by other authors (Diab *et al.*, 1995).

6.1 Summary of Results

- A strong relationship appeared between an aerosol discontinuity at 5km and the ~500hPa (~5km) absolutely stable layer. This layer is highly significant in controlling the vertical distribution of aerosols in most of the case studies. It was also identified by Swap and Tyson (1999) and Tyson and Preston-Whyte (2000) as a significant feature.

- The polluted lower atmosphere that was observed in the case studies supported the evidence for the relationship between anticyclonic circulation and high concentrations of aerosols. This observation is consistent with experiments undertaken during SAFARI-92 (Diab, *et al.*, 1996; Tyson, *et al.*, 1996).

- The contrast between an aerosol laden atmosphere prior to the passage of a frontal system and the relatively clean atmosphere after the frontal passage was highlighted. The influence of the passage of synoptic weather systems on pollution concentrations has also been noted by other authors (Diab *et al.*, 1995).

- A direct relationship between the vertical distribution of wind speed and the horizontal dispersion of aerosols was evident in the case studies. Strong upper air winds caused better dilution of aerosol-laden air, whereas weak wind speeds had less of a diluting effect.

- Anticyclonic flow showed a dynamical connection with recirculation of air at lower levels and a high concentration of aerosols in the study region. This observation was similar to earlier studies by Swap *et al.* (1996), Diab *et al.* (1996) and Tyson *et al.* (1996).

- A generally weak relationship between the origin of lower level back trajectories and aerosol concentrations in the lower troposphere was observed. Although different trajectory origins were noted, sometimes continental and sometimes once the Antarctic Ocean, the aerosol profile were invariably characterised by high concentration of aerosols. Further investigation based on a substantially greater number of profiles is needed to link high aerosol concentrations in the lower atmosphere to their origin.

- In the case of a well-developed anticyclone, a strong onshore flow over the eastern part of the subcontinent was present. This caused the transport of marine aerosols from the Indian Ocean in the lower troposphere and accounted for the near-surface aerosol peaks observed over this region. Along with the transportation of aerosols-

laden mid-tropospheric air circulating over South Africa and the recirculating air from either the Indian Ocean or South Atlantic Ocean, high aerosol concentrations were observed at 3-4km. Relatively high aerosol concentrations on the east coast occur in warm, moist air masses with weak pressure gradients. In addition, aerosols originating from inland (Mozambique and Zimbabwe) also generated high aerosol accumulation in the lower-troposphere. This observation is consistent with experiments undertaken by Held *et al.* (1994) and Piketh *et al.* (1999).

- The results of the back trajectory analysis in the upper troposphere (300, 500 and 700hPa) generally indicated an initial upward motion most likely due to the strong convective activity over tropical South Africa and the Atlantic Ocean and downward motion as the trajectory approached southern Africa due to the influence of anticyclonic circulation. This observation was similar to earlier studies by Swap *et al.* (1996), Tyson *et al.* (1996).

6.2 Limitation of this Study

It is recognised that the major limitation of this thesis was that the analysis was restricted to six different case studies only. However, this limitation was beyond the author's control. Originally it was intended to base this study on an analysis of aerosol profiles recorded by the new LIDAR installed in Durban. Instrumentalities problems precluded the incorporation of these data and it became necessary to rely on a historical data set. Undoubtedly, if the data had been collected on a continuous basis, then the results would have shown the relationship between atmospheric circulation and aerosol concentrations more precisely.

Furthermore, the laser beam of wavelength 589nm from the LIDAR identifies only the presence of aerosols in the atmosphere, and not the size distribution or the chemical composition of the aerosols. In addition, the high signal return from the low level molecules caused the photomultiplier to saturate, so that, aerosol data from 0-1km could not be utilised. The LIDAR is only able to function under cloud-free conditions.

Frequently, low-level stratus clouds develop over Durban at sunset, particularly during summer months, thus limiting the operation of the LIDAR.

Finally, the trajectory model was only run for standard pressure levels, it would have been preferable to run the model based on the aerosol peaks, to determine their source with certainty.

6.3 Future Studies

Several significant points emerged from this study which should be considered for further inquiry and research:

- This study has focused on six different days only. There is a need to confirm the relationships observed between the vertical distribution of aerosols and the stability structure by analysing a larger data set.

- During this study, the type and size of aerosols could not be determined from the old LIDAR system. Further inquiries with the new LIDAR will enable researchers to identify the type and size of the aerosols on this region.

- Further investigation of the source/s of high aerosol concentrations in the lower troposphere is needed to determine the relative roles of continental and maritime sources of aerosols.

- Forward trajectory modelling would be appropriate to extend the findings from the horizontal transport patterns of air masses over this region, and to link with similar observations of aerosol profiles over the island of Reunion in the Indian Ocean.

REFERENCES

Andreae, M. O. (1991). Biomass burning: its history, use and distribution and its impact on environmental quality and global climate. In **Global Biomass Burning: Atmospheric, Climate and Biospheric Implications,** edited by J.S. Levine, pp. 3-21, MIT Press, Cambridge, Massachusetts.

Andreae, M. O. (1993). Global distribution of fires seen from space. **Eos,** 74 (12), 129-134.

Andreae, M. O. (1995). Climatic effects of changing atmospheric aerosol levels. In **Future Climates of the World: A Modeling Perspective, World Survey of Climatology**, 16, edited by A. Henderson-Sellers, pp. 347-398, Elsevier, New York.

Andreae, M. O. and Crutzen, P. J. (1997). Atmospheric aerosols: biogeochemical sources and role in atmsopheric chemistry. **Science**, 276, 1052-1058.

Andreae, M. O., Atlas, E., Cachier, H., Cofer, W. R., Harris, W., Helas, G., Koppmann, R., Lacaux, J. P. and Ward, D. E. (1996). Trace gas and aerosol emissions from savanna fires. In **Biomass Burning and Global Change,** edited by J.S. Levine, pp. 278-295, MIT Press, Cambridge, Massachusetts.

Andreae, M. O., Browell, E. V., Garstang, M., Gregory, G. L., Harris, R. C., Hill, G. F., Jacob, D. J., Pereira, M. C., Sachse, G. W., Setzer, A. W., Silva Dias, P. L., Talbot, R. W., Torres, A. L. and Wofsy, S. C. (1988). Biomass-burning emissions and associated haze layers over Amazonia. **Journal of Geophysical Research**, 93(D2), 1509-1527.

Boubel, R. W., Donald, L. F., Stern, A. C. (1994). **Fundamentals of Air Pollution,** pp. 243-318, Academic Press (USA), USA.

Cacciani, M., Girolano, P., di Sarra, A., Fiocco, G. and Fua, D. (1993). Volcanic aerosol layers observed by lidar at South Pole, September 1991 – June 1992. **Geophysical Research Letters**, 20 (9), 807-810.

Cahill, T. A. (1996). Climate forcing by anthropogenic aerosols: the role of PIXE. **Nuclear Instruments and Methods in Physics Research**, B 150, 109-110.

Capaldo, K. P., Kasibhatla, P., and Pandis, S. N. (1999). Is aerosol production within the remote marine boundary layer sufficient to maintain observed concentrations? **Journal of Geophysical Research**, 104(D3), 3483-3500.

Chandra, S. (1993). Changes in stratospheric ozone and temperature due to eruption of Mt. Pinatubo. **Geophysical Research Letters**, 20 (1), 33-36.

Connors, V. S., Cahoon, D. R., Reichle, H. G., Brunke, E., Garstang, M., Seiler, W. and Scheel, H. E. (1991). Savanna burning and convective mixing in southern Africa: Implications for CO emissions and transport. In **Global Biomass Burning: Atmospheric, Climatic and Biospheric Implications,** edited by J.S. Levine, pp. 147-154, MIT Press, Cambridge, Massachusetts.

Cosijn, C. and Tyson, P. D. (1996). Stable discontinuities in the atmosphere over South Africa. **South African Journal of Science,** 92, 381-386.

D'Abreton, P. C. (1996). Lagrangian kinematic and isentropic trajectory models for aerosol and trace gas transport studies in southern Africa. **South African Journal of Science**. 92(3), 157-160.

D'Abreton, P. C., Zunckel, M. and Gondwe, P. M. (1998). Estimating mixing heights over southern Africa using surface-based measurements. **South African Journal of Science**. 94, 375-380.

Dentener, F. J., Carmichael, G. R., Zhang, Y., Lelieveld, J., and Crutzen, P. J. (1996). Role of mineral aerosols as a reactive surface in the global troposphere. **Journal of Geophysical Research**, 101(D17), 22869-22889.

Deshlar, T. and Hofmann, D. J. (1992). Measurements of unusual aerosol layers in the upper troposphere over Laramie, Wyoming in the spring of 1992: evidence for long range transport from the oil fields in Kuwait. **Geophysical Research Letters**, 19 (4), 385-388.

Diab, R. D. (1975). Stability and mixing layer characteristics over southern Africa. Unpublished M.Sc. thesis, University of Natal, Durban.

Diab, R. D. (1977). Weather influences on air pollution potential in southern Africa. Paper presented at the South African Geographical Society Conference, 22-26 June 1976, Bloemfontein, South Africa.

Diab, R. D. (1978). The spatial and temporal distribution of air pollution episode days over Southern Africa. **South African Geographical Journal,** 60(1), 13-22.

Diab, R. D. (1995). Wind Atlas of South Africa. Report to Department of Mineral and Energy Affairs, Pretoria.

Diab, R. D. and Preston-Whyte, R. A. (1995). State of the Environment Report for Durban Metropolitan Area: Air Sector Report, Physical Environmental Department, Durban.

Diab, R. D., Jury, M. R., Combrink, J. and Sokolic, F. (1996). A comparison of anticyclone and trough influences on the vertical distribution of ozone and meteorological conditions during SAFARI-92. **Journal of Geophysical Research**, 101(D19), 23809-23823.

Diab, R. D., Thompson, A. M., Zunkel, M., Coetzee, G. J. R., Combrink, J., Bodeker, G. E., Fishman, J., Sokolic, F., McNamara, D. P., Archer, C. B., Nganga, D. (1996). Vertical ozone distribution over southern Africa and adjacent oceans during SAFARI-92. **Journal of Geophysical Research**, 101(D19), 23823-23835.

Engardt, M. and Rodhe, H. (1993). A comparison between temperature trends and sulfate aerosol pollution. **Geophysical Research Letters**, 20 (2), 117-120.

Fishman, J., James, M. H., Bendura, R. D., Mcnneal, R. J. and Kirchhoff, V. W. J. H. (1996). NASA GTE TRACE A Experiment (September-October 1992): Overview (Paper 96JD00123). **Journal of Geophysical Research**, 101(D19), 23865-23881.

Fuelberg, H. E., Loring, R. O., Watson, M. W., Sinha, M. C., Pickering, K. E., Thompson, A. M., Sachse, G. W., Blake, D. R. and Schoebert, M. R. (1996). TRACE A trajectory intercomparison, 2. Isentropic and kinematic methods. **Journal of Geophysical Research**, 101, 23927-23939.

Garstang, M., Tyson, P. D., Swap, R., Edwards, M., Kallberg, P. and Lindesay, J. A. (1996). Horizontal and vertical transport of air over southern Africa, **Journal of Geophysical Research,** 101, D19, 23721-23736.

Gillette, D. A. and Goodwin, P. A. (1974). Microscale transport of sand sized soil aggregates eroded by wind. **Journal of Geophysical Research**. 79. 4080-4084.

Hao, M. W., Ward, E. D., Oldu, G., Baker, S. P. and Plummer, J. R. (1996). Emission of trace gases from fallow forest and woodland savannas in Zambia. In **Biomass Burning and Global Change,** edited by J. S. Levine, pp. 154-162, MIT Press, Cambridge, Massachusetts.

Haywood, J. M. and Shine, K. P. (1995). The effect of anthropogenic sulphate and soot aerosol on the clear sky planetary radiation budget. **Geophysical Research Letters**, 22 (5), 603-606.

Helas, G., Andreae, M. O., Schebeske, G. and Le Canut, P. (1995). SA'ARI-94: A preliminary view of results. **South African Journal of Science**. 91, 360-363.

IPCC. (1996). Climate Change, 1995. In **The Science of Climate Change**, edited by J. T. Houghton, L. G. Miera Filho, B. A. Callander, N. Harris, A. Kattenburg, and K. Maskell. pp. 350-372, Cambridge University Press, Cambridge.

Justice, C. O., Kendall, J. D., Dowty, P. R., Scholes, R. J. (1996). Satellite remote sensing of fires during the SAFARI campaign using NOAA advanced very high resolution radiometer data. **Journal of Geophysical Research**, 101(D19), 23851-23865.

Kaufman, Y. J., Gitelson, A., Karnieli, A., Ganor, E., Fraser, R. S., Nakajime, T., Mattoo, S. and Holben, B. N. (1994). Size distribution and scattering phase function of aerosol particles retrieved from sky brightness measurements. **Journal of Geophysical Research**, 99 (D5), 10341-10356.

Kemp, D. (1990). **Global Environmental Issues: a climatological approach**, pp. 97-116, Routledge, London.

King, M. D., Kaufman, Y. J., Difier, T. and Nakajima, T. (1999). Remote sensing of tropospheric aerosols from space: past, present, and future. **Bulletin of the American Meteorological Society,** 80 (11), 2229-2259.

Kirkman, G. A. (1998). Aerosols and Trace Gas Distribution Over South Africa. Unpublished MSc. Thesis. University of the Witwatersrand, South Africa.

Kuo, Y., Skumanich, H., Haagenson, P. and Chang, J. (1985). The accuracy of trajectory models as revealed by the observing system simulation experiment. **Monthly Weather Review**, 113, 1852-1867.

Kuppen, R. (1992). The Establishment of a Ground-Based Lidar System at Durban University of Natal. Unpublished MSc. thesis. University of Natal, Durban.

Kuppen, R. (1996). On The Interaction of Laser Beams with Air - with specific reference to refraction and scattering. Unpublished Ph.D. thesis. University of Natal, Durban.

Le Canut, P., Andreae, M. O., Harris, G. W., Wienhold, F. G. and Zenker, T. (1996). Airborne studies of emission from savanna fires in southern Africa: aerosol emission measured with a laser-optical particle counter. **Journal of Geophysical Research,** 101 (D19). 23615-23630.

Lenoble, J. (1991). The particulate matter from biomass burning: A tutorial and critical review of its radiative impact. In J. S. Levine (ed), **Global Biomass Burning**, MIT Press, London, 381-386.

Levine, J. S. (1990). Global biomass burning: Atmospheric, climatic and biospheric implications. **Eos,** 71(37), 1075-1077.

Levine, J. S. (Ed.) (1991). **Global Biomass Burning: Atmospheric, Climatic and Biospheric Implications,** 569pp. MIT Press, Cambridge, Massachusetts.

Li, Z. (1998). Influence of absorbing aerosols on the inference of solar surface radiation budget and cloud absorption. **Journal of Climate**. 11. 6-17.

Lindesay, J. A. (1992). Biomass burning as a factor in atmospheric chemistry and terrestrial ecology. **South African Journal of Science,** 88, 143-144.

Lindesay, J. A., Andreae, M. O., Goldammer, J. G., Harris, G., Annegarn, H. J., Garstang, M., Scholes, R. J. and van Wilgen, B. W. (1996). International Geosphere-Biosphere Programme/International Global Atmospheric Chemistry SAFARI-92 field experiment: Background and overview. **Journal of Geophysical Research**, 101(D19), 23521-23530.

Lindesay, J. A., Harrison, M. S. J. and Haffner, M. P. (1986). The southern oscillation and South African rainfall. **South African Journal of Science,** 82, 196-198.

Menaut, J. C., Abbadie, L., Lavenu, F., Loudjani, P. and Podaire, A. (1991). Biomass Burning in West African Savannas. In J. S. Levine (ed), **Global Biomass Burning**, MIT Press, London, 133-142.

Mitchell, J. F. B., Davis, R. A., Ingram, W. J. and Senior, C. A. (1995). On surface temperature, greenhouse gases and aerosol: models and observation, **Journal of Climate**, 8, 2365-2385.

Moorgawa, A. (1997). Application of scattering and refraction by atmospheric gases. Unpublished MSc. thesis. University of Natal, Durban.

Patterson, E. M. and Gillette, D. A. (1977). Commonalties in measurement size distribution for aerosols having a soil-derived component. **Journal of Geophysical Research**, 82 (15), 2074-2082.

Piketh, S. J., Annegarn, H. J. and Tyson, P. D. (1999a). Lower tropospheric aerosol loading over South Africa: The relative contribution of aeolian dust, industrial emissions, and biomass burning. **Journal of Geophysical Research**, 104(D1), 1597-1607.

Piketh, S. J., Formenti, P., Annegarn, H. J., Tyson, P. D. (1999b). Industrial aerosol characterisation at a remote site in South Africa. **Nuclear Instruments and Methods in Physics Research**, B 150, 350-355.

Piketh, S. J., Swap, R. J., Anderson, C. A., Freiman, M. T. and Held, G. (1999). The Ben Macdhui High Altitude Trace Gas and Aerosol Transport Experiment. **South African Journal of Science**. 95, 35-43.

Pinker, R. T., Ferrare, R. A., Karnieli, A., Aro, T. O., Kaufman, Y. J. and Zangvil, A. (1997). Aerosol optical depths in a semiarid region. **Journal of Geophysical Research**. 102 (D10), 11, 11123-11137.

Pinnick, R. G., Fernandez, G., Martinez-Andazola, E., Hinds, B. D., Hansen, A. D. A. and Fuller, K. (1993). Aerosol in the arid southwestern United States: measurement of mass loading, volatility, size distribution, absorption characteristics, black carbon content and vertical structure to 7km above sea level. **Journal of Geophysical Research**. 98 (D2). 2651-2666.

Preston-Whyte, R. A. (1968). The nature and significance of early morning winter air movement over Durban Bay. **The South African Journal of Science,** 64, 183-186.

Preston-Whyte, R. A. (1969). Sea breeze studies in Natal. **The South African Journal of Science,** 51, 38-43.

Preston-Whyte, R. A. (1970). Land breezes and rainfall on the Natal coast. **The South African Journal of Science,** 52, 38-43.

Preston-Whyte, R. A. (1974). Land breezes and mountain-plain winds over the Natal coast. **The South African Journal of Science,** 56(1), 27-35.

Preston-Whyte, R. A. and Diab, R. D. (1980). Local weather and air pollution: the case of Durban. **Environment Conservation,** 7, 241-244.

Preston-Whyte, R. A. and Tyson, P. D. (1988). **The Atmosphere and Weather of Southern Africa.** Oxford University Press, Cape Town.

Preston-Whyte, R. A., Diab, R. D. and Tyson, P. D. (1976). Towards an inversion climatology of southern Africa: Part I, surface inversions. **South African Geographical Journal,** 58(2), 151-163.

Preston-Whyte, R. A., Diab, R. D. and Tyson, P. D. (1976). Towards an inversion climatology of southern Africa: Part II, non-surface inversions. **South African Geographical Journal,** 59(1), 45-59.

Pruppacher, H. R. and Klett, J. D. (1980). **Microphysics of clouds and precipitation**. Reidel, Dordrecht.

Pye, K. (1987). **Aeolian Dust and Dust Deposits.** Academic Press, London.

Qian, Y., and Giorgi, F. (1999). Interactive coupling of regional climate and sulfate aerosol models over eastern Asia. **Journal of Geophysical Research**, 104(D6), 6477-6499.

Raes, F. (1995). Entrainment of free tropospheric aerosols as a regulating mechanism for cloud condensation nuclei in the remote marine boundary layer. **Journal of Geophysical Research**, 100 (D2), 2893-2903.

Rosenfeld, D. (1999). TRMM observed first direct evidence of smoke from forest fires inhibiting rainfall. **Geophysical Research Letters**, 26 (20), 3105-3108.

Rotstayn, L. D. (1999). Indirect forcing by anthropogenic aerosols: A global climate model calculation of the effective-radius and cloud-lifetime effects. **Journal of Geophysical Research**, 104(D8), 9369-9380.

Russell, P. B., Hobbs, P. V., Stowe, L. L. (1999). Aerosol properties and radiative effects in the United States East Coast haze plume: An overview of the Tropospheric Aerosol Radiative Forcing Observational Experiment (TARFOX). **Journal of Geophysical Research**, 104(D2), 2213-2222.

Schoebel, M. R., Bhartia, P. K. and Hisenrath, E. (1993). Tropical ozone loss following the eruption of Mt. Pinatubo. **Research Letters,** 20 (1), 29-32.

Scholes, R. J., Ward, D. E. and Justice, C. O. (1996). Emissions of trace gases and aerosol particles due to vegetation burning in southern hemisphere Africa. **Journal of Geophysical Research**, 101(D19), 23677-23683.

Shaw, E. G. (1996). **Encyclopedia of Climatology and Weather**. 1. Oxford University Press, London.

Sheridan, P. J., Schnell, R. C., Hoffmann, D. J., Harris, J. M. and Deshler, T. (1992). Electron Microscope Studies of Aerosol Layers with likely Kuwait Origins over Laramie, Wyoming during Spring 1991. **Geophysical Research Letters**, 19 (4). 389-392.

Stern, A. C. (1976). **Air Pollution: Air Pollution, Their Transformation and Transport, edited by** A. C. Stern, chapters 6-8, Academic Press, Inc., New York.

Swap, R. J. and Annegarn, H. J. (1999). Southern African regional science initiative: SAFARI 2000: Science plan.

Swap, R. J. and Tyson, P. D. (1999). Stable discontinuities as determinants of the vertical distribution of aerosols and trace gases in the atmosphere. **South African Journal of Science,** 95, 63-71.

Swap, R., Garstang, M., Macko, S. A. Tyson, P. D., Maenhaut, P., Artaxo, P., Kallberg, P., and Talbot, R. (1996). The long-range transport of southern African aerosols to the tropical south Atlantic. **Journal of Geophysical Research**, 101(D19), 23777-23793.

Taljaard, J. J. (1953). The mean circulation in the lower troposphere over southern Africa. **South African Geographical Journal,** 35, 33-43.

Thompson, A. M., Diab, R. D., Bodeker, G. E., Zunkel, M., Coetzee, G. J. R., Archer, C. B., McNamara, D. P., Pickering, K. E., Combrink, J., Fishman, J., and Nganga, D. (1996). Ozone over southern Africa during SAFARI-92/TRACE A. **Journal of Geophysical Research**, 101(D19), 23793-23809.

Twomey, S. A. (1977). **Atmospheric Aerosols**. Elsevier, New York.

Tyson, P. D. (1964). Berg winds of South Africa. **Weather,** 7-11.

Tyson, P. D. (1968). Southwesterly winds over Natal. **Journal of Geography III**, 3, 237-246.

Tyson, P. D. and Joubert, A. M. (1996). Equilibrium and fully coupled GCM simulations of future southern African climates. **South African Journal of Science,** 92, 471-483.

Tyson, P. D. and Preston-Whyte, R. A. (2000). **The atmosphere and weather of southern Africa**. Oxford University Press, Cape Town.

Tyson, P. D., Diab, R. D. and Preston-Whyte, R. A. (1979). Stability wind roses for southern Africa. **Environmental Studies,** Occasional Paper Number 21.

Tyson, P. D., Garstang, M. and Swap, R. (1996). Large-scale recirculation of air over southern Africa. **Journal of Applied Meteorology,** 35, 2218-2235.

Tyson, P. D., Garstang, M., Swap, R., Kallberg, and Edwards, M. (1999). An Air Transport Climatology for Subtropical Southern Africa. **International Journal of Climatology,** 16. 265-291.

Tyson, P. D., Garstang, M., Swap, R., Kallberg, P. and Edwards, M. (1996). An air transport climatology for subtropical Southern Africa. **International Journal of Climatology**, 16, 265-291.

Tyson, P. D., Kruger, F. J. and Louw, C. W. (1988). Atmospheric pollution and its implication in the eastern Transvaal Highveld. South African National Scientific Programmes Report Number 150, 104-116pp.

Warneck, P. (1988). Chemistry of the natural atmosphere. **International Geophysics Series**, 41, 280-84.

Wolf, M. E., and Hidy, G. M. (1997). Aerosols and climate: Anthropogenic emissions and trends for 50 years. **Journal of Geophysical Research**, 102(D10), 11113-11121.

Woods, D. C., Chuan, R. L., Cofer, W. R. and Levine, J. S. (1991). Aerosol Characterisation in Smoke Plumes from a Wetlands Fire. In J. S. Levine (ed), **Global Biomass Burning**, edited by J. S. Levine, pp. 240-244, MIT Press, Cambridge, Massachusetts.

APPENDIX 1

COMPUTER PACKAGES

1. Hlidar.pas : Written by R. Kuppen (1992)
2. Height.pas : Written by F. Sokolic (1998)
3. Clean.pas : Written by F. Sokolic (1999)

```
Program Lidar4Hercules;

{   This program controls the LIDAR hardware.                              }
{                                                                          }
{   Assembly Language routines by R. Grant (originally for HBASIC) and     }
{   modified for Turbo Pascal Version 6                                    }
{                                                                          }
{   Original Assembly Language routines by R Grant are ProcA - ProcG.      }
{                                                                          }


{$F-} {$O-} {$A+} {$G-} {$R-} {$S-}
{$V-} {$B-} {$X-} {$N-} {$E+} {$D-} {$L-}
{$M 8192,60000,180000}

Uses CRT,Dos,HGUI,Wins2,AutoBGI,AutoFont,Graph,Printer,PHercSc;

Const
    Control = $2BF;
    PortC   = $2BE;
    PortB   = $2BD;        {Ports on Laser Controller Card}
    PortA   = $2BC;
    Count   = 667;         {Number of Counts Recorded}

Var
   Colour  :Boolean;       {Colour Monitor}
   ColFF,
   ColBB,                  {Colours}
   ColF,
   ColB    :Byte;
   P       :^Byte;          {Assembly Language Data Stored Here}
   Drive   :String[2];      {Drive to be used for Data}

Procedure SetColorMode(C:Boolean);
Begin
  Colour:=C;
  If Colour Then
  Begin
    ColF:=14;
    ColB:=9;
    ColFF:=2;
    ColBB:=4;
  End
  Else
  Begin
    ColF:=7;
    ColB:=0;
    ColFF:=7;
    ColBB:=0;
  End
End;

Procedure DoHercAxis;        {Draw an axis on a Hercules Screen}
Const
  B=66.7;

Var
  I   :Byte;
  X   :Word;
  Temp:String;

Begin
  Line (52,0,52,300);
```

```
  Line (52,300,719,300);
  For I:=0 to 5 do
  Begin
    Line(50,I*50,54,I*50);
    If I=0 Then Temp:='' Else Str(300-I*50:3,Temp);
    OutTextXY(20,I*50-4,Temp);
  End;
  SetTextStyle(DefaultFont,VertDir,1);
  OutTextXY(10,120,'Counts');
  SetTextStyle(DefaultFont,HorizDir,1);
  For I:=1 to 10 do
  Begin
    X:=52+Trunc(I*B+0.5);
    Str(I*10,Temp);
    OutTextXY(X-6,306,Temp);
    Line(X,298,X,302);
  End;
  OutTextXY(52,306,'0');
  OutTextXY(330,320,'Altitude (km)');
End;

Procedure ProcA;       {Assembly Proc A - Configure the PCS}
Label
    Config,
    Settle,
    Wind_Up;

Var
    W1,
    W2  :Word;       {New Data Address}

Begin
  W1:=Seg(P^);
  W2:=Ofs(P^);

  Asm

    CONFIG:
            mov          es,W1
            mov          di,W2

            MOV AL,10010010B
            MOV DX,Control
            OUT DX,AL            {A,B INPUT C OUTPUT MODE 0}
            MOV DX,PortC
            MOV AL,11011111B
            OUT DX,AL
            MOV AL,11011110B     {TRIGGER GDL ON}
            OUT DX,AL
            MOV AL,11011111B
            OUT DX,AL
            MOV DX,PortB

    SETTLE:
            IN AL,DX
            AND AL,00000100B  {WAIT FOR GDL TO REACH ZERO AND GATE OFF}
            JNZ SETTLE

            MOV AL,11001101B
            {C=0, R/W=R B=0 SO ADD COUNTER CAN COUNT WE BAR HI}
            MOV DX,PortC
            OUT DX,AL
            MOV AL,11011111B  {PARALLEL LOAD ADD COUNTER WITH 0000}
            OUT DX,AL         {PULSE COUNTER BUFFERS TRI-STATE COUNT UP}
```

```
              MOV CX,Count

     WIND_UP:
              MOV AL,11010111B
              OUT DX,AL
              MOV AL,11011111B        {GENERATE COUNTER ADDRESS}
              OUT DX,AL
              LOOP WIND_UP

              CLD                  {COUNT UP WITH DI REGISTER}
              MOV CX,Count         {CLEAR DATA AREA SINCE DATA IS ADDED TO IT}
              MOV AX,0
              REP STOSW

              MOV AL,00111101B
              OUT DX,AL            {C=B=0 R/W=W ENABLE PULSE COUNTER BUFFERS}
              MOV AL,00111111B        {COUNT DOWN}
              OUT DX,AL

   End;
End;

Procedure ProcB;      {Reads the PCS RAM and Stores the data in P^}
Const                 {It also calculates the Figure of Merit}
    TopNinety = 600;
    Most      = 15;

Label
    Config,
    Read,
    Check,
    Test,
    Combine,
    Garbage,
    Quit;

Var
   NewDS,
   Storage,
   TempStore,
   Flag       : Word;

Begin
  NewDS:=Seg(P^);
  Storage:=Ofs(P^);
  TempStore:=Ofs(P^)+$800;
  Flag:=Ofs(P^)+$FFF;

  Asm
    CONFIG:
             push  ds
             mov   ax,NewDS
             mov   ds,ax

             MOV AL,11111101B     {ENABLE BUFFER TO READ}
             MOV DX,PortC
             OUT DX,AL            {DISABLE BOTH COUNTER BUFFERS}
             MOV AL,11011111B     {STATE OF C= R/W IS IRRELEVANT}
             OUT DX,AL

             MOV CX,Count
             MOV BX,TempStore     {POINT BX REG AT STORAGE FOR DATA}
             MOV DX,PortA
```

```
    READ:
            IN AL,DX            {GET BYTE FROM GDL RAM}
            MOV [BX],AL         {STORE RAW DATA}
            INC BX              {POINT BX AT NEXT LOCATION; BYTES REMEMBER}
            MOV AL,11010111B
            MOV DX,PortC
            OUT DX,AL
            MOV AL,11011111B
            OUT DX,AL           {INCREMENT ADDRESS, COUNT UP}
            MOV DX,PortA
            LOOP READ

    CHECK:
            MOV CX,TOPNINETY    {CHECK HIGHEST 600 COUNTS IE TOP 90 KM OF AIR}
            mov bx,TempStore    {POINT BX AT START OF RAW DATA IGNORE FIRST}
            add bx,4            {4 BYTES THE FIRST OF WHICH COLLECTS NOISE}
            MOV AL,MOST         {NO MORE THAN "MOST" COUNTS ALLOWED PER USEC}
    TEST:
            CMP AL,[BX]
            JS GARBAGE          {IF COUNTS MORE THAN MAX ALLOWED THEN QUIT}
            INC BX              {POINT AT NEXT LOCATION}
            LOOP TEST
            XOR AH,AH
            MOV BX,Flag
            MOV [BX],AH         {DATA IS OK SO CLEAR FLAG}

            MOV SI,TempStore
            MOV DI,Storage
            MOV CX,Count

    COMBINE:
            MOV AL,[SI]       {GET RAW DATA AS BYTES}
            ADD [DI],AX       {ADD TO OLD DATA AS WORDS}
            INC SI              {POINT AT NEXT RAW DATA BYTE}
            INC DI
            INC DI              {POINT AT NEXT GOOD DATA WORD IN STORAGE}
            LOOP COMBINE
            JMP QUIT            {FINISHED}

    GARBAGE:
            MOV AL,0AAH
            MOV BX,Flag
            MOV [BX],AL         {DATA WAS GARBAGE SO SET FLAG TO TELL BASIC}

    QUIT:
            pop     ds
  End;
End;

Procedure ProcC; Assembler;     {Wait for Laser to Fire.  Wait until end of}
Label                           {the PCS countdown}
   Config,
   Loop1;

Asm
  CONFIG:
          MOV DX,PortC
          MOV AL,00111111B    {COUNTERS TO COUNT DOWN}
          OUT DX,AL           {WHEN LASER TRIGGERS GDL}
          MOV DX,PortB
  LOOP1:
          IN AL,DX
          AND AL,00000100B    {WAIT FOR B2 TO GO HI}
          JZ LOOP1
```

```
End;

Procedure ProcD;        {Triggers the PCS On and Waits for End of PCS countdown
Label
     Config,
     Poll;

Begin
  Asm
    CONFIG:

            MOV DX,PortC
            MOV AL,00111110B
            OUT DX,AL
            MOV AL,00111111B        {GATE CLOCK ON}
            OUT DX,AL

            MOV DX,PortB

    POLL:
            IN AL,DX
            AND AL,00000100B        {WAIT FOR B2 TO GO LO IE FOR GDL TO FINISH}
            JNZ POLL                {ITS COUNTDOWN}

  End;
End;

Procedure ProcE;      {Plots the data stored in P^ to a Hercules Screen}

Const
   Screen = $B000;

Label
   Config,
   Draw,
   Okay,
   Start1;

Var
   NewSeg,
   Storage:Word;

Begin

  NewSeg :=Seg(P^);
  Storage:=Ofs(P^);

  Asm


    CONFIG:
           push   ds
           mov    ds,NewSeg
           MOV AX,Screen
           MOV ES,AX          {POINT ES AT THE SCREEN}
           MOV CX,Count       {NUMBER OF POINTS TO BE PLOTTED}
           SUB CX,3           {DO THIS TO SKIP THE LOWEST ALTITUDE COUNTS-}
                              {(GARBAGE)}
           MOV SI,Storage     {POINT SI AT START OF DATA}
           ADD SI,Count      {POINT SI AT LAST COUNT STORED IE FIRST RESULT TAKEN
           ADD SI,Count       {THEY ARE WORDS REMEMBER!}
           SUB SI,8           {POINT SI AT LAST LOCATION WRITTEN TO LESS TWO}
                              {AND SKIP THREE LOWEST ALTITUDE COUNTS}
           MOV AX,55          {X CO-ORD OF FIRST RESULT TO BE PLOTTED}
```

```
                    {(X=52 IS X AXIS)}
        MOV BX,300
        SUB BX,[SI]     {GENERATE FIRST Y VALUE IN BX (300-ACTUAL VALUE)}
                        {PLOT THE POINT IF [SI] LESS THAN 300}
        JNS Draw       {OTHERWISE LET THE POINT BE AT THE TOP OF THE SCREEN}
        XOR BX,BX       {SO SET BX = 0}

DRAW:

                    {PLOT THE POINT AX HAS X VALUE, BX HAS Y VALUE}

        { * * Start PROC Dot_Plot * * }
        { R. Grant had a separate Dot_Plot PROC here }

        push dx
        PUSH CX
        PUSH BX
        PUSH AX
        PUSH AX         {SAVE X VALUE ON THE STACK}
        PUSH BX         {SAVE Y VALUE ON THE STACK}
        AND BX,0003     {CALCULATE (Y MOD 4))
        MOV CX,BX       {PLACE INTO CL WITH 00 IN CH}
        INC CL          {MAKE SURE CL > 0}
        MOV BX,-2000H {IF (YMOD4)=0 THEN BX MUST BE 0}

START1:
        ADD BX,2000H
        LOOP START1     {CALCULATE 2000H * (Y MOD 4) AND PLACE IN BX}
        POP AX          {PUT Y COUNT INTO AX}
        SHR AX,1
        SHR AX,1        {PUT INTEGER Y/4 INTO AX}
        mov  dl,90
        mul  dl         {CALC 90*INTEGER(Y/4), RESULT IN AX}
        MOV DI,AX       {PLACE RESULT IN DI}
        POP AX          {PUT X VALUE IN AX}
        MOV CL,AL       {PLACE 8 LOWEST BITS IN CL}
        AND CL,00000111B {CALC XMOD8 IN CL}
        SHR AX,1
        SHR AX,1        {CALCULATE INTEGER X/8 IN AX}
        SHR AX,1
        ADD BX,AX       {ADD NEXT COMPONENT OF ADDRESS TO BX}
        MOV AL,10000000B
        SHR AL,CL       {PUT A 1 IN (7-XMOD8) BIT}
        OR  ES:[BX+DI],AL {TURN THE BIT ON}
        POP AX
        POP BX          {RESTORE CO-ORDS OF THE DOT PLOTTED}
        POP CX
        pop dx
                        {RESTORE INNOCENT REGISTERS}

        { * * End PROC DotPlot * * }

        DEC SI
        DEC SI          {POINT SI AT NEXT COUNT}
        MOV BX,300
        SUB BX,[SI]     {GENERATE NEXT DATA}
        JNS OKAY
        XOR BX,BX       {AGAIN LET POINT BE AT THE TOP OF THE SCREEN}
OKAY:
        INC AX          {GENERATE NEXT X VALUE}
        LOOP Draw

        pop ds
```

```
    { AX CONTAINS X VALUE BETWEEN 0 AND 719}
    { BX CONTAINS Y VALUE BETWEEN 0 AND 347}

  End;
End;

Procedure ProcG;    {Read and Subtract PCS Ram}

Label
   Config,
   Read,
   Okay;

Var
   NewSeg,
   NewOfs :Word;

Begin

  NewSeg :=Seg(P^);
  NewOfs :=Ofs(P^);

  Asm

    CONFIG:
            push  ds
            mov   ds,NewSeg

            MOV AL,11111101B      {ENABLE BUFFER TO READ}
            MOV DX,PortC
            OUT DX,AL             {DISABLE BOTH COUNTER BUFFERS}
            MOV AL,11011111B      {STATE OF C= R/W IS IRRELEVANT}
            OUT DX,AL

            MOV CX,COUNT
            MOV BX,NewOfs         {POINT BX REG AT STORAGE FOR DATA}
            MOV DX,PortA

    READ:
            IN AL,DX          {GET BYTE FROM GDL RAM}
            MOV AH,0          {CLEAR MOST SIG. WORD}
            SUB AX,[BX]       {SUBTRACT LAST DATA TO SUBTRACT DARK CURRENT}
            JNS OKAY          {NEVER LET THE PHOTON COUNT MINUS}
            XOR AX,AX         {NOISE BE LESS THAN ZERO}

    OKAY:
            MOV [BX],AX       {STORE NEW DATA}
            INC BX
            INC BX              {POINT BX AT NEXT LOCATION}
            MOV AL,11010111B
            MOV DX,PortC
            OUT DX,AL
            MOV AL,11011111B
            OUT DX,AL           {INCREMENT ADDRESS, COUNT UP}
            MOV DX,PortA
            LOOP READ

  End;
End;

Procedure ProcH; Assembler;    {Reconfigure PCS Hardware}

Label
   Config,
```

```
    Settle,
    Wind_Up;

Asm

  CONFIG:

          MOV AL,10010010B
          MOV DX,CONTROL
          OUT DX,AL          {A,B INPUT C OUTPUT MODE 0}
          MOV DX,PortC
          MOV AL,11011111B
          OUT DX,AL
          MOV AL,11011110B   {TRIGGER GDL ON}
          OUT DX,AL
          MOV AL,11011111B
          OUT DX,AL
          MOV DX,PortB

  SETTLE:
          IN AL,DX
          AND AL,00000100B   {WAIT FOR GDL TO REACH ZERO AND GATE OFF}
          JNZ SETTLE

          MOV AL,11001101B
          {C=0, R/W=R B=0 SO ADD COUNTER CAN COUNT WE BAR HI}
          MOV DX,PortC
          OUT DX,AL
          MOV AL,11011111B
          OUT DX,AL          {PULSE COUNTER BUFFERS TRI-STATE COUNT UP}

          MOV CX,COUNT

  WIND_UP:
          MOV AL,11010111B
          OUT DX,AL               {DX STILL HAS PORT C ADDRESS}
          MOV AL,11011111B        {GENERATE COUNTER ADDRESS}
          OUT DX,AL
          LOOP WIND_UP

          MOV AL,00111101B
          OUT DX,AL          {C=B=0 R/W=W ENABLE PULSE COUNTER BUFFERS}
          MOV AL,00111111B       {COUNT DOWN}
          OUT DX,AL

End;

Procedure Once;    {Test Hardware Once}
Var
  C:Char;

Begin
  InitHerc('');

  Repeat
    ProcA;
    ProcD;
    ProcB;
    ProcE;
    Repeat
      C:=PutString(100,100,'Run Once (A)gain or Quit to (M)enu?');
    Until C in ['A','M'];
  Until C='M';
  CloseGraph;
```

```
End;

Procedure WriteZone(At:Word;NewVal:Byte);

{   Writes the value NewVal At bytes into the Variable P^.                    }

Var
   T:^Byte;
   OldT:Pointer;

Begin
  New(T);
  OldT:=T;
  T:=Ptr(Seg(P^),Ofs(P^)+At);
  T^:=NewVal;
  T:=OldT;
  Dispose(T);
End;

Function ReadZone(At:Word):Word;

{ Reads the byte At bytes into the P^ data. }

Var
   T:^Byte;
   OldT:Pointer;

Begin
  New(T);
  OldT:=T;
  T:=Ptr(Seg(P^),Ofs(P^)+At);
  ReadZone:=T^;
  T:=OldT;
  Dispose(T);
End;

Procedure SaveData(Batch:Word;Pulse:Word); {Save P^}
Var
  Temp:String;
  F   :File;
  Err :Word;

Begin
  {$I-}
  WriteZone(2*667+1,Pulse Div 256);
  WriteZone(2*667,Pulse - Pulse Div 256);
  Str(Batch,Temp);
  Temp:=Concat(Drive,'BATCH',Temp);
  Assign(F,Temp);
  Rewrite(F,1);
  Err:=IOResult;
  If Err>0 Then Exit;
  BlockWrite(F,P^,1402);
  Close(F);
  Err:=IOResult;
  {$I+}
End;

Procedure ShowDateTime;    {Display Date and Time}

Const
   Day:Array[0..6] of String[9] = ('Sunday','Monday','Tuesday',
                                   'Wednesday','Thursday','Friday','Saterday')
   Month:Array[1..12] of String[9] = ('January','February','March','April',
```

```
                                        'May','June','July','August',
                                        'September','October','November',
                                        'December');

Var
   A,B,C,D:Word;

Begin
  GetDate(A,B,C,D);
  WriteLn(Day[D],', ',C,' ',Month[B],', ',A,'.');
  WriteLn;
  GetTime(A,B,C,D);
  WriteLn(A,':',B,':',C,'.');
End;

Function PlotOptions(Var Dump,Pulse:Word):Boolean;
{Returns False if user wants to abort to menu}

{    Options Menu given to the user during / after the graph is          }
{    being plotted.                                                      }

Var
   SS:Pointer;
    C:Char;

   Procedure ViewNumbers;   {Show P^ Data}
   Var
      StrN,
      Temp  :String[40];
      X,
      Y,
      Z,
      Marker:Word;

   Begin
     Marker:=2*667;
     Repeat
       X:=Marker;
       Y:=0;
       Z:=Marker Div 2;
       Z:=667-Z;
       Repeat
         Str(Z:3,StrN);
         Str(256*ReadZone(X+1)+ReadZone(X):6,Temp);
         Temp:=Concat(StrN,'. ',Temp);
         OutTextXY(330,120+10*Y,Temp);
         Dec(X,2);
         Inc(Y);
         Inc(Z);
       Until X=Marker-30;
       C:=Readkey;
       If Keypressed Then C:=ReadKey;

       If C='Q' Then
       Begin
         If Marker>34 Then Dec(Marker,30) Else Marker:=30;
       End
       Else
       If C='I' Then
       Begin
         If Marker<2*643 Then Inc(Marker,30) Else Marker:=2*667;
       End;
       If C='O' Then Marker:=30;
       If C='G' Then Marker:=2*667;
```

```
      Bar(316,116,580,266);
    Until C=#27;
  End;

  Procedure PrintNumbers;     {Print P^ Data}
  Var
    I,
    X:Word;
    StrN,
    Temp:String[80];

  Begin
    OutTextXY(370,130,'Print Numerical Data');
    OutTextXY(330,200,'Press (Esc) to abort, any');
    OutTextXY(330,215,'other key continues.');
    C:=ReadKey;
    If C=#27 Then
    Begin
      Bar(316,116,580,265);
      Exit;
    End;
    Bar(330,200,550,230);
    OutTextXY(330,210,'Printing, Please Wait.');

    I:=2*667;
    X:=0;
    Repeat
      Str(256*ReadZone(I+1)+ReadZone(I),Temp);
      Str(X,StrN);
      Temp:=Concat(StrN,'. ',Temp);
      WriteLn(Lst,Temp);
      Dec(I,2);
      Inc(X);
    Until I=0;

    Bar(316,116,580,265);
  End;

  Procedure Dump2Disk;        {Save P^ Dump}
  Var
     T2,
     T1 :String[20];
     F  :File;

  Begin
    {$I-}
    Inc(Dump);
    Str(Dump,T1);
    Str(Pulse,T2);
    T1:=Concat(Drive,'D',T1,'P',T2);
    WriteZone(2*667+1,Pulse Div 256);
    WriteZone(2*667,Pulse-(Pulse Div 256));
    Assign(F,T1);
    Rewrite(F,1);
    BlockWrite(F,P^,1402);
    Close(F);
    {$I+}
  End;

Begin
  GetMem(SS,50000);
  GetImage(300,100,600,280,SS^);
  SetFillStyle(SolidFill,0);
  Bar(300,100,600,280);
```

```
    Box(310,110,590,270,15,15,2);
    Repeat
      OutTextXY(420,120,'Options');
      OutTextXY(320,140,'1 Continue');
      OutTextXY(320,150,'2 Save / Menu');
      OutTextXY(320,160,'3 Print Screen');
      OutTextXY(320,170,'4 Dump to Disk');
      OutTextXY(320,180,'5 View Numerical Data');
      OutTextXY(320,190,'6 Numerical Data Print');
      C:=Upcase(ReadKey);
      Bar(316,116,580,265);
      Case C Of
         '2':Begin
               PlotOptions:=True;
               FreeMem(SS,50000);
               Exit;
             End;
         '3':Begin
               PutImage(300,100,SS^,CopyPut);
               ProcF;
               Bar(300,100,600,280);
               Box(310,110,590,270,15,15,2);
             End;
         '4':Dump2Disk;
         '5':ViewNumbers;
         '6':PrintNumbers;
      End;
    Until C in ['1','C'];

    PutImage(300,100,SS^,CopyPut);
    FreeMem(SS,50000);
    PlotOptions:=False;
  End;

  Procedure LIDARSys;

  {   Offer the user the options and then start the LIDAR plot.                }

  Var
     Temp     :String;
     T        :LongInt;
     C,
     Trig,
     Noise    :Char;
     Dump,
     Batch,
     B2,
     Pulse,
     Rejects,
     Merit,
     OldMerit,
     Wait,
     Code,
     BatchTot,
     PulseTot:Word;
     Quit     :Boolean;

  Begin
    Quit:=False;
    Merit:=0;
    Rejects:=0;
    Pulse:=0;
    Batch:=1;
    Dump:=0;
```

```
BackShade(1,2,80,24,177);
ShadowBox(10,8,70,15,176);          {Open Box}
ClearBottom(ColFF,ColBB);
VideoColor(ColBB,ColFF);
GotoXY(11,9);
Pad(19,32);
Write('Run the LIDAR System');              {Heading}
Pad(20,32);
GotoXY(2,24);
Write('Select the options you require.  [Esc] for Default Values.');
VideoColor(ColF,ColB);

GotoXY(12,11);
Write('Number of Pulses to be Integrated (50) : ');                    {Prompt}
GetString(WhereX,WhereY,4,True,Temp);          {Get Temp String}
If Length(Temp)>0 Then
Begin
   Val(Temp,T,Code);
   If (T>0) And (T<9999) Then
     PulseTot:=T
   Else
     PulseTot:=50;
End
Else
  PulseTot:=50;

GotoXY(12,13);
Write('(S)ubtract Noise or (A)llow Counts to Accumulate (A) : ');
GetString(WhereX,WhereY,1,True,Temp);          {Get Temp String}
If Length(Temp)>0 Then
Begin
  If Temp[1] in ['A','S'] Then
    Noise:=Temp[1]
  Else
    Noise:='A';
End
Else
  Noise:='A';

GotoXY(12,11);
Pad(56,32);
GotoXY(12,13);
Pad(56,32);

GotoXY(12,11);
Write('Number of Data Batches to be Taken (1) : ');                    {Prompt}
GetString(WhereX,WhereY,4,True,Temp);          {Get Temp String}
If Length(Temp)>0 Then
Begin
   Val(Temp,T,Code);
   If (T>0) And (T<9999) Then
     BatchTot:=T
   Else
     BatchTot:=1;
End
Else
  BatchTot:=1;

GotoXY(12,13);
Write('(C)omputer Trigger or (E)xternal Trigger (E) : ');          {Prompt}
GetString(WhereX,WhereY,1,True,Temp);          {Get Temp String}
If Length(Temp)>0 Then
Begin
  If Temp[1] in ['C','E'] Then
```

```
      Trig:=Temp[1]
    Else
      Trig:='E';
  End
  Else
    Trig:='E';

  GotoXY(12,11);
  Pad(56,32);
  GotoXY(12,13);
  Pad(56,32);

  If Trig='C' Then
  Begin
    GotoXY(12,13);
    Write('Trigger Delay Between Pulses in Seconds (1) : ');        {Prompt}
    GetString(WhereX,WhereY,2,True,Temp);          {Get Temp String}
    If Length(Temp)>0 Then
    Begin
       Val(Temp,T,Code);
       If (T>0) And (T<60) Then
         Wait:=1000*T       {Number of milliseconds}
       Else
         Wait:=1000;
    End
    Else
      Wait:=1000;

    GotoXY(12,13);
    Pad(56,32);
  End;

  GotoXY(12,11);
  WriteLn('Insert your Data Disk in '+Drive+' and press a key');
  GotoXY(12,13);
  WriteLn('Press any key during the display for options.');
  C:=ReadKey;

  InitHerc('');

  Repeat
    ClearDevice;
    DoHercAxis;
    OutTextXY(240,338,'Pulse 0   of Batch         0 Rejects.');
    OutTextXY(10,338,'Sum:      Dif:');
    SetFillStyle(SolidFill,0);
    Bar(388,338,439,346);
    Str(Batch,Temp);
    Temp:=Concat(Temp,'.');
    OutTextXY(394,338,Temp);

    ProcA;

    Repeat

      If Trig='C' Then
      Begin
        Delay(Wait);
        Port[688]:=170;    {Fire Laser}
        Delay(10);
        Port[688]:=0;
      End
      Else
        ProcC;
```

```
      Repeat
        B2:=Port[701] And 4;
      Until B2<>4;

      ProcB;

      OldMerit:=Merit;
      Merit:=ReadZone($FFC)+256 * ReadZone($FFD);
      WriteZone($FFC,0);
      WriteZone($FFD,0);
      Bar(44,338,84,346);
      Bar(124,338,164,346);
      Str(Merit,Temp);
      OutTextXY(44,338,Temp);
      Str(Merit-OldMerit,Temp);
      OutTextXY(124,338,Temp);

      If ReadZone($FFF)<>0 Then
      Begin
        Inc(Rejects);
        Bar(440,338,468,346);
        Str(Rejects,Temp);
        OutTextXY(440,338,Temp);
        ProcH;
      End
      Else
      Begin
        If Noise='S' Then
        Begin
          ProcD;
          ProcG;
        End;
        ProcE;
        Inc(Pulse);
        Bar(280,338,318,346);
        Str(Pulse,Temp);
        OutTextXY(288,338,Temp);
      End;
      If Keypressed Then Quit:=PlotOptions(Dump,Pulse);
    Until (Pulse=PulseTot) Or Quit;
    SaveData(Batch,Pulse);
    Quit:=PlotOptions(Dump,Pulse);
    Pulse:=0;
  Until (Batch=BatchTot) or Quit;
  CloseGraph;
  WriteLn;
  WriteLn(BatchTot,' Batches of ',PulseTot,' Pulses Completed.');
  WriteLn;
  ShowDateTime;
  WriteLn;
  WriteLn('Press any key.');
  Temp[1]:=Readkey;
End;

Procedure ChangeDrive;    {Change Storage Drive}
Var
   C:Char;

Begin
  ClearBottom(ColFF,ColBB);
  VideoColor(ColBB,ColFF);
  GotoXY(2,24);
  Write('Enter the new Drive Letter:');
```

```
  C:=UpCase(ReadKey);
  If C in ['A'..'Z'] Then Drive[1]:=C;
End;

Procedure Options;
{Setup options for this program}

Var
   Choices      :MenuArray;        {Possible Coices }
   UserChoice   :Byte;             {Number of Choice}

Begin
  Drive:='A:';
  Choices[1]:='1 Run the Hardware Once';
  Choices[2]:='2 Run the LIDAR System';
  Choices[4]:='4 Quit';
  Choices[5]:='';

  Repeat                                {Until User Selects 'Quit'}
    Choices[3]:='3 Change Drive from '+Drive;
    CursorSize($20,$20);
    ClearBottom(ColFF,ColBB);
    VideoColor(ColF,ColB);
    BackShade(1,2,80,23,177);           {Remove any old message boxes}
    ShadowBox(37,8,76,18,176);          {Open a new Box}
    VideoColor(ColBB,ColFF);                        {Reverse}
    GotoXY(2,24);
    Write('Press either the number of your choice, or use the cursor keys.');
    GotoXY(1,1);
    Write(' LIDAR Control Centre     Ver 2.00     ');
    GotoXY(38,9);
    Pad(14,32);
    Write('Main  Menu');                {Display heading for this box}
    Pad(14,32);

    UserChoice:=Menu(ColF,ColB,40,12,1,36,Choices);
    {Goto the menu and get a choice}
    Case UserChoice Of
      1:Once;
      2:LIDARSys;
      3:ChangeDrive;
    End;    {End Case}
  Until UserChoice=4     {Stop giving the menu when user selects 'Quit'}

End;  {Options}

Begin                                   {Start Main Program}
  UseHerc;                              {Use a Hercules Video Card}
  GetMem(P,8192);                       {Reserve Memory for Assembly Procs}
  SetColorMode(True);
  If ParamCount>0 Then
    If (ParamStr(1)='/m') Or (ParamStr(1)='/M') Then
      SetColorMode(False);
  VideoColor(7,0);
  ClrScr;                               {Clear Screen}
  CursorSize ($20,$20);
  Options;                              {Go to the Menu}
  VideoColor(7,0);
  ClrScr;
  CursorSize (CSizeMax-2,CSizeMax-1);
End.                                    {End Main Program}
```

```
program CalculateHeight;

    (*************************************************************************)
    (* This program calculates heights of pressure surfaces from             *)
    (* temperature, pressure and humidity readings. It is based on a BASIC   *)
    (* program supplied by Miloud Bessafi from the University of Reunion.    *)
    (*                                                                       *)
    (* Input:  The input for the program must be in a text file with air     *)
    (*         pressure, temperature, humidity and dew point temperature     *)
    (*         in the first 4 columns. The contents of the other columns     *)
    (*         (if any) are unimportant.                                     *)
    (*                                                                       *)
    (* Output: The output is the same as the input except that the height    *)
    (*         reading is inserted in column 5. The output file will over-   *)
    (*         write the input file.                                         *)
    (*                                                                       *)
    (* Usage:  HEIGHT <input filename>                                       *)
    (*                                                                       *)
    (* Written by: Frank Sokolic                                             *)
    (*             Geographical and Environmental Sciences                   *)
    (*             University of Natal                                       *)
    (*             Durban                                                    *)
    (*                                                                       *)
    (* Compiler: Turbo Pascal  Version 7.0                                   *)
    (*                                                                       *)
    (* Date: March 1996                                                      *)
    (*************************************************************************)

const
  StationHeight = 14;  (* Height of Durban International Airport *)
  Path = 'C:\USER\';

var
  Source  : text;
  Dest    : text;
  DataStr : string;
  POld    : real;
  TOld    : real;
  UOld    : real;
  TdOld   : real;
  ZOld    : real;
  PNew    : real;
  TNew    : real;
  UNew    : real;
  TdNew   : real;
  ZNew    : real;

(*****************************************************************************)

function Power (Base, Pwer: real): real;

begin
  Power := exp (Pwer * ln(Base));
end;  (* end of function Power *)

(*****************************************************************************)

function FnTv (P, T, U : real) : real;

    (*************************************************************************)
    (* This function calculates the virtual temperature in Kelvin at the     *)
    (* Pressure P, temperature T and humidity U.                             *)
    (*************************************************************************)

var
  E  : real;
  Ew : real;
  Tk : real;
  W  : real;

begin
  Tk   := T + 273.15;
  Ew   := 6.1078 * Power (10, ((7.5 * T / (237.3 + T))));
  E    := Ew * (U / 100);
  W    := 0.622 * E / (P - E);
  FnTv := Tk * (1 + W / 0.622) / (1 + W);
end;
```

```
(*****************************************************************************)

function FnDZtr (P1, T1, U1, P2, T2, U2 : real) : real;

    (*************************************************************************)
    (* This function calculates the thickness of a layer by using the       *)
    (* hypsometric equation.                                                 *)
    (*                                                                       *)
    (* Inputs:                                                               *)
    (* P1, T1 and U1 are the pressure, temperature and humidity at the       *)
    (* bottom of the layer                                                   *)
    (* P2, T2 and U2 are the pressure, temperature and humidity at the top   *)
    (* of the layer                                                          *)
    (* P1 and P2 are in hPa                                                  *)
    (* T1 and T2 are in degrees Celsius                                      *)
    (* H1 and H2 are in %                                                    *)
    (*                                                                       *)
    (* Output:                                                               *)
    (* The thickness of the layer                                            *)
    (*************************************************************************)

var
  Tv1 : real;  (* Virtual temperature at P1 *)
  Tv2 : real;  (* Virtual temperature at P2 *)
  Tv  : real;  (* Mean virtual temperature for the layer *)
  Ra  : real;  (* Gas constant                           *)
  g   : real;  (* Acceleration due to gravity            *)

begin
  (* assign constants *)
  Ra := 287.05;  (* J/deg/kg *)
  g  := 9.806;   (* m/s^2    *)

  (* Calculate the mean virtual temperature for the layer *)
  Tv1 := FnTv(P1, T1, U1);
  Tv2 := FnTv(P2, T2, U2);
  Tv  := (Tv1 + Tv2) / 2;

  (* Calculate the thickness of the layer *)
  FnDZtr := Ra / g * Tv * ln(P1 / P2);
end;

(*****************************************************************************)

begin
  assign  (Source, path + paramstr(1) + '.SIG');
  reset   (Source);
  assign  (Dest, 'TEMPFILE');
  rewrite (Dest);
  readln (Source, POld, TOld, UOld, TdOld, DataStr);
  ZOld := StationHeight;
  writeln (Dest, POld:6:1, TOld:6:1, UOld:5:0, TdOld:6:1, ZOld:6:0, DataStr);
  while NOT (eof (Source)) do
    begin
      readln (Source, PNew, TNew, UNew, TdNew, DataStr);
      ZNew := ZOld + FnDZtr (POld, TOld, UOld, PNew, TNew, UNew);
      ZOld := ZNew;
      POld := PNew;
      TOld := TNew;
      UOld := UNew;
      writeln (Dest, PNew:6:1, TNew:6:1, UNew:5:0, TdNew:6:1, ZNew:6:0, DataStr);
    end;
  close (Source);
  close (Dest);
  erase (Source);
  rename (Dest, path + paramstr(1) + '.SIG');
end.
```

```
program CleanData;

var
 source, Dest: text;
 DataStr : string [65];
 Counter : longint;
 NoDataPos : integer;

begin
  assign (Source, paramstr(1));
  reset (Source);
  assign (Dest, paramstr(2));
  rewrite (Dest);
  Counter := 1;
  repeat
    read (Source, DataStr);

    (* replace ********** with ***** *)
    while (Pos('**********', DataStr) > 0) do
      begin
        NoDataPos := (Pos ('**********', DataStr));
        delete (DataStr, NoDataPos, 10);
        insert ('       NaN', DataStr, NoDataPos);
      end;

    (* replace ***** with NaN *)
    while (Pos('*****', DataStr) > 0) do
      begin
        NoDataPos := (Pos ('*****', DataStr));
        delete (DataStr, NoDataPos, 5);
        insert ('  NaN', DataStr, NoDataPos);
      end;

    (* replace bar with space *)
    while (Pos('|', DataStr) > 0) do
      begin
        NoDataPos := (Pos ('|', DataStr));
        delete (DataStr, NoDataPos, 1);
        insert (' ', DataStr, NoDataPos);
      end;

    (* replace / with nothing *)
    while (Pos('/', DataStr) > 0) do
      begin
        NoDataPos := (Pos ('/', DataStr));
        delete (DataStr, NoDataPos, 1);
      end;

    write (Dest, DataStr);
    if (Counter/10000 = Counter div 10000)
      then writeln ('processed ' , Counter, ' lines');
    inc (Counter);
  until (eof (Source));
  close (Source);
  close (Dest);
end.
```

```
program CleanData;

var
 source, Dest: text;
 DataStr : string [81];
 Counter : longint;
 NoDataPos : integer;

begin
  assign (Source, paramstr(1));
  reset (Source);
  assign (Dest, paramstr(2));
  rewrite (Dest);
  Counter := 1;
  repeat
    read (Source, DataStr);

    (* replace ********** with ***** *)
    while (Pos('**********', DataStr) > 0) do
      begin
        NoDataPos := (Pos ('**********', DataStr));
        delete (DataStr, NoDataPos, 10);
        insert ('       NaN', DataStr, NoDataPos);
      end;

    (* replace ***** with NaN *)
    while (Pos('*****', DataStr) > 0) do
      begin
        NoDataPos := (Pos ('*****', DataStr));
        delete (DataStr, NoDataPos, 5);
        insert ('  NaN', DataStr, NoDataPos);
      end;

    (* replace bar with space *)
    while (Pos('|', DataStr) > 0) do
      begin
        NoDataPos := (Pos ('|', DataStr));
        delete (DataStr, NoDataPos, 1);
        insert (' ', DataStr, NoDataPos);
      end;

    (* replace / with nothing *)
    while (Pos('/', DataStr) > 0) do
      begin
        NoDataPos := (Pos ('/', DataStr));
        delete (DataStr, NoDataPos, 1);
      end;

    write (Dest, DataStr);
    if (Counter/10000 = Counter div 10000)
      then writeln ('processed ' , Counter, ' lines');
    inc (Counter);
  until (eof (Source));
  close (Source);
  close (Dest);
end.
```

APPENDIX 2

DATA

1. Standard Pressure Data from South African Weather Bureau.
2. Significant Pressure Data from South African Weather Bureau.
3. Surface Pressure Data from Automatic Weather Station.
4. Surface Wind Data from Automatic Weather Station.

Standard Pressure Data From SAWB, 1997

Station Number	Date	Time of release	Pressure (hPa)	Temp (C)	Humidity (%)	Height asl (gpkm)	Wind dir (deg)	Wind Speed (m/s)
68588	3-Jul-97	1241	1023.8	20.1	45	0.014	150	3.5
68588	3-Jul-97	1241	1000	17.5	39	0.216	205	3
68588	3-Jul-97	1241	925	11.6	47	0.875	245	4
68588	3-Jul-97	1241	850	8.7	36	1.578	265	7.4
68588	3-Jul-97	1241	700	4.4	5	3.164	230	11.9
68588	3-Jul-97	1241	500	-11.8	23	5.824	250	15.5
68588	3-Jul-97	1241	400	-23.2	9	7.496	240	13.8
68588	3-Jul-97	1241	300	-38.4	18	9.533	215	24.4
68588	3-Jul-97	1241	250	-46.8	11	10.759	220	25.8
68588	3-Jul-97	1241	200	-55.4	4	12.215	270	18.4
68588	3-Jul-97	1241	150	-60.9	2	14.02	260	22.1
68588	3-Jul-97	1241	100	-69.5	1	16.489	275	19.3
68588	3-Jul-97	1241	70	-68.2	1	18.612	290	12.3
68588	3-Jul-97	1241	50	-65.9	1	20.624	255	8.4
68588	3-Jul-97	1241	30	-60.6	1	23.761	220	2.8
68588	3-Jul-97	1241	20	-55.2	1	26.313	270	8.3
68588	23-Jul-97	1235	1013.3	26.9	43	0.014	360	3
68588	23-Jul-97	1235	1000	24.9	38	0.129	245	1.5
68588	23-Jul-97	1235	925	23.6	19	0.813	210	1.9
68588	23-Jul-97	1235	850	17.7	25	1.542	180	3
68588	23-Jul-97	1235	700	4.6	23	3.16	330	5.9
68588	23-Jul-97	1235	500	-10.8	6	5.83	270	9.1
68588	23-Jul-97	1235	400	-23.5	3	7.499	290	17.9
68588	23-Jul-97	1235	300	-38.9	5	9.536	275	19.8
68588	23-Jul-97	1235	250	-46.8	5	10.764	275	29.9
68588	23-Jul-97	1235	200	-56	4	12.211	270	27.3
68588	23-Jul-97	1235	150	-64.5	4	13.999	280	34
68588	23-Jul-97	1235	100	-67.6	1	16.448	285	26
68588	23-Jul-97	1235	70	-70.1	1	18.567	275	22.5
68588	23-Jul-97	1235	50	-63.9	1	20.596	280	18.3
68588	23-Jul-97	1235	30	-56.7	1	23.766	280	7.4
68588	23-Jul-97	1235	20	-49.2	1	26.375	330	11.8
68588	23-Jul-97	1235	10			31.013		
68588	8-Aug-97	1237	1022.1	22.4	59	0.014	20	5
68588	8-Aug-97	1237	1000	19.2	53	0.204	5	6.9

68588	8-Aug-97	1237	925	18.1	18	0.873	15	1.5
68588	8-Aug-97	1237	850	12.9	14	1.588	225	4.6
68588	8-Aug-97	1237	700	3.8	10	3.187	235	16.4
68588	8-Aug-97	1237	500	-14.2	10	5.833	235	17.6
68588	8-Aug-97	1237	400	-23.4	12	7.494	255	26.4
68588	8-Aug-97	1237	300	-38	11	9.538	265	29.3
68588	8-Aug-97	1237	250	-48	12	10.765	275	28.4
68588	8-Aug-97	1237	200	-58.3	11	12.199	285	28.7
68588	8-Aug-97	1237	150	-64.5	5	13.974	270	28.1
68588	8-Aug-97	1237	100	-67.6	1	16.419	260	19.2
68588	8-Aug-97	1237	70	-64.3	1	18.581	275	11.7
68588	8-Aug-97	1237	50	-59.7	1	20.665	300	2.1
68588	8-Aug-97	1237	30	-55.2	1	23.872	60	11.4
68588	8-Aug-97	1237	20	-51.9	1	26.489	30	10.7
68588	8-Aug-97	1237	10			31.075		
68588	21-Aug-97	1236	1011.6	23.6	65	0.014	40	5
68588	21-Aug-97	1236	1000	21.1	59	0.113	320	1.9
68588	21-Aug-97	1236	925	19.4	24	0.785	215	3.9
68588	21-Aug-97	1236	850	15.1	22	1.505	225	9.4
68588	21-Aug-97	1236	700	1.9	31	3.108	265	17
68588	21-Aug-97	1236	500	-14.8	2	5.728	250	27.9
68588	21-Aug-97	1236	400	-26	1	7.382	265	33.2
68588	21-Aug-97	1236	300	-39.1	3	9.407	260	44.3
68588	21-Aug-97	1236	250	-46.9	2	10.635	260	51.3
68588	21-Aug-97	1236	200	-54	1	12.092	265	48.3
68588	21-Aug-97	1236	150	-59.5	1	13.914	275	43.3
68588	21-Aug-97	1236	100	-65.2	1	16.414	275	40.6
68588	21-Aug-97	1236	70	-68	1	18.596	295	11.3
68588	21-Aug-97	1236	50	-59.9	1	20.642	235	9.3
68588	21-Aug-97	1236	30	-54.6	1	23.896	45	5.2
68588	21-Aug-97	1236	20	-48.8	1	26.525	65	9.4
68588	26-Sep-97	1242	1020	24.4	66	0.014	40	8
68588	26-Sep-97	1242	1000	21	62	0.186	50	9.3
68588	26-Sep-97	1242	925	16.3	77	0.854	20	11.3
68588	26-Sep-97	1242	850	16.8	21	1.576	5	10.1
68588	26-Sep-97	1242	700	10.4	36	3.219	260	4.7
68588	26-Sep-97	1242	500	-9.4	40	5.914	260	11.9

68588	26-Sep-97	1242	400	-22.9	47	7.592	265	15.6
68588	26-Sep-97	1242	300	-37	20	9.643	255	20
68588	26-Sep-97	1242	250	-47.4	30	10.876	265	19.9
68588	26-Sep-97	1242	200	-54.5	6	12.325	280	23.9
68588	26-Sep-97	1242	150	-64.6	5	14.119	290	23.1
68588	26-Sep-97	1242	100	-73.7	4	16.54	300	17.7
68588	26-Sep-97	1242	70	-68.6	2	18.644	295	5
68588	26-Sep-97	1242	50	-66.6	1	20.669	25	3.2
68588	26-Sep-97	1242	30	-58.9	1	23.843	30	12.4
68588	26-Sep-97	1242	20	-52.1	1	26.433	30	8.4
68588	20-Oct-97	1244	1014	26.8	55	0.014	30	7.5
68588	20-Oct-97	1244	1000	23.6	50	0.135	60	6.8
68588	20-Oct-97	1244	925	25.1	24	0.816	160	5.1
68588	20-Oct-97	1244	850	19.8	26	1.55	205	5.7
68588	20-Oct-97	1244	700	5.3	35	3.177	215	11.5
68588	20-Oct-97	1244	500	-11.4	1	5.835	205	2.7
68588	20-Oct-97	1244	400	-23.5	1	7.503	150	4.3
68588	20-Oct-97	1244	300	-36.6	9	9.553	145	21.2
68588	20-Oct-97	1244	250	-47.3	13	10.786	140	18.4
68588	20-Oct-97	1244	200	-52.8	4	12.233	150	12
68588	20-Oct-97	1244	150	-61	2	14.063	195	16
68588	20-Oct-97	1244	100	-68.3	2	16.528	220	9
68588	20-Oct-97	1244	70	-67.2	1	18.666	75	3
68588	20-Oct-97	1244	50	-63.4	1	20.72	60	11.3
68588	20-Oct-97	1244	30	-53.3	1	23.917	60	15.5
68588	20-Oct-97	1244	20	-47	1	26.566	65	24.4

Significant Pressure Data From SAWB, 1997

Station Number	Date	Time of release	Pressure (hPa)	Temp (C)	Humidity (%)	Dew Point T (C)	Flight time (minutes)
68588	3-Jul-97	1241	1023.8	20.1	45	7.8	0
68588	3-Jul-97	1241	917.4	11	50	1	2.6
68588	3-Jul-97	1241	860.3	9.3	46	-1.7	4
68588	3-Jul-97	1241	827.8	8.3	9	-22.8	4.8
68588	3-Jul-97	1241	724.3	3.4	1	-48.3	7.5
68588	3-Jul-97	1241	707.2	4.6	2	-41.1	8
68588	3-Jul-97	1241	666.1	2.9	28	-13.8	9.3
68588	3-Jul-97	1241	631.1	0.8	20	-19.6	10.5
68588	3-Jul-97	1241	562.8	-6.7	30	-21.4	12.8
68588	3-Jul-97	1241	449.9	-16.4	10	-41.1	17.1
68588	3-Jul-97	1241	270.6	-44.9	16	-60.6	26.5
68588	3-Jul-97	1241	221.1	-50.1	6	-72.2	29.5
68588	3-Jul-97	1241	187.0	-58.5	4	-81.5	32
68588	3-Jul-97	1241	150.3	-61.1	2	-87.7	35.8
68588	3-Jul-97	1241	144.9	-59.5	2	-86.5	36.5
68588	3-Jul-97	1241	102.0	-70.5	1	-98.4	42.6
68588	3-Jul-97	1241	101.0	-69.7	1	-97.8	42.8
68588	3-Jul-97	1241	80.1	-71.2	1	-98.9	47
68588	3-Jul-97	1241	68.5	-67.7	1	-96.4	49.8
68588	3-Jul-97	1241	61.2	-70.6	1	-98.5	51.8
68588	3-Jul-97	1241	55.8	-70.5	1	-98.4	53.5
68588	3-Jul-97	1241	48.5	-65.1	1	-94.5	56
68588	3-Jul-97	1241	29.2	-60.1	1	-90.9	64.6
68588	3-Jul-97	1241	27.1	-61.4	1	-91.9	65.8
68588	3-Jul-97	1241	23.8	-56.1	1	-88.1	68
68588	3-Jul-97	1241	21.5	-57	1	-88.7	69.6
68588	3-Jul-97	1241	14.6	-50.3	1	-84	76
68588	23-Jul-97	1235	1013.3	26.9	43	13.3	0
68588	23-Jul-97	1235	999.2	24.9	38	9.7	0.3
68588	23-Jul-97	1235	974.4	26.3	26	5.3	1
68588	23-Jul-97	1235	750.0	8.7	28	-8.8	7
68588	23-Jul-97	1235	703.6	4.7	23	-14.7	8.5
68588	23-Jul-97	1235	643.7	0.8	13	-24.6	10.5
68588	23-Jul-97	1235	628.4	2.2	4	-36	11
68588	23-Jul-97	1235	420.6	-21.6	7	-48.5	19.1

68588	23-Jul-97	1235	273.2	-43.6	5	-68.4	27.6
68588	23-Jul-97	1235	197.1	-56.7	4	-80.1	34.3
68588	23-Jul-97	1235	156.6	-64.8	4	-86.5	38.8
68588	23-Jul-97	1235	137.8	-66.7	3	-89.6	41.5
68588	23-Jul-97	1235	100.5	-67.6	1	-96.3	47.3
68588	23-Jul-97	1235	86.7	-71.7	1	-99.3	49.8
68588	23-Jul-97	1235	53.6	-67.2	1	-96	58.6
68588	23-Jul-97	1235	46.9	-63.2	1	-93.1	61
68588	23-Jul-97	1235	39.6	-64.5	1	-94.1	63.8
68588	23-Jul-97	1235	34.7	-57.4	1	-89	66
68588	23-Jul-97	1235	31.1	-55.4	1	-87.6	68
68588	23-Jul-97	1235	28.9	-58	1	-89.4	69.1
68588	23-Jul-97	1235	27.1	-54.4	1	-86.9	70.1
68588	23-Jul-97	1235	12.4	-42.6	1	-78.6	82.8
68588	23-Jul-97	1235	12.2	-42.8	1	-78.8	83.1
68588	8-Aug-97	1237	1022.1	22.4	59	14	0
68588	8-Aug-97	1237	1014.2	20	50	9.3	0.1
68588	8-Aug-97	1237	986.1	18	55	8.9	0.8
68588	8-Aug-97	1237	966.8	20.9	21	-2.2	1.3
68588	8-Aug-97	1237	730.5	4.1	24	-14.7	7.5
68588	8-Aug-97	1237	708.2	4.4	9	-25.8	8.1
68588	8-Aug-97	1237	685.6	4.3	4	-34.5	8.8
68588	8-Aug-97	1237	479.1	-16.6	11	-40.3	16
68588	8-Aug-97	1237	371.8	-26	9	-49.8	20.8
68588	8-Aug-97	1237	331.8	-33.2	21	-48.2	22.8
68588	8-Aug-97	1237	312.6	-35.5	10	-56.5	23.8
68588	8-Aug-97	1237	230.6	-52.9	17	-67	29.1
68588	8-Aug-97	1237	181.3	-62.2	11	-78	33.6
68588	8-Aug-97	1237	149.4	-64.6	4	-86.3	37.5
68588	8-Aug-97	1237	113.5	-68.9	2	-93.6	42.5
68588	8-Aug-97	1237	100.2	-67.6	1	-96.3	44.8
68588	8-Aug-97	1237	85.3	-63.9	1	-93.7	47.6
68588	8-Aug-97	1237	75.5	-68	1	-96.6	49.8
68588	8-Aug-97	1237	64.0	-62	1	-92.3	52.8
68588	8-Aug-97	1237	51.3	-59	1	-90.1	56.8
68588	8-Aug-97	1237	46.7	-61	1	-91.6	58.5
68588	8-Aug-97	1237	21.8	-50.7	1	-84.3	71.6
68588	8-Aug-97	1237	18.0	-51.9	1	-85.1	74.8

68588	8-Aug-97	1237	16.0	-47.1	1	-81.8	76.8
68588	8-Aug-97	1237	11.5	-44.2	1	-79.8	82.3
68588	21-Aug-97	1236	1011.6	23.6	65	16.7	0
68588	21-Aug-97	1236	989.0	19.5	65	12.8	0.6
68588	21-Aug-97	1236	960.2	18.7	60	10.8	1.5
68588	21-Aug-97	1236	936.9	19.8	27	0.3	2.1
68588	21-Aug-97	1236	871.5	16.9	20	-6.2	4.1
68588	21-Aug-97	1236	679.8	-0.1	33	-14.5	10.3
68588	21-Aug-97	1236	620.3	-3.6	15	-26.6	12.3
68588	21-Aug-97	1236	519.4	-15.3	12	-38.4	16.3
68588	21-Aug-97	1236	506.3	-14.1	1	-59.5	16.8
68588	21-Aug-97	1236	397.4	-26.5	1	-67.7	22
68588	21-Aug-97	1236	370.5	-28.6	1	-69.1	23.5
68588	21-Aug-97	1236	316.3	-37.7	10	-58.3	26.8
68588	21-Aug-97	1236	248.2	-47.3	2	-77.5	32.3
68588	21-Aug-97	1236	188.7	-56.1	1	-88.1	38
68588	21-Aug-97	1236	121.4	-61.6	1	-92	47
68588	21-Aug-97	1236	104.6	-66.4	1	-95.5	49.8
68588	21-Aug-97	1236	100.6	-65.1	1	-94.5	50.5
68588	21-Aug-97	1236	90.1	-62.1	1	-92.4	52.5
68588	21-Aug-97	1236	76.3	-63.9	1	-93.7	55.3
68588	21-Aug-97	1236	67.0	-69.4	1	-97.6	57.3
68588	21-Aug-97	1236	66.4	-69.5	1	-97.7	57.5
68588	21-Aug-97	1236	46.2	-56.2	1	-88.2	63.8
68588	21-Aug-97	1236	28.7	-54.4	1	-86.9	72.1
68588	21-Aug-97	1236	20.4	-48.6	1	-82.8	78.1
68588	21-Aug-97	1236	18.3	-50.6	1	-84.2	80
68588	21-Aug-97	1236	14.5	-44.2	1	-79.8	84.1
68588	26-Sep-97	1242	1020.0	24.4	66	17.7	0
68588	26-Sep-97	1242	1012.2	21.9	57	13	0.1
68588	26-Sep-97	1242	938.9	16.1	78	12.3	1.8
68588	26-Sep-97	1242	881.0	18.4	24	-2.5	3.3
68588	26-Sep-97	1242	806.8	15.5	38	1.3	5.3
68588	26-Sep-97	1242	787.6	17.8	27	-1.4	5.8
68588	26-Sep-97	1242	558.7	-4.3	51	-12.9	13.3
68588	26-Sep-97	1242	550.2	-3.5	13	-28	13.6
68588	26-Sep-97	1242	505.5	-8.9	44	-19	15.5

68588	26-Sep-97	1242	430.2	-18.9	54	-25.9	18.6
68588	26-Sep-97	1242	412.6	-21.6	44	-30.7	19.5
68588	26-Sep-97	1242	304.7	-36	17	-52.5	25.3
68588	26-Sep-97	1242	239.0	-50	31	-59.9	30.1
68588	26-Sep-97	1242	208.6	-52.9	6	-74.4	33.1
68588	26-Sep-97	1242	152.8	-64.7	5	-85.1	39.5
68588	26-Sep-97	1242	100.7	-73.6	3	-95	47.1
68588	26-Sep-97	1242	96.9	-74.8	4	-94.4	47.8
68588	26-Sep-97	1242	83.2	-72.9	4	-92.9	50.5
68588	26-Sep-97	1242	78.7	-69.4	4	-90.1	51.5
68588	26-Sep-97	1242	61.6	-69	1	-97.3	55.8
68588	26-Sep-97	1242	56.0	-66	1	-95.2	57.5
68588	26-Sep-97	1242	51.8	-67.3	1	-96.1	58.8
68588	26-Sep-97	1242	33.7	-57.8	1	-89.3	66.3
68588	26-Sep-97	1242	31.4	-59.3	1	-90.4	67.5
68588	26-Sep-97	1242	14.9	-47.3	1	-81.9	80.1
68588	20-Oct-97	1244	1014.0	26.8	55	17	0
68588	20-Oct-97	1244	1007.6	24	48	12.4	0.1
68588	20-Oct-97	1244	969.0	22.4	47	10.6	1.1
68588	20-Oct-97	1244	942.4	25.7	23	3.1	1.8
68588	20-Oct-97	1244	892.4	23.5	18	-2.1	3.1
68588	20-Oct-97	1244	638.6	-1.6	51	-10.4	10.5
68588	20-Oct-97	1244	617.7	-3.3	32	-17.7	11.1
68588	20-Oct-97	1244	607.1	-1.4	6	-34.5	11.5
68588	20-Oct-97	1244	415.4	-22	1	-64.7	18.8
68588	20-Oct-97	1244	319.7	-32.8	6	-58.5	23.5
68588	20-Oct-97	1244	256.8	-46	17	-61.1	27.8
68588	20-Oct-97	1244	222.0	-53.7	13	-69.7	30
68588	20-Oct-97	1244	207.4	-52.6	6	-74.2	31.3
68588	20-Oct-97	1244	170.2	-55.1	2	-83.2	35.1
68588	20-Oct-97	1244	111.6	-69.2	2	-93.8	43
68588	20-Oct-97	1244	100.3	-68.3	2	-93.1	45
68588	20-Oct-97	1244	91.0	-66.3	2	-91.6	46.8
68588	20-Oct-97	1244	78.0	-71.1	1	-98.9	49.5
68588	20-Oct-97	1244	60.8	-63.8	1	-93.6	54.1
68588	20-Oct-97	1244	51.9	-63.2	1	-93.1	57
68588	20-Oct-97	1244	47.9	-63.8	1	-93.6	58.5
68588	20-Oct-97	1244	28.2	-50.8	1	-84.4	67.8

						-81.7	74
68588	20-Oct-97	1244	20.0	-47	1	-82.1	78.5
68588	20-Oct-97	1244	15.3	-47.6	1		

Surface Wind Data from AWS, 1997

3-Jul

Hours	Wind Direction	Wind Speed
1	0	0
2	310	1.5
3	310	1.6
4	300	1.9
5	310	2
6	300	1.6
7	270	1.9
8	300	1.8
9	300	1.9
10	250	3.8
11	230	4.7
12	190	4.1
13	160	3.5
14	150	3.7
15	120	3.4
16	80	2.9
17	60	1.9
18	20	2
19	310	2.2
20	310	2.4
21	320	2
22	330	2.8
23	330	1.9
24	330	2

23-Jul

Hours	Wind Direction	Wind Speed
1	320	2.2
2	310	2.1
3	320	1.8
4	330	1.9
5	340	1.7
6	320	1.6
7	330	1.5
8	350	1.6
9	360	2
10	10	2.5
11	20	1.7
12	10	2.4
13	10	3.3
14	20	2.7
15	20	3.4
16	20	3.6
17	20	3.6
18	10	3.2
19	350	1.8
20	330	1.6
21	320	2.1
22	310	2.1
23	310	1.7
24	330	1.7

8-Aug

Hours	Wind Speed	Wind Direction
1	2.3	320
2	2.1	310
3	2	330
4	2.2	10
5	3.4	10
6	3.2	20
7	3.3	10
8	2.5	10
9	4.1	360
10	5.3	10
11	4	20
12	4.2	30
13	4.9	30
14	5.5	30
15	5.6	30
16	5.6	30
17	5.4	30
18	2.9	20
19	2.1	360
20	2.5	330
21	2.2	320
22	2	320
23	1.6	310
24	1.9	330

21-Aug

Hours	Wind Speed	Wind Direction
1	1.5	200
2	1.7	320
3	1.7	350
4	2.5	360

26-Sep

Hours	Wind Speed	Wind Direction
1	1.5	320
2	1.9	330
3	1.6	330
4	1.5	310

20-Oct

Hours	Wind Speed	Wind Direction
1	4.7	10
2	4.7	360
3	2.2	340
4	1.5	310

5	2.4	350	5	1.6	340	5	1.6	320
6	2.1	350	6	1.8	330	6	1.8	350
7	3.5	360	7	1.9	350	7	2.7	360
8	4	360	8	3.9	20	8	3.3	360
9	4.7	10	9	6.5	20	9	3.4	20
10	3.9	20	10	7.7	30	10	4.4	30
11	3	30	11	8.3	30	11	5.5	30
12	3.3	40	12	8.6	40	12	6.5	30
13	4.3	30	13	10.1	50	13	7.5	20
14	4.1	30	14	9.7	40	14	7.3	20
15	3	60	15	10.3	30	15	7.8	20
16	3.1	130	16	10.1	30	16	8.6	20
17	3.7	190	17	9.5	20	17	7.6	20
18	3.6	200	18	9.3	20	18	6.7	20
19	3.6	220	19	10	20	19	5.3	20
20	2.9	210	20	10.5	20	20	4.4	20
21	2.4	230	21	9.9	20	21	3.8	30
22	3.4	230	22	8.7	20	22	2.6	10
23	4	230	23	7.7	20	23	3.4	10
24	3.1	230	24	8.3	10	24	3.6	10

Surface Pressure Data from AWS, 1997

July 3,1997		23-Jul-97		8-Aug-97	
Hours	Pressure (hPa)	Hours	Pressure(hPa)	Hours	Pressure(hPa)
1	1026.2	1	1018.4	1	1028.3
2	1026.1	2	1017.9	2	1027.8
3	1026.1	3	1017.1	3	1027.1
4	1026	4	1017.1	4	1026.5
5	1026.2	5	1017.0	5	1025.9
6	1026.8	6	1017.1	6	1025.8
7	1027	7	1017.1	7	1026.0
8	1027.7	8	1017.2	8	1026.3
9	1028	9	1017.2	9	1026.1
10	1028.1	10	1016.9	10	1025.8
11	1027.5	11	1016.2	11	1025.1
12	1026.3	12	1015.2	12	1024.2
13	1026.3	13	1014.1	13	1023.4
14	1023.8	14	1013.6	14	1023.0
15	1023.5	15	1013.1	15	1023.0
16	1023.4	16	1013.0	16	1023.1
17	1023.5	17	1013.0	17	1023.5
18	1023.7	18	1012.8	18	1023.9
19	1024	19	1013.1	19	1024.2
20	1024.3	20	1013.1	20	1024.0
21	1024.3	21	1012.8	21	1023.9
22	1024	22	1012.8	22	1024.0
23	1024.4	23	1012.8	23	1024.1
24	1024.5	24	1012.6	24	1024.2

Surface Pressure Data from AWS, 1997

21-Aug-97		September 26,1997		20-Oct-97	
Hours	Pressure	Hours	Pressure	Hours	Pressure
1	1021.5	1	1026.0	1	1018.8
2	1020.4	2	1025.9	2	1018.3
3	1019.5	3	1025.6	3	1017.5
4	1018.6	4	1025.6	4	1017.5
5	1018.2	5	1025.9	5	1017.3
6	1017.9	6	1026.3	6	1017.4
7	1017.5	7	1026.5	7	1017.4
8	1017.1	8	1026.3	8	1017.2
9	1016.4	9	1025.9	9	1017.0
10	1015.5	10	1024.8	10	1016.8
11	1014.9	11	1023.7	11	1016.2
12	1013.9	12	1022.4	12	1015.6
13	1012.7	13	1020.9	13	1015.2
14	1012.8	14	1020.0	14	1014.5
15	1013.1	15	1019.3	15	1014.0
16	1014.4	16	1018.7	16	1013.5
17	1015.6	17	1018.3	17	1013.6
18	1016.3	18	1018.1	18	1014.1
19	1017.2	19	1017.9	19	1014.4
20	1018.5	20	1017.0	20	1015.0
21	1019.8	21	1016.9	21	1015.4

Hours	Pressure
22	1020.7
23	1020.9
24	1021.1

Hours	Pressure
22	1016.0
23	1014.7
24	1013.5

Hours	Pressure
22	1015.2
23	1015.0
24	1014.6

APPENDIX 3

TRAJECTORY MODELLING RESULTS

- Trajectory results at Standard Pressure Levels (300, 500, 700, 850, 925 and 1000hPa) for different case studies from the Climatology Research Group, University of Witwatersrand, Johannesburg.

Backward Trajectories (Centroid Only)
Origin 29.9S 30.9E (Site unknown)
Height at Origin 1300 hPa on 3 July 1997 12.00 UTC

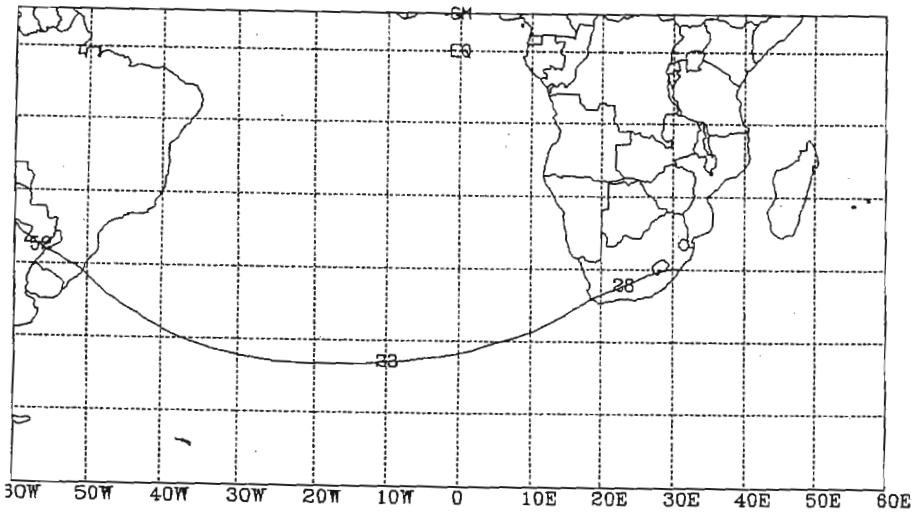

Backward Trajectories (Centroid Only)
Origin 29.9S 30.9E (Site unknown)
Height at Origin 1500 hPa on 3 July 1997 12.00 UTC

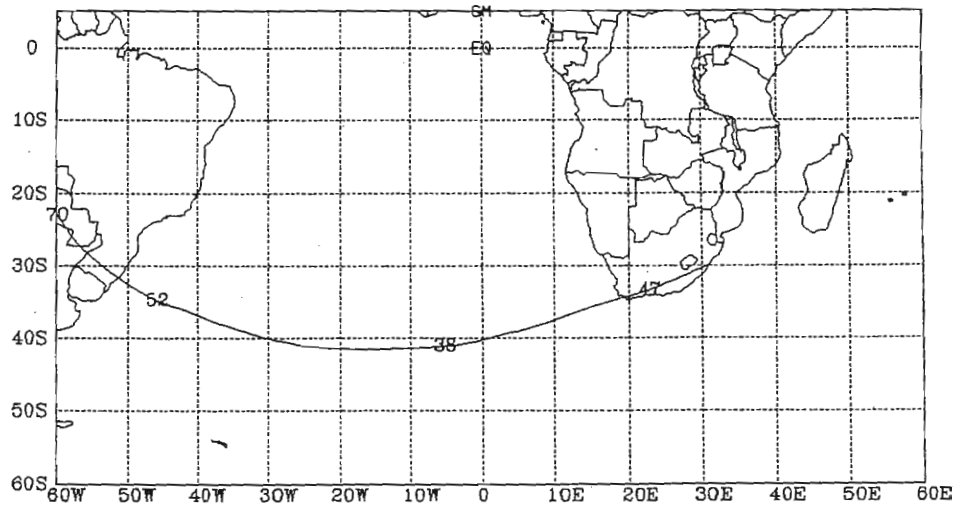

Backward Trajectories (Centroid Only)
Origin 29.9S 30.9E (Site unknown)
Height at Origin 1850 hPa on 3 July 1997 12.00 UTC

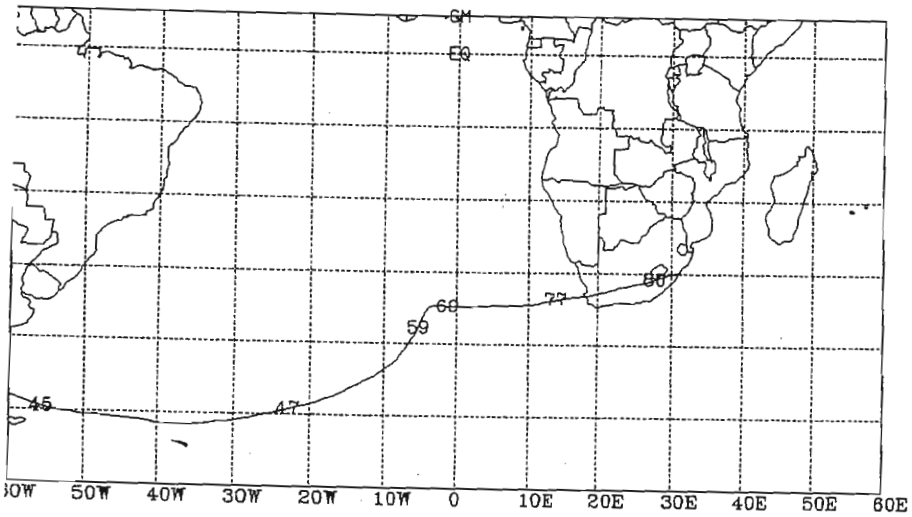

Backward Trajectories (Centroid Only)
Origin 29.9S 30.9E (Site unknown)
Height at Origin 1700 hPa on 3 July 1997 12.00 UTC

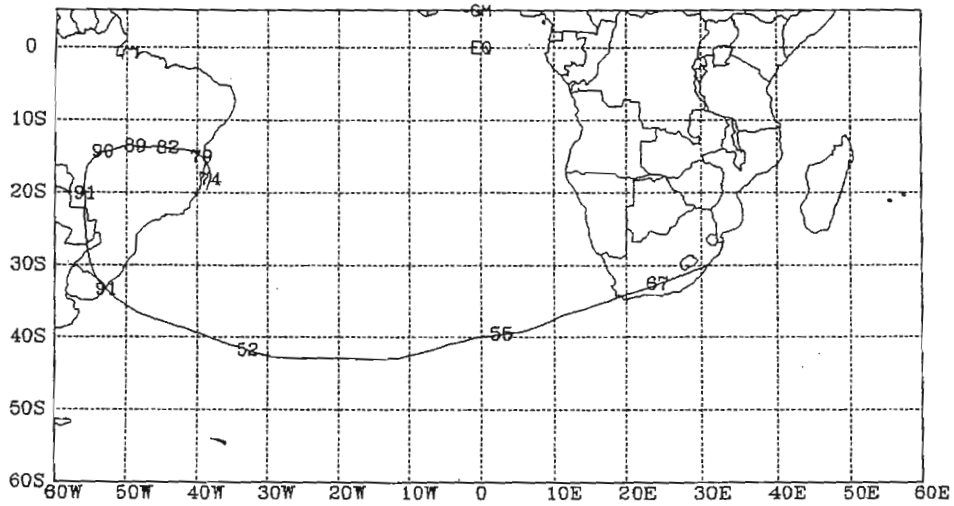

Backward Trajectories (Centroid Only)
Origin 29.9S 30.9E (Site unknown)
Height at Origin 925 hPa on 3 July 1997 12.00 UTC

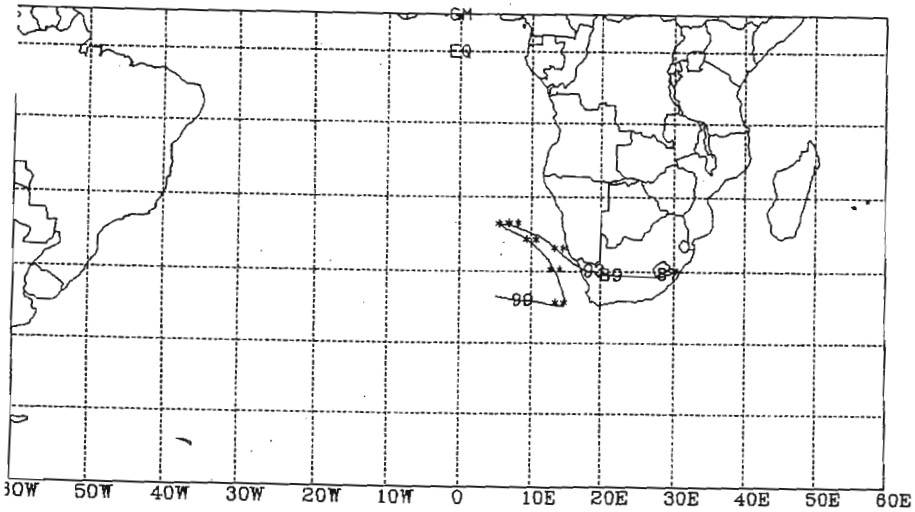

Backward Trajectories (Centroid Only)
Origin 29.9S 30.9E (Site unknown)
Height at Origin 1000 hPa on 3 July 1997 12.00 UTC

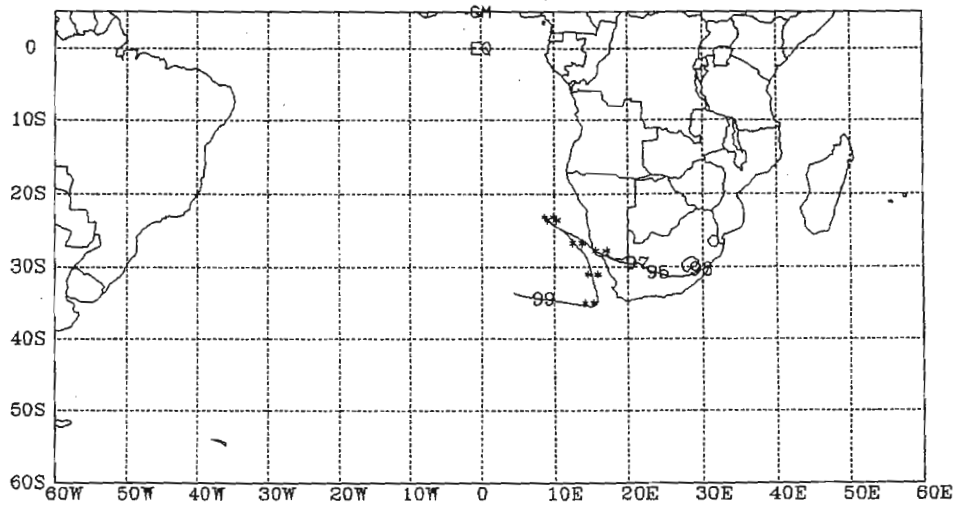

Backward Trajectories (Centroid Only)
Origin 29.9S 30.9E (Site unknown)
Height at Origin 1500 hPa on 23 July 1997 12.00 UTC

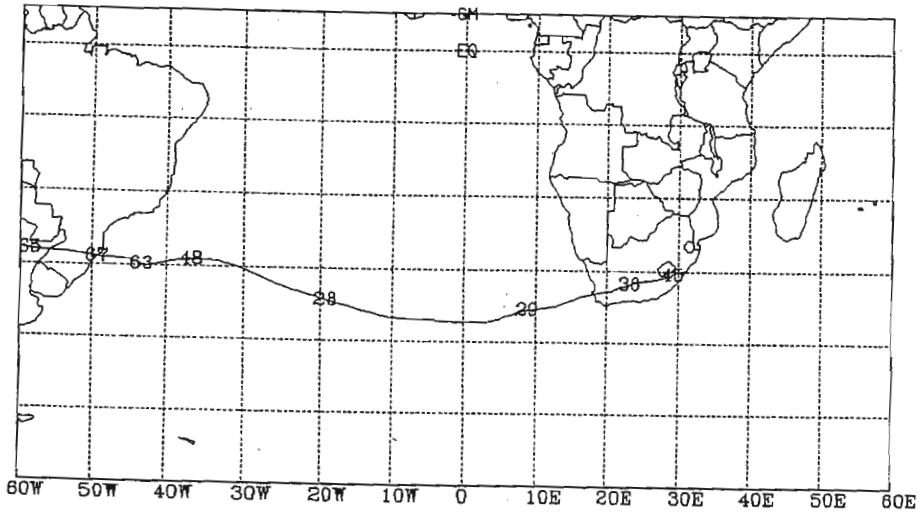

Backward Trajectories (Centroid Only)
Origin 29.9S 30.9E (Site unknown)
Height at Origin 1300 hPa on 23 July 1997 12.00 UTC

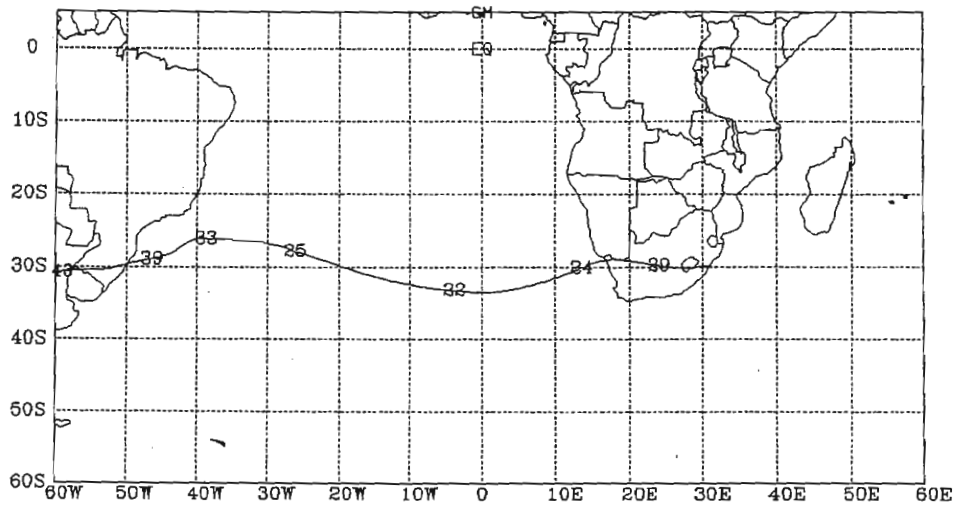

Backward Trajectories (Centroid Only)
Origin 29.9S 30.9E (Site unknown)
Height at Origin 1850 hPa on 23 July 1997 12.00 UTC

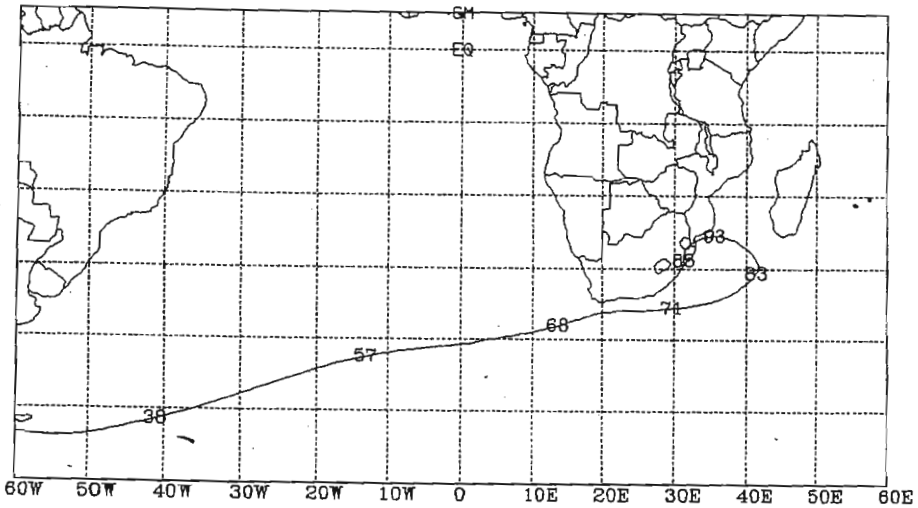

Backward Trajectories (Centroid Only)
Origin 29.9S 30.9E (Site unknown)
Height at Origin 1700 hPa on 23 July 1997 12.00 UTC

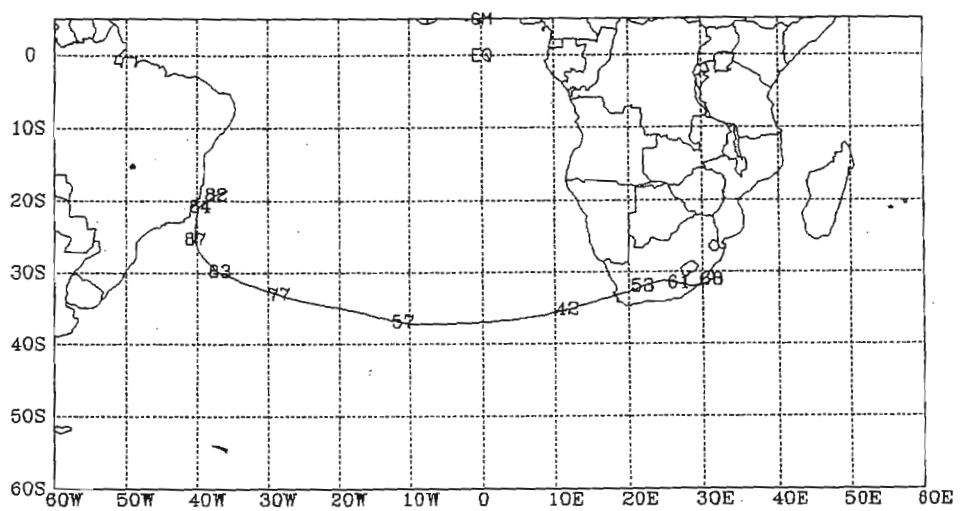

Backward Trajectories (Centroid Only)
Origin 29.9S 30.9E (Site unknown)
Height at Origin 925 hPa on 23 July 1997 12.00 UTC

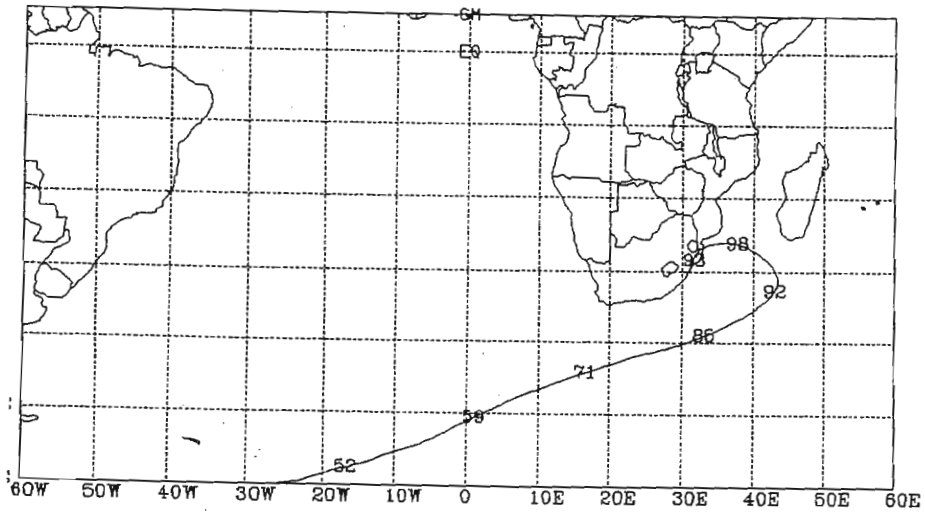

Backward Trajectories (Centroid Only)
Origin 29.9S 30.9E (Site unknown)
Height at Origin 1000 hPa on 23 July 1997 12.00 UTC

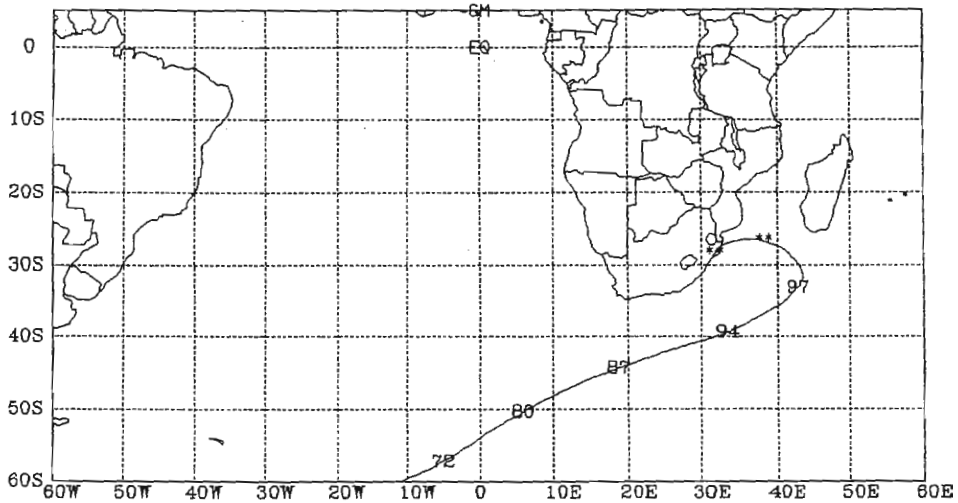

Backward Trajectories (Centroid Only)
Origin 29.9S 30.9E (Site unknown)
Height at Origin 1300 hPa on 8 August 1997 12.00 UTC

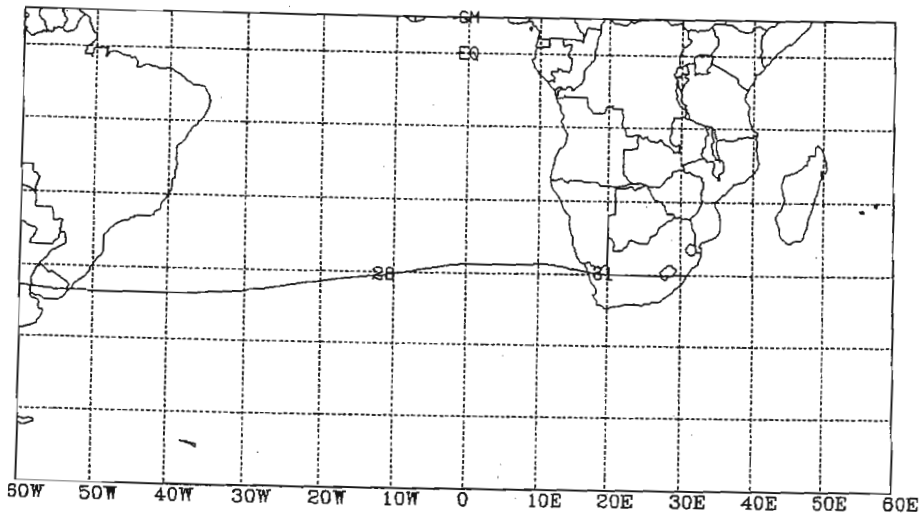

Backward Trajectories (Centroid Only)
Origin 29.9S 30.9E (Site unknown)
Height at Origin 1500 hPa on 8 August 1997 12.00 UTC

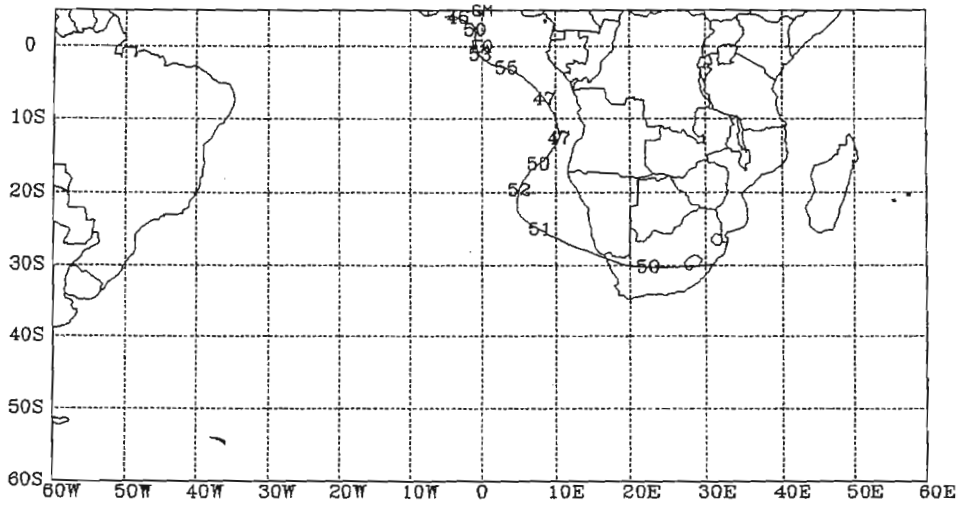

Backward Trajectories (Centroid Only)
Origin 29.9S 30.9E (Site unknown)
Height at Origin 1850 hPa on 8 August 1997 12.00 UTC

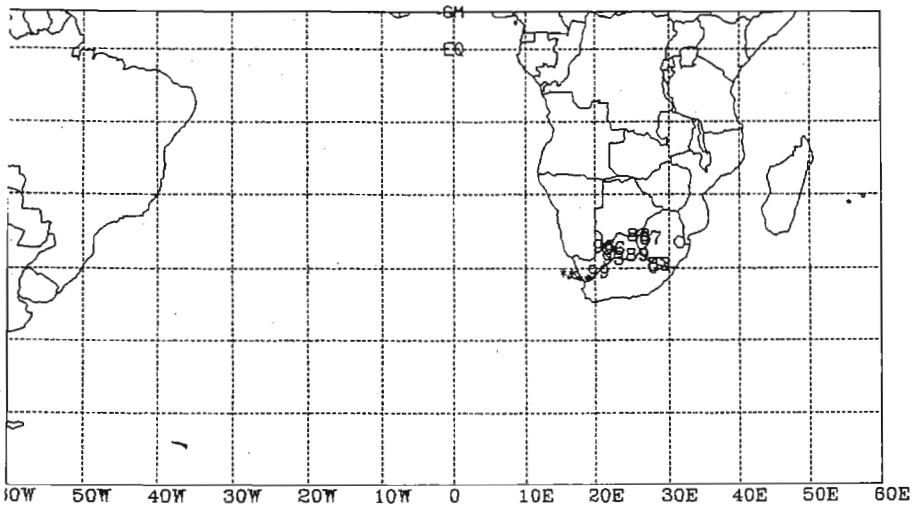

Backward Trajectories (Centroid Only)
Origin 29.9S 30.9E (Site unknown)
Height at Origin 1700 hPa on 8 August 1997 12.00 UTC

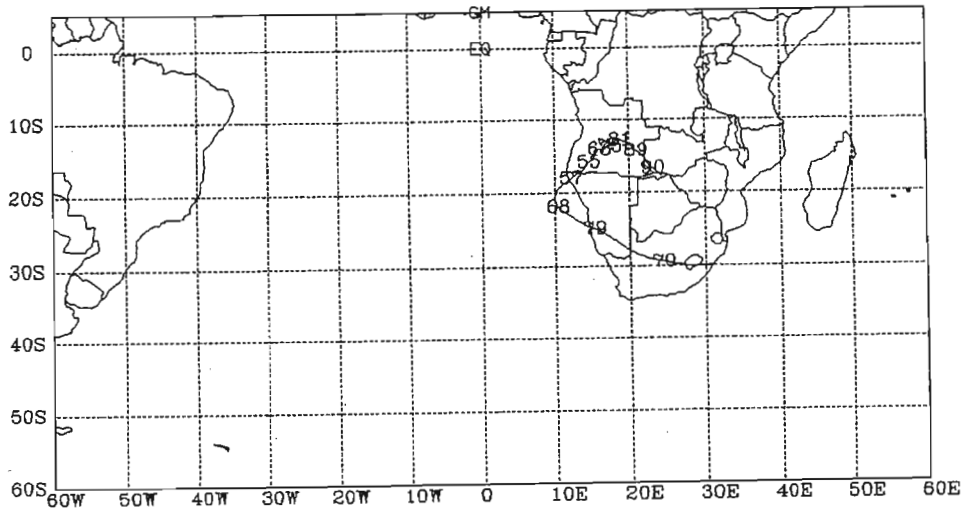

Backward Trajectories (Centroid Only)
Origin 29.9S 30.9E (Site unknown)
Height at Origin 1000 hPa on 8 August 1997 12.00 UTC

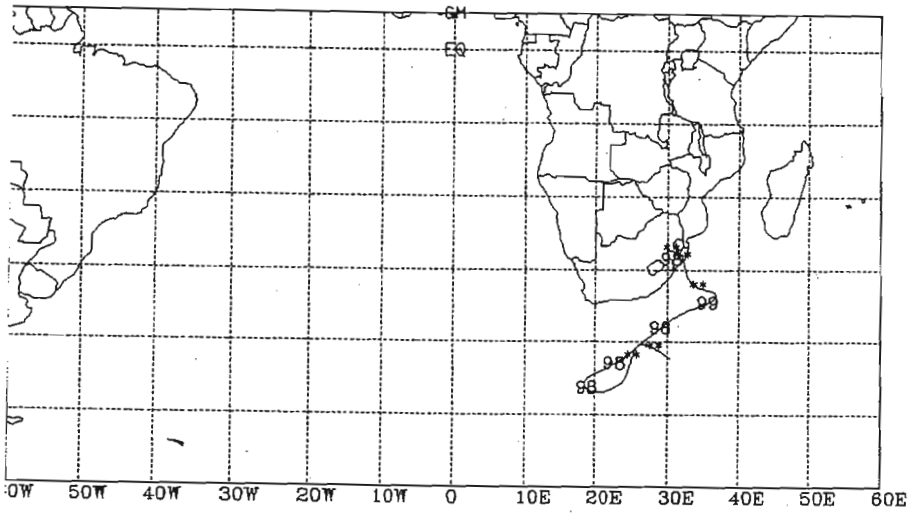

Backward Trajectories (Centroid Only)
Origin 29.9S 30.9E (Site unknown)
Height at Origin 925 hPa on 8 August 1997 12.00 UTC

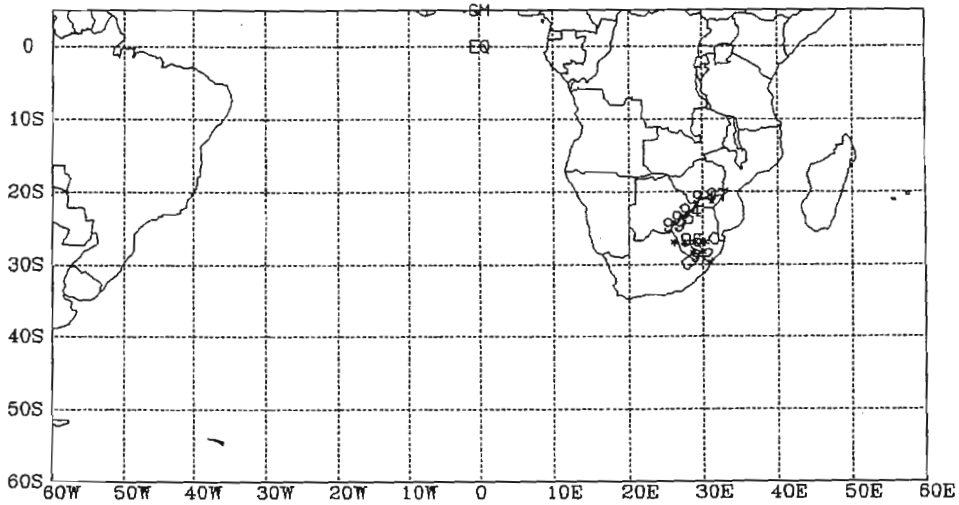

Backward Trajectories (Centroid Only)
Origin 29.9S 30.9E (Site unknown)
Height at Origin 1500 hPa on 21 August 1997 12.00 UTC

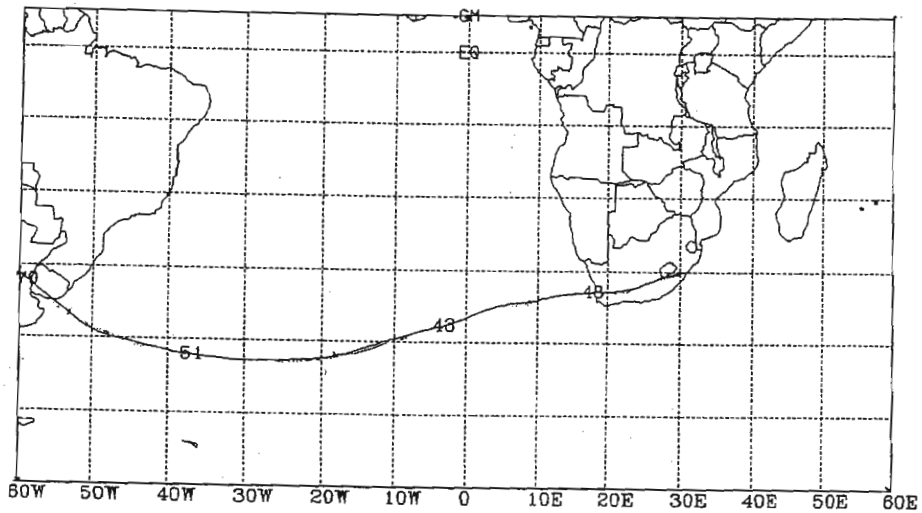

Backward Trajectories (Centroid Only)
Origin 29.9S 30.9E (Site unknown)
Height at Origin 1300 hPa on 21 August 1997 12.00 UTC

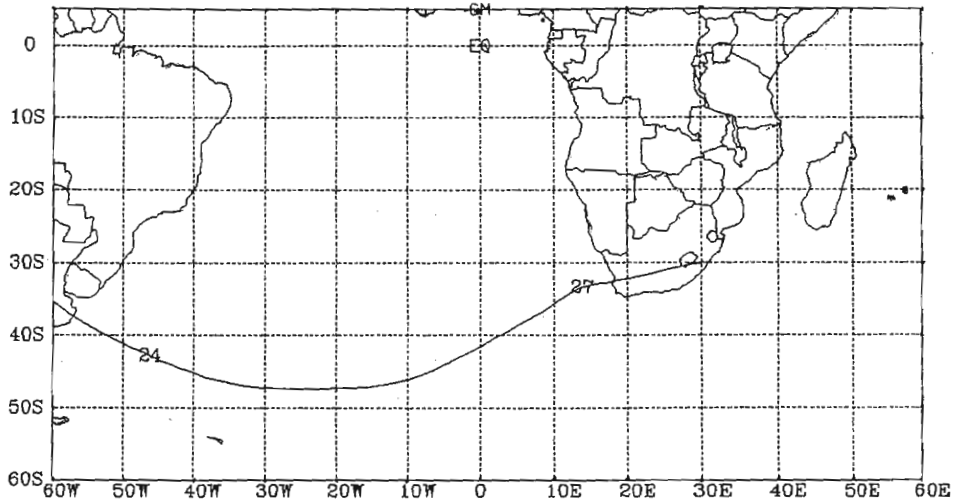

Backward Trajectories (Centroid Only)
Origin 29.9S 30.9E (Site unknown)
Height at Origin 1850 hPa on 21 August 1997 12.00 UTC

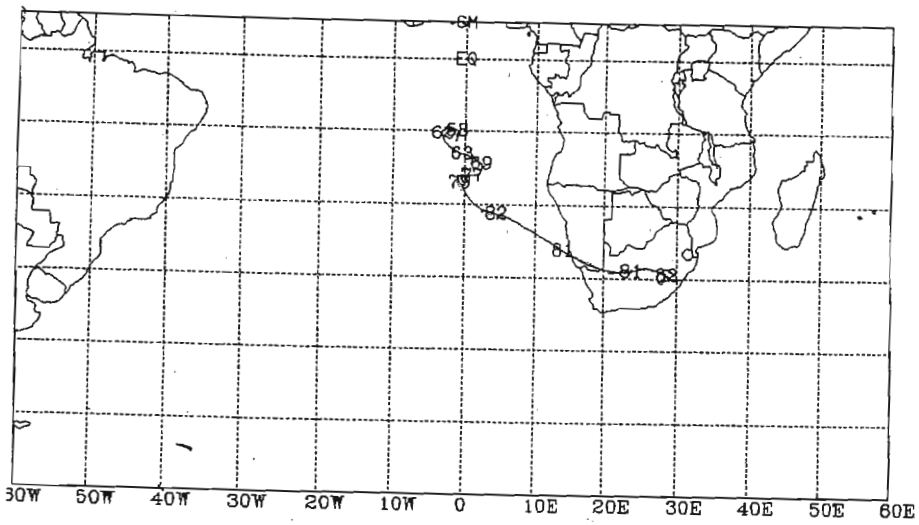

Backward Trajectories (Centroid Only)
Origin 29.9S 30.9E (Site unknown)
Height at Origin 1700 hPa on 21 August 1997 12.00 UTC

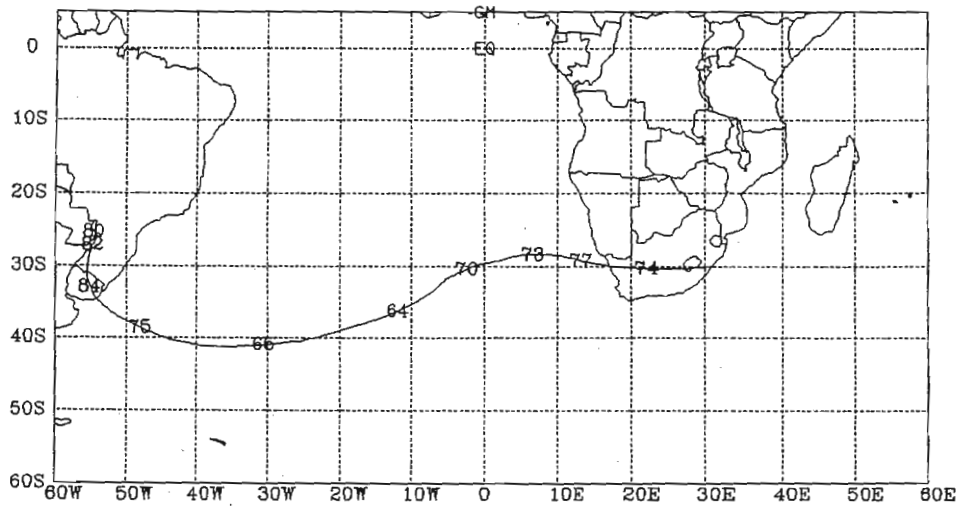

Backward Trajectories (Centroid Only)
Origin 29.9S 30.9E (Site unknown)
Height at Origin 1000 hPa on 21 August 1997 12.00 UTC

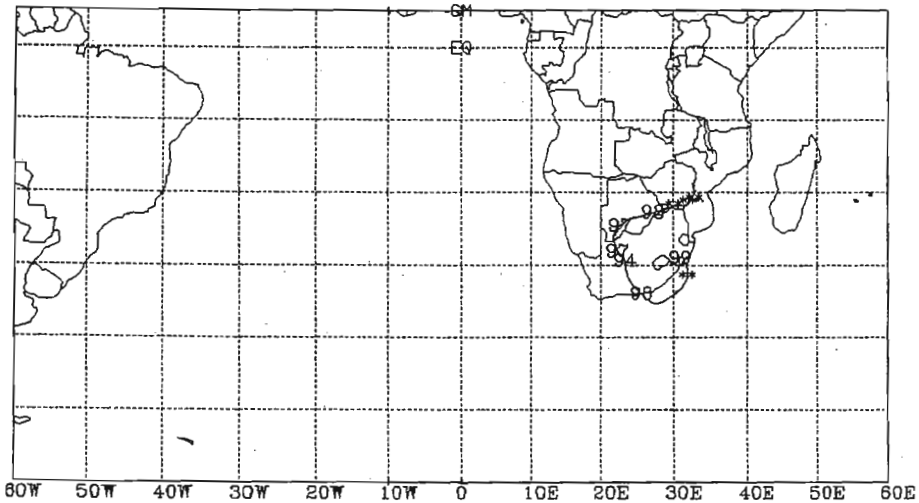

Backward Trajectories (Centroid Only)
Origin 29.9S 30.9E (Site unknown)
Height at Origin 925 hPa on 21 August 1997 12.00 UTC

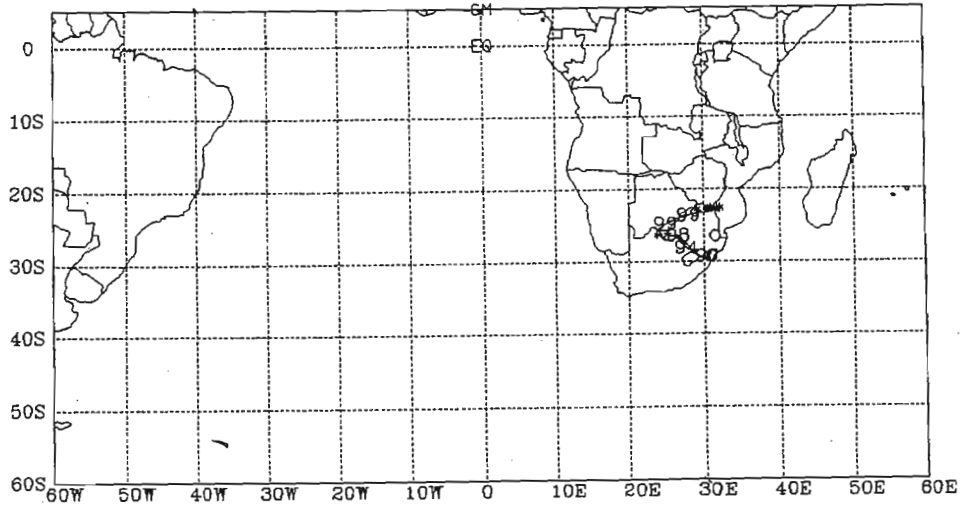

Backward Trajectories (Centroid Only)
Origin 29.9S 30.9E (Site unknown)
Height at Origin 1500 hPa on 26 September 1997 12.00 UTC

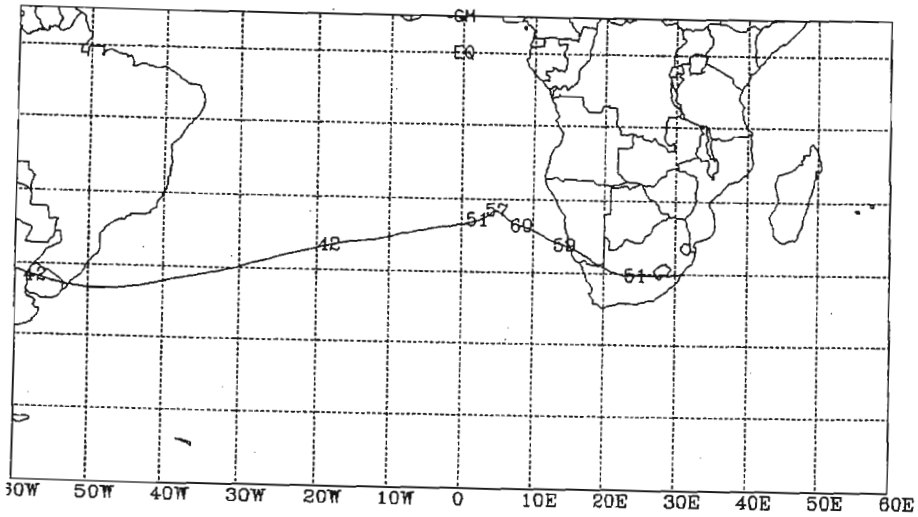

Backward Trajectories (Centroid Only)
Origin 29.9S 30.9E (Site unknown)
Height at Origin 1300 hPa on 26 September 1997 12.00 UTC

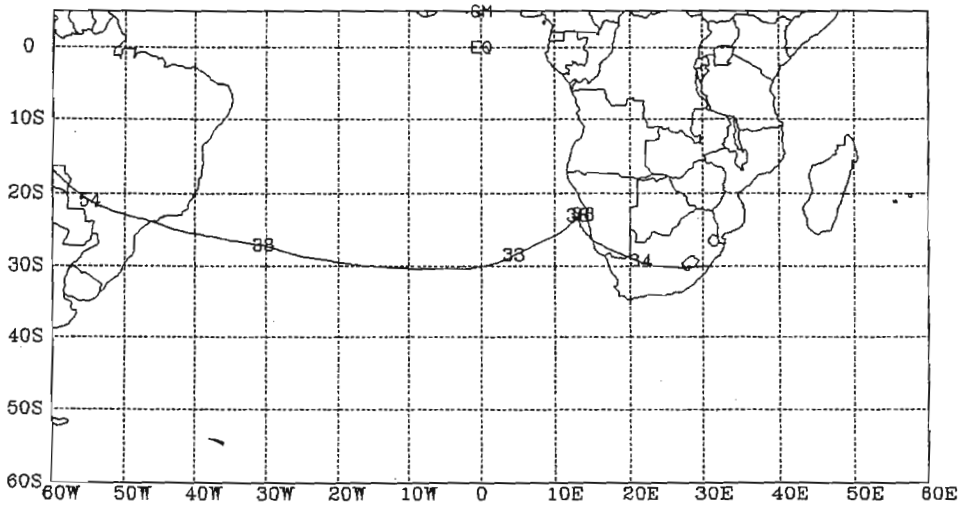

Backward Trajectories (Centroid Only)
Origin 29.9S 30.9E (Site unknown)
Height at Origin 1850 hPa on 26 September 1997 12.00 UTC

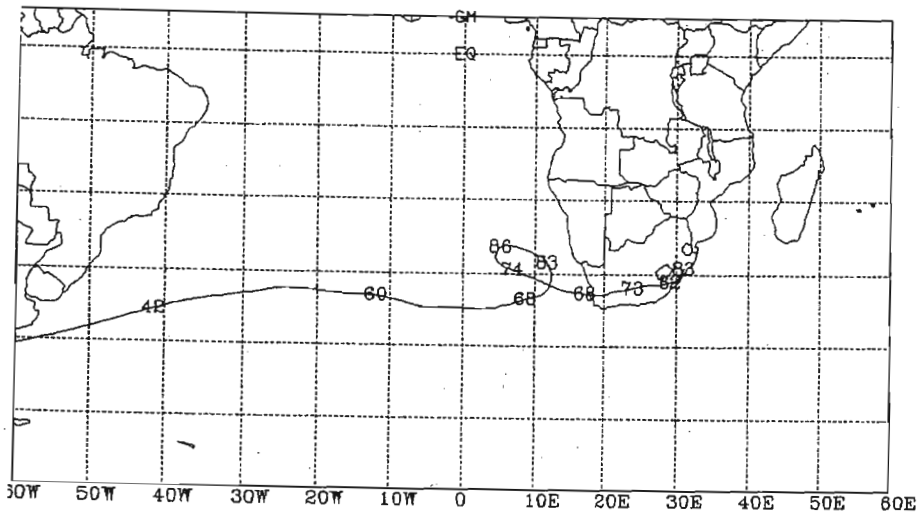

Backward Trajectories (Centroid Only)
Origin 29.9S 30.9E (Site unknown)
Height at Origin 1700 hPa on 26 September 1997 12.00 UTC

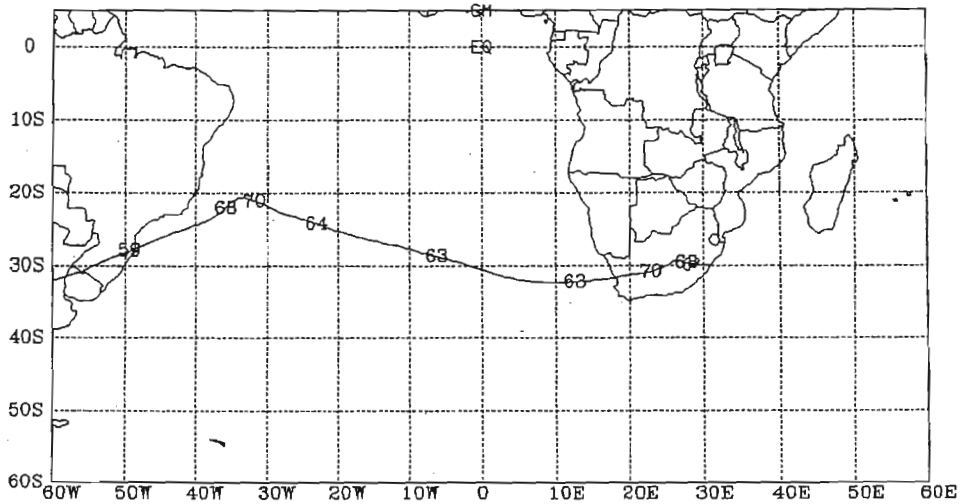

Backward Trajectories (Centroid Only)
Origin 29.9S 30.9E (Site unknown)
Height at Origin 925 hPa on 26 September 1997 12.00 UTC

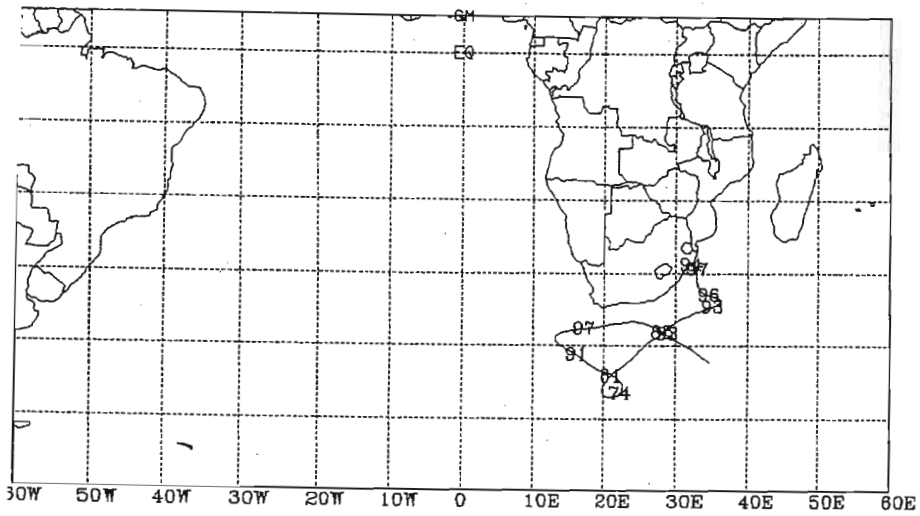

Backward Trajectories (Centroid Only)
Origin 29.9S 30.9E (Site unknown)
Height at Origin 1000 hPa on 26 September 1997 12.00 UTC

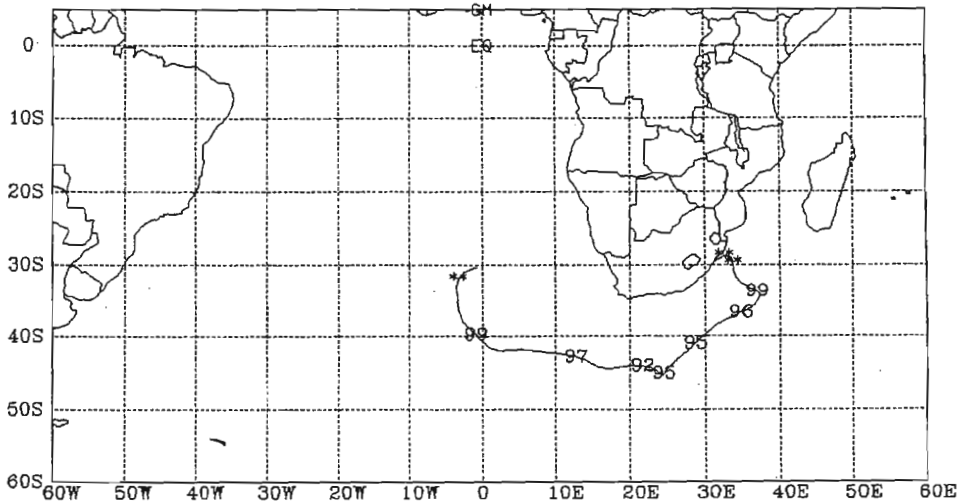

Backward Trajectories (Centroid Only)
Origin 29.9S 30.9E (Site unknown)
Height at Origin 1500 hPa on 20 October 1997 12.00 UTC

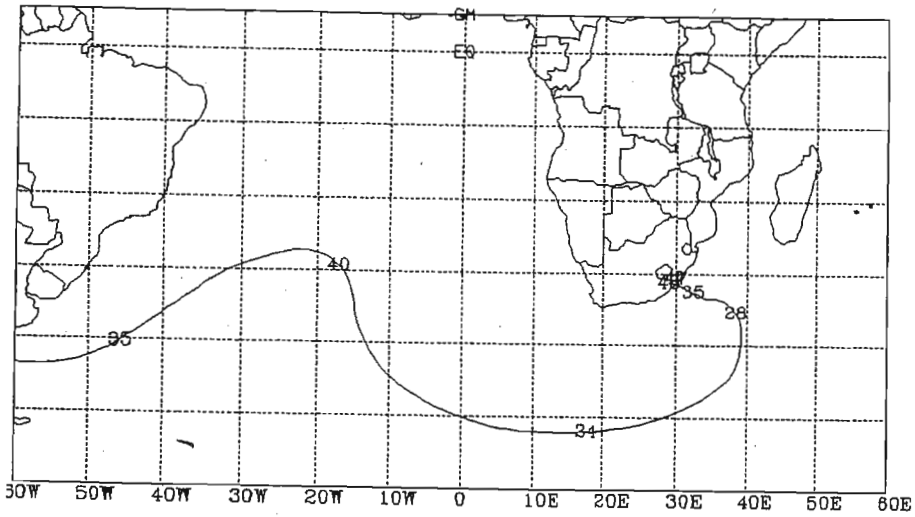

Backward Trajectories (Centroid Only)
Origin 29.9S 30.9E (Site unknown)
Height at Origin 1300 hPa on 20 October 1997 12.00 UTC

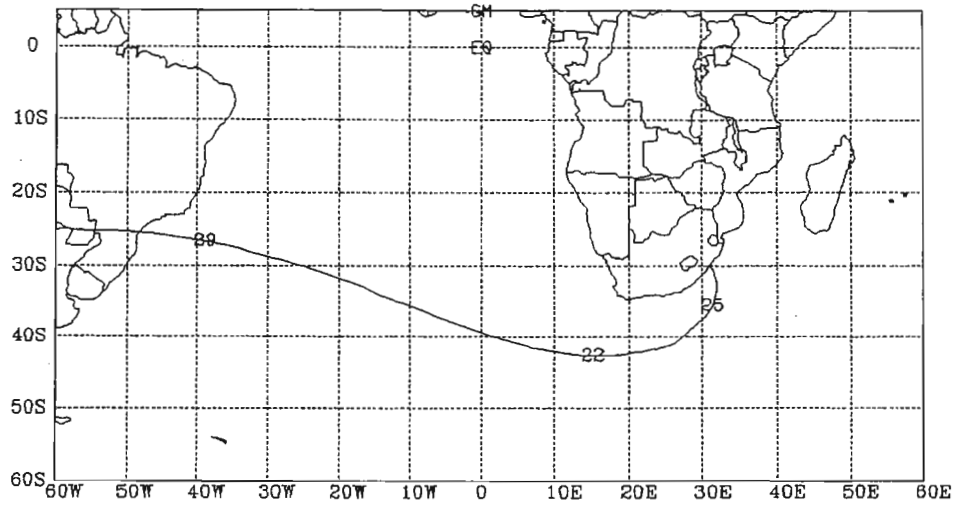

Backward Trajectories (Centroid Only)
Origin 29.9S 30.9E (Site unknown)
Height at Origin 1700 hPa on 20 October 1997 12.00 UTC

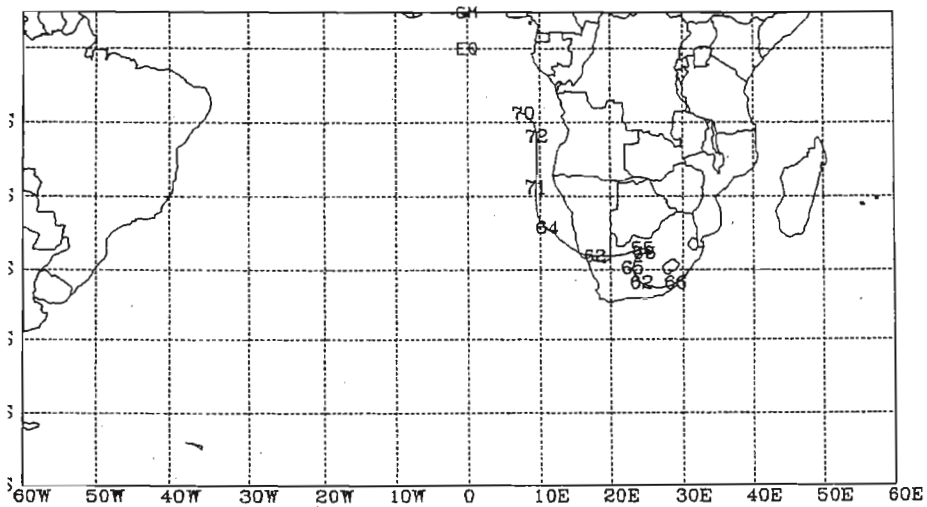

Backward Trajectories (Centroid Only)
Origin 29.9S 30.9E (Site unknown)
Height at Origin 1850 hPa on 20 October 1997 12.00 UTC

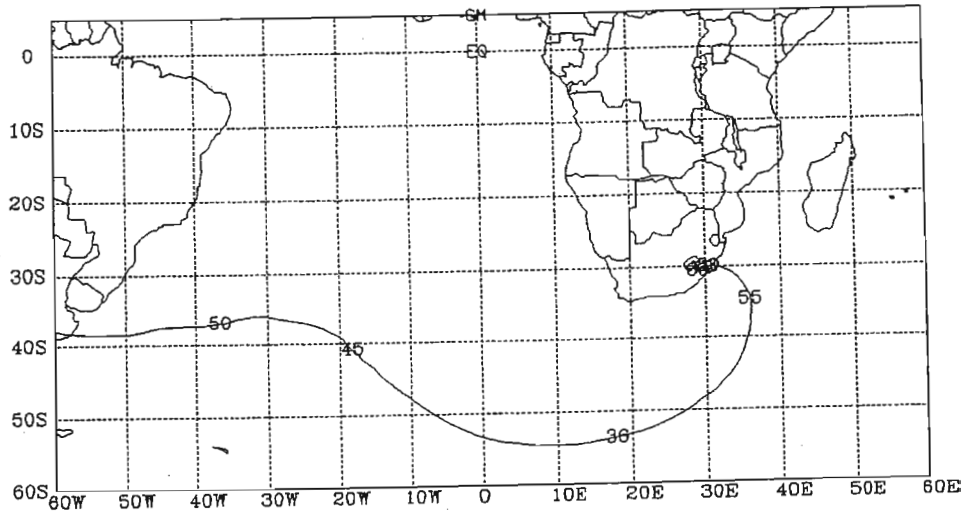

Backward Trajectories (Centroid Only)
Origin 29.9S 30.9E (Site unknown)
Height at Origin 925 hPa on 20 October 1997 12.00 UTC

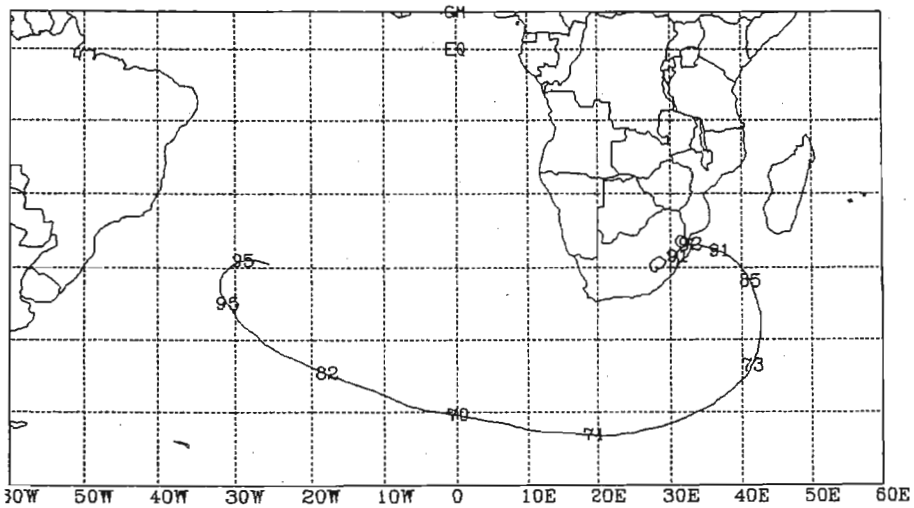

Backward Trajectories (Centroid Only)
Origin 29.9S 30.9E (Site unknown)
Height at Origin 1000 hPa on 20 October 1997 12.00 UTC

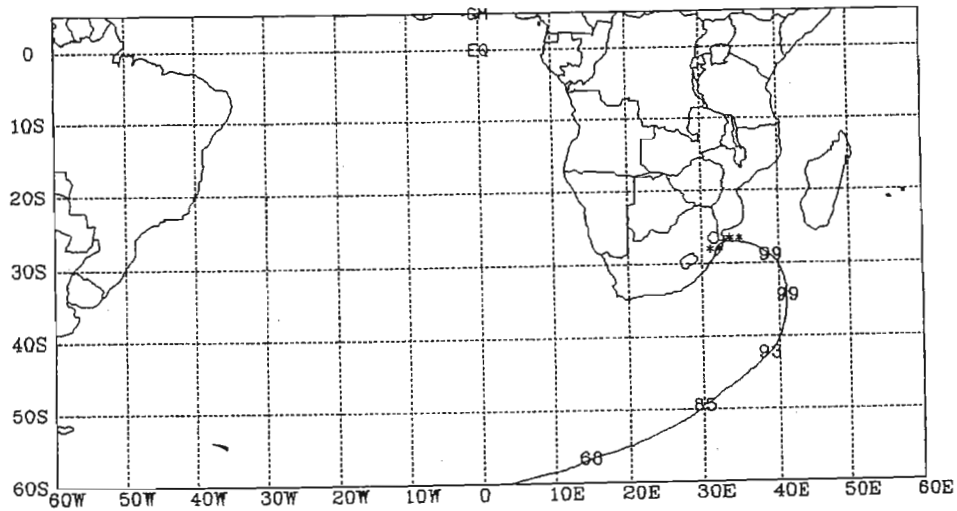

Backward Trajectories (Centroid Only)
Origin 29.9S 30.9E (Site unknown)
Height at Origin 1500 hPa on 20 October 1997 12.00 UTC

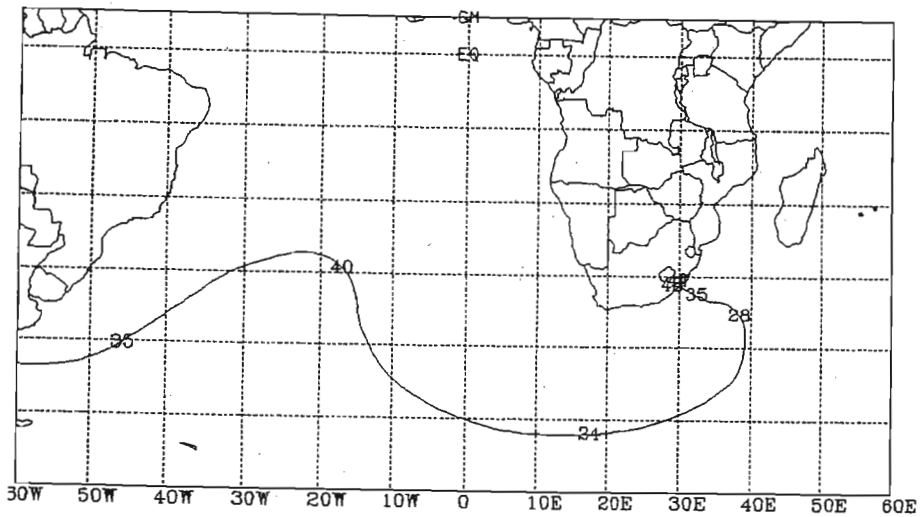

Backward Trajectories (Centroid Only)
Origin 29.9S 30.9E (Site unknown)
Height at Origin 1300 hPa on 20 October 1997 12.00 UTC

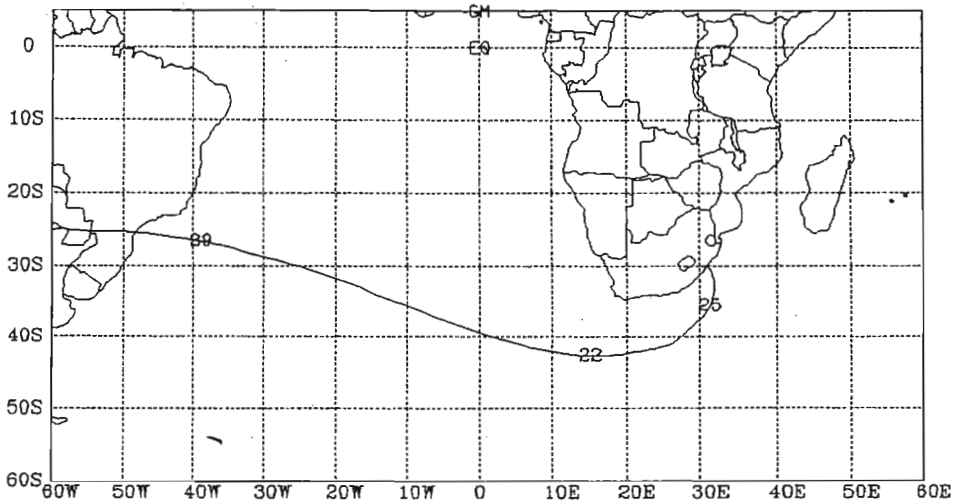

Backward Trajectories (Centroid Only)
Origin 29.9S 30.9E (Site unknown)
Height at Origin 1700 hPa on 20 October 1997 12.00 UTC

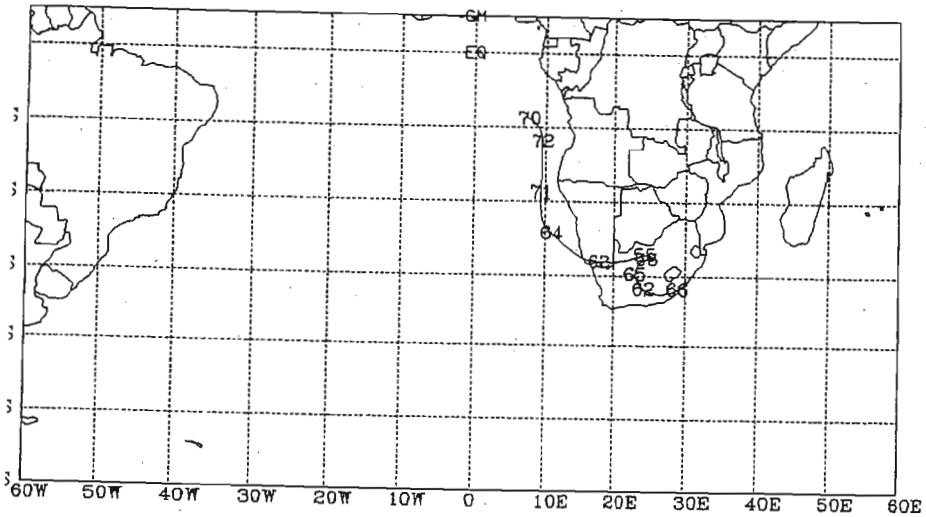

Backward Trajectories (Centroid Only)
Origin 29.9S 30.9E (Site unknown)
Height at Origin 1850 hPa on 20 October 1997 12.00 UTC

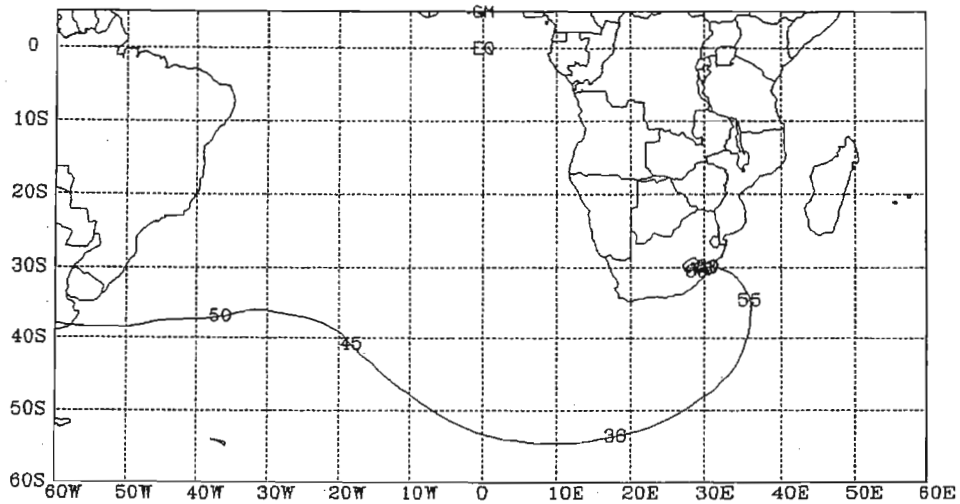

Backward Trajectories (Centroid Only)
Origin 29.9S 30.9E (Site unknown)
Height at Origin 925 hPa on 20 October 1997 12.00 UTC

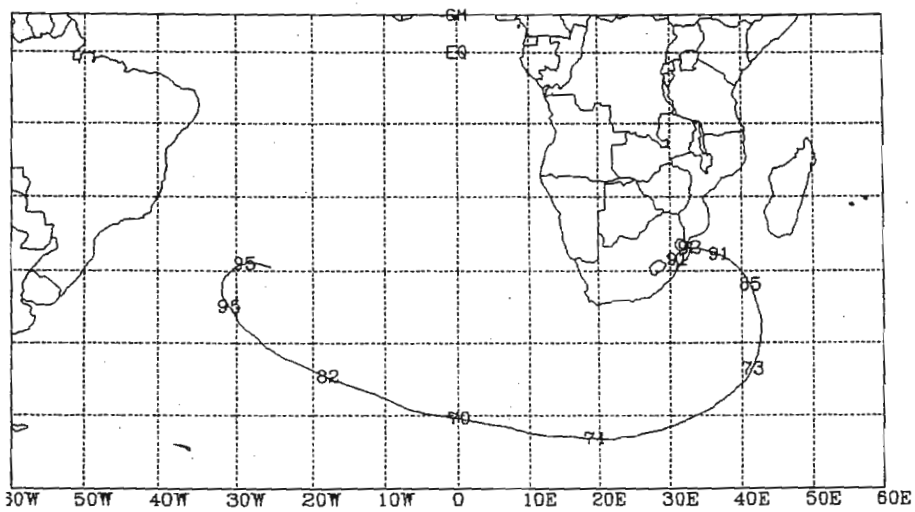

Backward Trajectories (Centroid Only)
Origin 29.9S 30.9E (Site unknown)
Height at Origin 1000 hPa on 20 October 1997 12.00 UTC